



The University of
Nottingham

UNITED KINGDOM • CHINA • MALAYSIA

Computational Modelling of Polymer-Based Drug Delivery Systems

Robert Mackenzie BSc

Thesis submitted to the University of Nottingham

for the degree of Doctor of Philosophy

September 2014

Abstract

Polymer-based drug delivery systems have fantastic potential in chemotherapy as they can reduce drug side effects, help in patient compliance and provide targeting. Nanoprecipitation is used to encapsulate small drug molecules into polymer nanoparticles to form a drug delivery system.

A major obstacle in polymer-based drug delivery systems reaching the clinic is their inability to load sufficient drug molecules. Little is known about the processes involved in the encapsulation of drug molecules into these delivery systems. An insight into the processes that govern the formation of these particles and encapsulation of small drug molecules within them is therefore desirable.

We used molecular dynamics to model nanoprecipitation by simulating the dispersion of an acetone drop, containing polymer, into water containing drug. To allow sufficient dispersion of acetone a large amount of water is required, thus coarse-graining becomes mandatory. However, we maintain accuracy for our polymer-drug interactions by using a multiscale force field. Atomistic polymer and drug molecules contain coarse-grain virtual sites which facilitate interactions with the coarse-grain solvent molecules. We also

employed fully atomistic reference simulations via resolution transformation to optimise our multiscale force field.

This thesis details the theory and design behind this model of nanoprecipitation including how other techniques produced inferior results. Initial simulations with our multiscale model matched an experimental trend and were shown to be accurate relative to atomistic reference simulations.

We also analysed a fully atomistic simulation of nanoprecipitation that took several months to complete. This atomistic simulation was used as a reference to update the multiscale force field. The updated force field improved on some aspects of the simulation but there are still areas that need improvement.

Insight from the simulations provides an understanding of the experimental results and trends. The transferability of the model should help in designing more efficient polymer-based drug delivery systems in the future.

We conclude with future work on modelling polymer-based drug delivery systems including alternate methods to gain understanding of not only drug incorporation but also drug release.

Acknowledgements

Firstly I would like to thank Charlie Laughton for his support and encouragement during my PhD. Charlie inspired me to do this project when it was pitched to a small group of us at AstraZeneca four years ago. His enthusiasm in the explanation of this project assured me that this was the PhD I should spend the next three years of my life on. Since then I have never looked back. My other supervisors Martin, Cameron and Jon have also been a great help. I hope that my work has helped unlock some of the secrets of how PGA behaves at the molecular level. I still remember the enthusiasm Martin had after I showed the initial simulations I completed. All of this positive encouragement was a huge driving force during my PhD and for that I am grateful.

The DTC/CDT has also been essential to me. The freedom and blue-sky thinking that the CDT provides allows for the creation of the toughest and most interesting PhD projects at Nottingham. Continued funding from EPSRC and AZ enables this fantastic research to continue after I finish.

The Molecular Recognition Group has seen many changes whilst I have been a part of it. I would like to thank everyone I got to know in the group as you were all inspirational to me and a great source of interest when I became

tired of my own work! I hope our discussions in lab meetings were helpful to all of you and that you will continue being the great collaborative group you are. Ioanna and Eleanor good luck tackling those polymers and do not hesitate to contact me for any tips/ideas!

To my collaborators Sarah and Matt; I had tons of fun helping out on your projects and it is a shame I cannot include your work in this thesis. I wish you both the best of luck in the future.

Finally I would like to thank my friends and family back in London. I cannot guess how many hours were spent on the train to and from St Pancras but it was fantastic to almost always have something to look forward to at the weekend.

Thanks Mum and Dad for being supportive and interested in what I have done these past years. Mum thank you for teaching me how to be industrious and Dad for reminding me to think outside of the box.

Claire you were there right at the very start and have followed me all the way through. Now we are finally together and this is all finished I am sure we will look back on it and remember the fantastic weekends we spent together be it in my tiny flat, a house filled with undergraduates or the lovely Carey Gardens. Thank you.

List of Contents

| | |
|--|----|
| Abstract..... | 2 |
| Acknowledgements..... | 4 |
| List of Contents..... | 6 |
| List of Figures..... | 11 |
| List of Tables | 22 |
| List of Abbreviations | 23 |
| Chapter 1..... | 25 |
| Introduction..... | 25 |
| 1.1 Motivation..... | 26 |
| 1.2 Nanoprecipitation..... | 27 |
| 1.3 Theoretical Work | 29 |
| 1.3.1 Modelling Nanoprecipitation | 30 |
| 1.3.2 Nanoparticle Encapsulation Efficiency..... | 35 |
| 1.3.3 Single Drug Interactions | 49 |
| 1.4 Multiscale Modelling | 57 |
| 1.5 Poly(glycerol adipate)..... | 61 |

| | |
|--|----|
| 1.6 Thesis Aims | 68 |
| Chapter 2..... | 70 |
| Methodology..... | 70 |
| 2.1 Experimental Work..... | 70 |
| 2.1.1 Polymer Synthesis..... | 70 |
| 2.1.2 Polymer Designations | 73 |
| 2.2 Theoretical Work | 74 |
| 2.2.1 Molecular Dynamics | 74 |
| 2.2.2 Interaction Potential | 76 |
| 2.2.3 Coarse-Grain Molecular Dynamics | 79 |
| 2.2.4 Nanoprecipitation Model | 79 |
| 2.3 Simulation Setup..... | 81 |
| 2.3.1 Molecular Dynamics | 81 |
| 2.3.2 Multiscale Force Field | 83 |
| 2.3.3 Simulation Setup | 84 |
| 2.4 Analysis..... | 85 |
| 2.4.1 Resolution Transformation | 85 |
| 2.4.2 Comparative Analysis of Multiscale and Atomistic Simulations | 86 |
| 2.4.3 Drug Loading and Encapsulation Efficiency | 87 |
| Chapter 3..... | 89 |
| Designing a Model to Study Polymer Drug Interactions | 89 |
| 3.1 An Acetone Drop Nanoprecipitation Model..... | 90 |

| | |
|---|-----|
| 3.2 Coarse-Grained Solvent | 93 |
| 3.3 Coarse-Grained Polymer | 96 |
| 3.3.1 Improving the CG interactions | 97 |
| 3.3.2 A new CG model | 101 |
| 3.4 Coarse-Grained Drug | 104 |
| 3.5 Multiscale Modelling | 105 |
| 3.6 Multiscale Model Optimisations | 106 |
| 3.6.1 Polymer-Drug Interactions | 106 |
| 3.6.2 DXMP Orientation | 111 |
| 3.6.3 Drug Solvent Interactions | 113 |
| 3.7 Conclusion | 114 |
| Chapter 4..... | 116 |
| Incorporation of DXMP into PGA Nanoparticles: Multiscale Model..... | 116 |
| 4.1 Simulation of PGA ₁₀₀ nanoprecipitation in the presence of DXMP..... | 118 |
| 4.2 Simulation of PGA ₂₀ -co-C18PGA ₈₀ nanoprecipitation in the presence of DXMP | 122 |
| 4.3 Simulation of C18PGA ₁₀₀ nanoprecipitation in the presence of DXMP | 124 |
| 4.4 Model validation through resolution transformation | 125 |
| 4.5 Encapsulation Efficiency and Drug Loading | 128 |
| 4.6 Testing Drug Binding Affinity..... | 131 |
| 4.7 The Importance of Acetone Dispersion | 132 |

| | |
|--|-----|
| 4.8 Explanation for the Experimental Trend..... | 135 |
| 4.9 Conclusion | 141 |
| Chapter 5..... | 143 |
| Incorporation of DXMP into PGA Nanoparticles: Atomistic Model..... | 143 |
| 5.1 Acetone Dispersion | 145 |
| 5.1.1 Molecular Dynamics Optimisation | 147 |
| 5.2 Fully Atomistic Simulation of PGA ₂₀ -co-C18PGA ₈₀ nanoprecipitation in the presence of DXMP | 148 |
| 5.3 Encapsulation Efficiency and Drug Loading | 153 |
| 5.4 Sodium Ion Interactions | 154 |
| 5.5 Drug Cluster Binding to the Polymer Nanoparticle..... | 156 |
| 5.6 Conclusion | 158 |
| Chapter 6..... | 160 |
| Incorporation of DXMP into PGA Nanoparticles: Updated Multiscale Model | 160 |
| 6.1 Optimisation..... | 162 |
| 6.1.1 Acetone Dispersion | 162 |
| 6.1.2 PGA ₂₀ -co-C18PGA ₈₀ Radius of Gyration | 166 |
| 6.2 Simulation of PGA ₂₀ -co-C18PGA ₈₀ nanoprecipitation in the presence of DXMP | 169 |
| 6.3 Simulation of C18PGA ₁₀₀ nanoprecipitation in the presence of DXMP (MS2_salt)..... | 174 |

| | |
|--|-----|
| 6.4 Simulation of PGA ₁₀₀ nanoprecipitation in the presence of DXMP (MS2_salt)..... | 176 |
| 6.5 Drug Loading and Encapsulation Efficiency | 177 |
| 6.6 Conclusion | 179 |
| Chapter 7..... | 181 |
| Conclusions and Future Work | 181 |
| References..... | 192 |
| Appendix..... | 197 |
| WS_RM Acetone Topology | 197 |
| Multiscale DXMP.gro | 198 |
| Multiscale DXMP.itp..... | 199 |
| grompp.mdp for Multiscale Simulations | 209 |
| MS2 force field | 210 |

List of Figures

| | |
|---|----|
| Figure 1.1 Cartoon of the process of nanoprecipitation. Polymer dissolved in acetone (blue droplet) is added to water in a beaker under constant stirring. As acetone disperses the polymer chains aggregate into nanoparticles. If drug molecules are present in either solvent they can be encapsulated in the nanoparticles as they form. | 28 |
| Figure 1.2 Snapshots taken from a system with favourable solute-polymer interaction at time points 12.5 μ s, 17.5 μ s, 25 μ s and 100 μ s. Solute bead (blue), PS block (red), PEG block (transparent grey). Taken from Ref ¹⁶ | 33 |
| Figure 1.3 Schematic of a microreactor used for nanoprecipitation. Taken from Ref ¹⁷ | 34 |
| Figure 1.4 The chemical structure of Gantrez AN119 (A), Gliclazide (B) and Silymarin (C). | 36 |
| Figure 1.5 Chemical structures of the molecules involved in this study. Taken from Ref ²⁰ | 37 |
| Figure 1.6 Snapshot taken at 900ns into a high concentration simulation of PAE-PEG with CPT. A vesicle forms with a hydrophobic layer of PAE (green) and hydrophilic PEG (purple). Orange spheres are camptothecin. Taken from Ref ²⁰ | 39 |

| | |
|--|----|
| Figure 1.7 Cross-section views of (a) blank micelle, (b) schematic of blank micelle, (c) DOX loaded micelle. PCL (blue), DEA (pink/red), PEG (green). Taken from Ref ²¹ | 40 |
| Figure 1.8 (A) Snapshot of propofol (yellow/pink) encapsulated within a GCPQ micelle. Chitosan (orange), glycol (red), quaternary ammonium (blue), palmitoyl (green). Structures of GCPQ (B) and propofol (C) with circles designating the atoms that make up the CG beads used in the model. Taken from Ref ²² | 43 |
| Figure 1.9 Solute encapsulation is measured over time for pre-assembled micelles and micelles that form in co-association with solute. The interaction between polymer solvent-phobic head particles (ϵ_{hh}) was set at 1.2 and 1.5 for comparison purposes. Taken from Ref ²³ | 45 |
| Figure 1.10 Snapshot of a worm-like micelle. Part of the micelle is sectioned to reveal the internal structure. Taken from Ref ²⁵ | 47 |
| Figure 1.11 Chemical structures of (A) Curcubitacin B and (B) Curcubitacin I. | 49 |
| Figure 1.12 Chemical structures of curcumin (A), paclitaxel (B) and Vitamin D3 (C). | 52 |
| Figure 1.13 PMFs calculated over a distance from the dendrimer centre of mass. PAMAM dendrimer (G5), G5NP (PAMAM non-protonated). Taken from Ref ²⁹ | 53 |
| Figure 1.14 The spatial distribution of PEO (blue) and PPO (green) around curcumin is calculated. Taken from Ref ³⁰ | 56 |
| Figure 1.15 A summary of mesoscale simulations; atomistic being the most accurate and DPD the most simplistic yet fastest. Taken from Ref ³² | 57 |

| | |
|---|----|
| Figure 1.16 A diagram showing how AdResS (adaptive resolution scheme) works. Water is shown in its CG and AA representations at the top. In the middle and at the ends are transition regions where the CG and AA representations interchange. Taken from Ref ³³ . | 59 |
| Figure 1.17 Atomistic butane (yellow) has CG virtual sites (red) to allow it to interact with the surrounding CG butane molecules (grey). Taken from Ref ³⁵ . | 60 |
| Figure 1.18 Chemical structures of PGA and two functionalised PGA polymers. The structure of the chemotherapeutic DXMP is also shown. | 62 |
| Figure 1.19 Effect of % acylation and PGA backbone molecular weight on DXMP encapsulation efficiency for a C18 acyl chain. Taken from Ref ¹² . | 63 |
| Figure 1.20 DXMP release from PGA polymers at various acylation % at 37°C in water over 25 days. Taken from Ref ¹¹ . | 65 |
| Figure 1.21 A contact angle can be measure for a drop of solvent on a surface coated with polymer. Taken from Ref ³⁷ . | 67 |
| Figure 2.22 Synthesis of PGA by poly-condensation reaction of glycerol and divinyl adipate. | 71 |
| Figure 2.23 GPC plot showing a highly poly disperse polymer with a Mw of nearly 9kDa. This polymer was used for the nanoprecipitation experiments... | 72 |
| Figure 2.24 Functionalisation of PGA with a stearate chain via an acid chloride reaction. | 72 |
| Figure 2.25 In nanoprecipitation polymer dissolved in acetone is added drop-wise to water containing hydrophilic drug molecules. | 73 |
| Figure 2.26 A plot of a 6-12 Lennard Jones potential. | 77 |

| | |
|---|----|
| Figure 2.27 A graph of a harmonic oscillator used for bond lengths in molecular dynamics. The given bond length (r_0) is maintained due to the increase in potential energy upon bond compression or extension. | 78 |
| Figure 2.28 (A-C) The dispersion of acetone in a periodic box of water. | 80 |
| Figure 2.29 Molecules used in this work including their chemical structures and their in silico representations. | 82 |
| Figure 2.30 Interactions involved in the multiscale force field. AA interactions are labelled in green whilst CG interactions are in red. Note there are no CG interactions between the CG virtual sites on the AA molecules to prevent doubling with AA interactions already present. | 84 |
| Figure 2.31 Resolution transformation procedure. (A) An 11nm sided..... | 86 |
| Figure 2.32 A cartoon depicting the calculation of the difference in the distance (Δ distance) from two atoms at opposite ends of DXMP to the centre of mass of the polymer nanoparticle. | 87 |
| Figure 3.33 Snapshot taken from the end of a simulation of five 50mers of PGA ₁₀₀ in pure water. Each polymer chain is shown in a different colour to emphasize the lack of polymer chain entanglement. | 91 |
| Figure 3.34 The mean square displacement of acetone in water over 5ns using the GROMOS 53a6 AA force field (red), MARTINI force field (green) and a corrected CG force field (blue)..... | 95 |
| Figure 3.35 Two separate simulations of acetone dispersing in water using two different force fields: AA (red) and CG (blue). Water is not shown for clarity. | 95 |
| Figure 3.36 Snapshots taken from simulations of PGA ₁₀₀ in water. Polymers are represented as lines with different colours for the CG beads in the structure. | |

| | |
|--|-----|
| The AA structures were mapped to CG representations at the end of the simulation for a clearer comparison. | 97 |
| Figure 3.37 CG mapping scheme used for PGA ₁₀₀ . Every 3-4 non hydrogen atoms are mapped to a single CG bead..... | 97 |
| Figure 3.38 The RDF of a blue bead to green beads. Seven green beads are located at a distance r from the central blue bead..... | 98 |
| Figure 3.39 CG potentials required for PGA ₁₀₀ : Non-bonded (green), Bonds (black), Angles (red)..... | 99 |
| Figure 3.40 During iterative Boltzmann inversion RDFs from a CG simulation of PGA ₁₀₀ in water are plotted at different cycles during the process. The CG RDFs begin to converge to the AA reference RDF until a refined CG potential was obtained after 25 cycles..... | 100 |
| Figure 3.41 CG structure of a PGA ₁₀₀ nanoparticle in water using the CG potentials obtained with VOTCA. The structure more closely resembles the AA structure seen in Figure 3.36..... | 101 |
| Figure 3.42 Plots for the solvent accessible surface area (SASA) of PGA ₁₀₀ over 40ns. The new CG tabulated potentials offered good agreement with the AA simulation compared with the MARTINI force field. | 101 |
| Figure 3.43 Two simulations of 250 monomers of PGA ₁₀₀ in water using the MARTINI force field and the VOTCA refined CG force field. The MARTINI force field generates a bilayer like construct whereas the VOTCA force field generates a spherical nanoparticle. | 103 |
| Figure 3.44 Multiscale model used for DXMP (A) and PGA (B). The transparent CG beads are virtual sites that are positioned at the centre of mass of the atoms they represent. The atomistic molecules interact with surrounding | |

| | |
|--|-----|
| CG solvent molecules through these virtual sites using the MARTINI CG force field..... | 105 |
| Figure 3.45 Snapshot taken during a 20ns multiscale simulation of DXMP (green/orange) with PGA ₁₀₀ (blue/red) in CG water. Black dashed lines show the distance between charged oxygen atoms on the phosphate of DXMP to hydroxyl groups on PGA ₁₀₀ . The CG water molecules are not shown for clarity. | 108 |
| Figure 3.46 Snapshot taken at the end of a 20ns multiscale simulation of DXMP with PGA ₁₀₀ in AA water. There is counter charge present for the DXMP molecule and so it adopts a different orientation with respect to the polymer. Only water atoms in close proximity to the DXMP phosphate group are shown for clarity. | 109 |
| Figure 3.47 The radius of gyration for PGA ₁₀₀ in water using an AA force field (red) is compared with the multiscale force field at $\epsilon_r = 6$ (green). | 110 |
| Figure 3.48 Snapshots comparing the final atomistic structure with a corrected multiscale (hybrid) force field. Water is not shown for clarity. PGA ₁₀₀ (blue/red), DXMP (green/orange). | 111 |
| Figure 3.49 The orientation of DXMP in relation to a PGA nanoparticle in water was analysed over four different 5ns simulations. AA (red), multiscale ($\epsilon_r = 6$) (green), multiscale ($\epsilon_r = 1$) (blue), multiscale ($\epsilon_r = 15$) (pink). | 111 |
| Figure 3.50 Snapshots taken at the end of 10ns simulations showing the partitioning of DXMP in acetone/water. With an AA force field (left) and multiscale (right). Water (red dots), acetone (blue dots). | 114 |
| Figure 4.51 Snapshots taken during the 80ns multiscale simulation of PGA ₁₀₀ with DXMP. A: 5ns (with acetone shown), B: 5ns, C: 30ns, D: 50ns, E: 80ns | |

| | |
|---|-----|
| (with acetone shown), F: 80ns. DXMP (red/blue), PGA (white), acetone (blue). Water and CG virtual sites not shown for clarity. | 119 |
| Figure 4.52 Snapshot taken from a simulation of PGA ₁₀₀ with DXMP. DXMP molecules position themselves at the surface of the acetone drop in a specific orientation..... | 120 |
| Figure 4.53 Snapshots taken during the 80ns multiscale simulation of PGA ₂₀ - co-C18PGA ₈₀ with DXMP. A: 5ns (with acetone shown), B: 5ns, C: 30ns, D: 50ns, E: 80ns (with acetone shown), F: 80ns. DXMP (red/blue/white), PGA (white), C18 chains (yellow), acetone (blue). Water and CG virtual sites not shown for clarity..... | 122 |
| Figure 4.54 Snapshots taken during the 80ns multiscale simulation of C18PGA ₁₀₀ with DXMP. A: 5ns (with acetone shown), B: 5ns, C: 30ns, D: 50ns, E: 80ns (with acetone shown), F: 80ns. DXMP (red/blue/white), PGA (white), C18 chains (yellow), acetone (blue). Water and CG virtual sites not shown for clarity..... | 124 |
| Figure 4.55 Analysis for PGA ₁₀₀ (top) PGA ₂₀ -co-C18PGA ₈₀ (bottom) with DXMP. Left: Two snapshots from the end of the 5ns simulations. DXMP (multi), PGA (white with C18 chains yellow). Graphs for the total radius of gyration of the polymer cluster (middle) and the orientation of DXMP in relation to the centre of mass of the polymer chains (right). Atomistic (red), multiscale (green). | 127 |
| Figure 4.56 Snapshots taken during a 20ns pure water simulation of the final nascent nanoparticles from the 80ns nanoprecipitation simulation of PGA ₁₀₀ (A,B,C) and PGA ₂₀ -co-C18PGA ₈₀ (D,E,F) with A and D being the start, B and E middle and C and F the end of the simulation. PGA (white), C18 chains | |

| | |
|---|-----|
| (yellow) and DXMP (multi). For clarity only a single drug molecule with no CG solvent or virtual sites are shown. | 132 |
| Figure 4.57 Snapshot taken at the end of a simulation containing three chains of PGA ₁₀₀ with cytarabine. PGA ₁₀₀ (white), cytarabine (multi). CG solvent and virtual sites are not shown for clarity. | 135 |
| Figure 4.58 Number of DXMP molecules within 1.2 nm of the polymer chains is analysed for all three polymers over the 80ns simulations. Error bars are included for the standard error of the mean from triplicate repeats. PGA ₁₀₀ (red), PGA _{20-co-C18PGA₈₀} (blue), C18PGA ₁₀₀ (green). | 136 |
| Figure 4.59 Snapshots taken from a PGA _{20-co-C18PGA₈₀} multiscale simulation with DXMP. (A-E) A drug cluster binds to the surface of the polymer nanoparticle. (F) A drug cluster in solution formed during the 80ns simulation. | 137 |
| Figure 4.60 Snapshots taken at the around the 20ns time point of the nanoprecipitation simulations. PGA ₁₀₀ (A,D), PGA _{20-co-C18PGA₈₀} (B,E), C18PGA ₁₀₀ (C,F). Acetone is shown on the top row of snapshots to indicate the size of the acetone drop. PGA (white) and C18 chains (yellow). Water is not shown for clarity. | 139 |
| Figure 4.61 The radius of gyration of the all the polymers in each system over the 10-50ns time period of the 80ns multiscale simulation. Error bars are included for the standard error of the mean from triplicate repeats. PGA ₁₀₀ (red), PGA _{20-co-C18PGA₈₀} (blue), C18PGA ₁₀₀ (green). | 140 |
| Figure 5.62 Chemical structure of acetone showing methyl groups and central carbonyl group. | 146 |

| | |
|--|-----|
| Figure 5.63 Snapshots taken during the 50ns atomistic simulation of PGA ₂₀ -co-C18PGA ₈₀ with DXMP. A: 2ns, B: 10ns, C: 20ns, D: 30ns, E: 40ns , F: 50ns. DXMP (red/blue/white), PGA (white), C18 chains (yellow), acetone (blue). Water and acetone not shown for clarity. | 150 |
| Figure 5.64 Snapshot taken at the end of the 50ns atomistic nanoprecipitation simulation. Some drug molecules are buried into the nanoparticle whilst others rest on the surface. | 151 |
| Figure 5.65 The location of acetone at the start (A) and end (B) of the 50ns fully atomistic nanoprecipitation simulation. | 152 |
| Figure 5.66 The dispersion of atomistic acetone over 50ns during the fully atomistic nanoprecipitation simulation..... | 154 |
| Figure 5.67 (A) A large cluster of DXMP molecules forms with sodium counter ions for the phosphate charge. (B) Phosphate groups on DXMP molecules encapsulated by PGA ₂₀ -co-C18PGA ₈₀ interact with surrounding ions..... | 155 |
| Figure 5.68 The process of a DXMP cluster merging with the surface of the polymer nanoparticle is shown over 2ns A-E. F: Close-up of where the drug bound to the surface of the polymer (drug shown with liquorice representation for clarity). | 157 |
| Figure 6.69 Plots for the mean squared displacement of acetone in water using various force fields. Original ATB AA (cyan), original multiscale (MS1) (pink), MARTINI CG (blue), WS_RM AA (green), new multiscale (MS2) (red)..... | 163 |

| | |
|---|-----|
| Figure 6.70 The dispersion of acetone differs between the original MS1 force field (left) and the atomistic force field WS_RM (right). Acetone is shown as a single sphere in both images for comparison. | 164 |
| Figure 6.71 The MSD of acetone in water during 50ns of nanoprecipitation simulation time. Original multiscale (blue), fully atomistic (red), optimised multiscale (green). | 165 |
| Figure 6.72 The total radius of gyration for a two polymer cluster is analysed over a 50ns nanoprecipitation simulations. Fully AA (green), MS2 (red). | 166 |
| Figure 6.73 View in landscape orientation. The dispersion of acetone is shown over the 50ns nanoprecipitation simulation using the fully atomistic force field (top) and MS2 force field (bottom). Snapshots were taken at 0, 10, 20, 30, 40 and 50ns from bottom to right. | 168 |
| Figure 6.74 View in landscape orientation. Snapshots taken during the 50ns MS2 simulation of PGA ₂₀ -co-C18PGA ₈₀ with DXMP (bottom). Snapshots from the fully atomistic are shown for comparison (top). A: 2ns, B: 10ns, C: 20ns, D: 30ns, E: 40ns, F: 50ns. DXMP (red/blue/white), PGA (white). Water and acetone not shown for clarity. | 170 |
| Figure 6.75 Snapshots taken at the end of the nanoprecipitation simulation of PGA ₂₀ -co-C18PGA ₈₀ with DXMP using the MS2 force field (left) and atomistic force field (right). Acetone surrounding the polymer is shown for comparison. | 171 |
| Figure 6.76 The binding of DXMP to PGA ₂₀ -co-C18PGA ₈₀ during the MS2 simulation (left). If DXMP binds an ion the orientation of the drug molecule is reversed. | 172 |

| | |
|---|-----|
| Figure 6.77 Snapshots taken during the 50ns MS2 simulation of PGA ₂₀ -co-C18PGA ₈₀ with DXMP salt. A: 2ns, B: 10ns, C: 20ns, D: 30ns, E: 40ns, F: 50ns. DXMP (red/blue/white), PGA (white). Water and acetone not shown for clarity. | 172 |
| Figure 6.78 Snapshots taken from the 10ns wash simulation in pure CG water at the start (left) and end (right) of the simulation using the MS2 force field. | 173 |
| Figure 6.79 The radius of gyration (R_g) for the PGA ₂₀ -co-C18PGA ₈₀ nanoparticle during a 10ns wash simulation (blue) is overlaid with the R_g from the last 10ns of the MS2 simulation (red) and fully atomistic simulation (green)..... | 174 |
| Figure 6.80 Snapshots taken during the 50ns MS2 simulation of C18PGA ₁₀₀ with DXMP salt. A: 2ns, B: 10ns, C: 20ns, D: 30ns, E: 40ns, F: 50ns. DXMP (red/blue/white), PGA (white). Water and acetone not shown for clarity..... | 175 |
| Figure 6.81 Snapshots taken during the 50ns MS2 simulation of PGA ₁₀₀ with DXMP salt. A: 2ns, B: 10ns, C: 20ns, D: 30ns, E: 40ns, F: 50ns. DXMP (red/blue/white), PGA (white). Water and acetone not shown for clarity..... | 176 |
| Figure 7.82 An alternative model for nanoprecipitation where the aqueous and organic phases are separated into planes and allowed to mix during the simulation. | 188 |

List of Tables

Table 4.1.....128

Table 5.1.....145

Table 6.1.....175

List of Abbreviations

| | |
|--------------|--|
| AA | All-Atom (atomistic) |
| ATB | Automated Topology Builder |
| C18-PGA | Stearate functionalised poly(glycerol adipate) |
| CPT | Camptothecin |
| CG | Coarse-Grain |
| COM | Centre Of Mass |
| CWC | Critical Water Concentration |
| CYT | Cytarabine |
| DL | Drug Loading |
| DPD | Dissipative Particle Dynamics |
| DXMP | Dexamethasone Phosphate |
| EE | Encapsulation efficiency |
| ϵ_r | Relative dielectric constant |
| fs | femtosecond |
| GROMACS | GRONingen MACHine for Chemical Simulations |
| GROMOS | GRONingen MOlecular Simulation |
| KB | Kirkwood-Buff |
| LINCS | LINear Constraint Solver |

| | |
|---------|--|
| MARTINI | MARrink's Toolkit INItiative |
| MD | Molecular Dynamics |
| MS1 | Multiscale force field version 1.0 |
| MS2 | Multiscale force field version 2.0 |
| ns | nanosecond |
| PAE | Poly(amino ester) |
| PEG | Poly(ethylene glycol) |
| PEO | Poly(ethylene oxide) |
| PGA | Poly(glycerol adipate) |
| PME | Particle Mesh Ewald |
| PPO | Poly(propylene oxide) |
| ps | picosecond |
| QM | Quantum Mechanics |
| R_g | Radius of Gyration |
| VDW | van der Waals |
| VOTCA | Versatile Object Orientated Toolkit for Coarse-graining Applications |
| WS | Weerasinghe and Smith (acetone model) |
| WS_RM | Weerasinghe and Smith and Robert Mackenzie (acetone model) |

Chapter 1

Introduction

This thesis details the analysis of drug-polymer interactions through molecular dynamics simulations. Small drug molecules can be encapsulated within polymer nanoparticles through a technique called nanoprecipitation¹. The resulting drug polymer nanoparticle is referred to as a polymer-based drug delivery system. Drug molecules encapsulated within a carrier will be slowly released throughout the body. The carrier can also reduce off-target effects of the drug and provide targeting to specific organs or tissues in the body. One example is the enhanced permeability retention effect where nanoparticles are preferentially retained in tumour sites due to leaky vasculature and poor lymphatic drainage. For these reasons several drug delivery systems have been designed for various existing chemotherapeutics²⁻⁶.

Whilst the potential for polymer drug delivery systems is very high there are several hurdles stopping them from entering the clinic. Historically the most difficult obstacle for polymer-based drug delivery systems is achieving useful levels of drug loading into the nanoparticles⁷⁻⁹. Whilst trial and error experimentation with various polymers is possible, there is a lack of

understanding of the underlying principles of drug incorporation and polymer drug interactions at the molecular level. Molecular dynamics provides a unique insight that is unobtainable by experimental methods. Computational simulations allow detailed analysis of drug polymer interactions that help comprehend experimental results and could potentially aid in the design of more efficient polymer-based drug delivery systems.

In this chapter we will explore the motivation for this work. Nanoprecipitation will be explained and we will look at theoretical work that has been performed previously to analyse polymer-drug interactions. Additionally the experimental work that is the basis for this PhD is evaluated. The aims of this thesis will be presented at the end of this chapter.

1.1 Motivation

Molecular dynamics has been used to simulate the behaviour of molecules for several decades. With the steady increase in computational power every year, the accuracy and scale of computational simulations increases facilitating the exploration of new and larger systems¹⁰. Traditionally molecular dynamics has been used to model the behaviour of proteins or lipid bilayers. Whilst many proteins are relatively small at around 10 nm in diameter, nanoparticles are often much larger - around 100-200 nm in diameter^{11,12}. With molecular dynamics the size of a system is directly related to its speed as an increase in the number of molecules, increases the number of interactions to be computed. As such, until recently there has been little work using molecular dynamics to model the formation of full-scale polymer nanoparticles.

When this project was started it was decided that computational power had grown sufficiently that simulations on the formation of polymer-based drug delivery systems could be attempted. Whilst mesoscale modelling techniques may have to be used, the goal was to design a computational model of nanoprecipitation. An accurate model has many useful features; firstly it could give an understanding of the processes involved in encapsulating drug molecules inside polymer nanoparticles. Secondly the model could be used to predict the encapsulation efficiency of various drug and polymer combinations. A computer model can be easily edited allowing easy exploration of new molecules and their interactions¹³.

1.2 Nanoprecipitation

Whilst there are several techniques used to prepare polymer-based drug delivery systems¹⁴; nanoprecipitation is fast, does not require mechanical work and generates particles with a relatively narrow size range¹. Droplets of a water-insoluble polymer in a water-miscible organic solvent are added to a large excess of water. Drug can either be present in the organic polymer solution, or the aqueous receiving solution, depending on the drug properties (Figure 1.1).

As each acetone drop hits the water it quickly disperses into the water. This exposes the hydrophobic polymer chains within the acetone and results in their aggregation with each other. Nearby, drug molecules diffuse through the water and will interact with the polymer chains during aggregation. Drug molecules that interact strongly with the polymer nanoparticle will be retained during subsequent washing steps and are considered encapsulated.

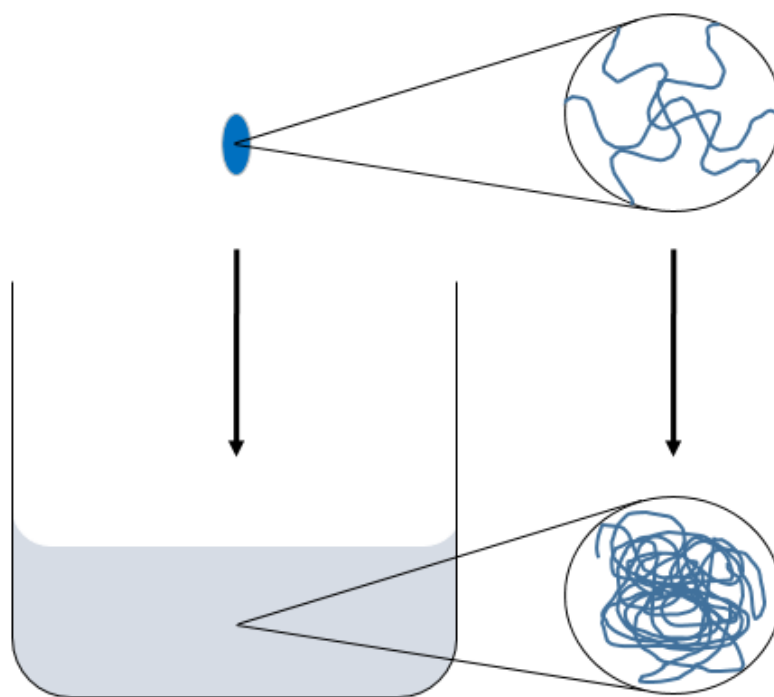


Figure 1.1 Cartoon of the process of nanoprecipitation. Polymer dissolved in acetone (blue droplet) is added to water in a beaker under constant stirring. As acetone disperses the polymer chains aggregate into nanoparticles. If drug molecules are present in either solvent they can be encapsulated in the nanoparticles as they form.

Conceptually, nanoprecipitation involves a number of processes that will be to some extent interdependent in a complex way. Firstly there is the solvent diffusion process, whereby the water-miscible organic solvent disperses into bulk water, and water enters into the volume of the original droplet. This change in the solvent environment of the (hydrophobic) polymer results in other processes; such as change in the polymer chains from an extended to a compacted conformation, intramolecular collapse, intramolecular aggregation and polymer chain entanglement. At the same time the drug molecules will be diffusing into the region in response to their concentration gradient, modulated by their affinity for the various species present. This makes modelling nanoprecipitation a difficult task as there are so many factors to replicate. We will see that much of the current literature ignores some of

these processes. If we want to use computational models to help understand and predict experimental results all these factors must be considered.

1.3 Theoretical Work

Computational models are widely used throughout several industries to tackle difficult problems such as predicting the weather or traffic flow^{15,16}. A model can help understand complex situations and ideas.

Recently the Nobel Prize for Chemistry was awarded to Karplus, Warshel and Levitt for their work on computational models for chemistry¹⁷. Their models were the first of their kind and looked at the folding of proteins and cleavage of glycoside bonds by lysozyme¹⁸. These microscopic processes are hard to observe with current experimental techniques such as transmission electron microscopy. By modelling how these molecules interact we can gain a greater understanding of the processes involved.

40 years after this pioneering work the field of computational chemistry has grown tremendously thanks in part due to the increase in computer power following Moore's law¹⁰. As computers become more powerful they are able to tackle large systems faster and more accurately. Processes that were originally unable to be simulated are now being investigated, with polymer drug interactions in nanoparticles being a prime example.

Whilst there is a large amount of work done on molecular dynamics with biomacromolecules, its application to polymer-based drug delivery systems is more limited. A pub-med search for "polymer molecular dynamics" returns ~600 results whilst "protein molecular dynamics" returns 4443 results.

With this in mind we will look at a selection of relevant models that have been created to analyse polymer-drug interactions. It should be noted that whilst not all of the studies have looked at recreating nanoprecipitation *in silico*, there are various other ways to gain a greater understanding of polymer-based drug delivery systems. In general most of the literature on polymer-drug nanoparticles tends to not focus on the formation of the particles themselves but the polymer-drug interactions that occur within them.

1.3.1 Modelling Nanoprecipitation

Spaeth et al. used dissipative particle dynamics (DPD) to model Flash NanoPrecipitation¹⁹. Flash NanoPrecipitation differs from nanoprecipitation as the mixture of anti-solvent with solvent is rapid (over a few milliseconds) and not drop-wise. The technique has been used to make nanoparticles of controllable size with various polymers experimentally.

However, as with nanoprecipitation there is a lack of understanding of the molecular interactions involved during Flash NanoPrecipitation. This study by Spaeth et al. attempts to address this by simulating the process using DPD. The model was parameterised based on experimental work. The authors found an implicit-solvent model using Brownian dynamics to produce incorrect aggregation dynamics. Conversely, an explicit solvent approach produced reasonable aggregation dynamics. This result is expected as implicit solvation treats solvent as a continuous medium instead of explicit solvent molecules.

Simulating Flash NanoPrecipitation at experimental conditions is challenging for several reasons: the concentration of polymer and solute results in roughly 200,000 solvent molecules per solute molecule, nanoparticles

formed were 100-200 nm in diameter and the mixing time was estimated to be a few milliseconds. The authors speculate that to form a single nanoparticle 10^5 solute molecules with 10^9 solvent molecules would need to be simulated over a few milliseconds which is beyond the scope of the computational resources available.

Multiple steps were taken to overcome this problem. Firstly a single solvent particle was used and its interactions with the solute were changed over time to mimic the change in solvent environment that occurs during Flash NanoPrecipitation. Solvent molecules were coarse-grained using DPD to reduce the degrees of freedom in the simulation. To further reduce the number of solvent molecules, the solute and polymer concentrations were 10-20 fold greater than experimental conditions. Finally the simulations were only run for 200 μ s, far less than the few milliseconds required. Whilst there are several caveats involved here they were all necessary to simulate Flash NanoPrecipitation. However, these changes must be factored into the discussion of any results generated by a model that is sufficiently different from experimental conditions.

DPD is a mesoscale modelling technique that uses repulsive forces between particles, with a random force and a frictional force as a thermostat to sample the NVT ensemble. Each molecule in the system is coarse-grained into particles 1 nm in diameter. For polystyrene, 1 CG particle represents two monomers of the polymer.

For the simulations, both polystyrene-b-poly(ethylene glycol) (PS₁₀-b-PEG₆₈) and the antifungal itraconazole were placed in a periodic box with solvent particles. By simplifying the molecules used in DPD a large timestep of

0.36 ps is used for the 200 μ s simulations. DPD produces accelerated dynamics compared with molecular dynamics so the simulation times were rescaled accordingly.

First the authors analysed the effect of mixing time by increasing the duration for the solvent interactions to fully change from instantaneous (0 μ s) to 200 μ s. As expected shorter mixing times caused nanoparticles to form more rapidly. Additionally a short mixing time reduced the amount of polymer and solute molecules in each nanoparticle formed.

Solute-polymer interactions were adjusted such that they were either favourable or unfavourable. Unfavourable interactions led to the formation of empty micelles with the solute forming aggregates separately. By the end of the simulation a large solute aggregate formed with only a few polymer molecules stabilising it. Favourable solute-polymer interactions allowed polymer micelles to form with solute incorporated in the process. The solute-polymer ratio was increased resulting in a steady increase in the number of solutes per nanoparticle up to a ratio of 4:1. This also produced larger nanoparticles due to the increase in solute content.

The polymer used in this study contains both a hydrophilic PEG block and a hydrophobic PS block. As the length of the PEG block increased the number of solutes per nanoparticle decreased whether the solute interactions were favourable or unfavourable. This was due to a decrease in particle size with an increase of PEG block. With a smaller particle size there is less space for solute in each nanoparticle. With an increase in the PS block length the number of solutes per nanoparticle does not change significantly.

When solute polymer interactions are favourable the solute clusters over the first 15 μ s of the simulation and polymer micelles form around the solute clusters (Figure 1.2). There is equal mixing of the polystyrene particles with the solute particles at the centre of the micelles. When the solute polymer interactions are unfavourable, solute is still encapsulated within the micelles but the solute is phase separated from the PS block of the copolymer.

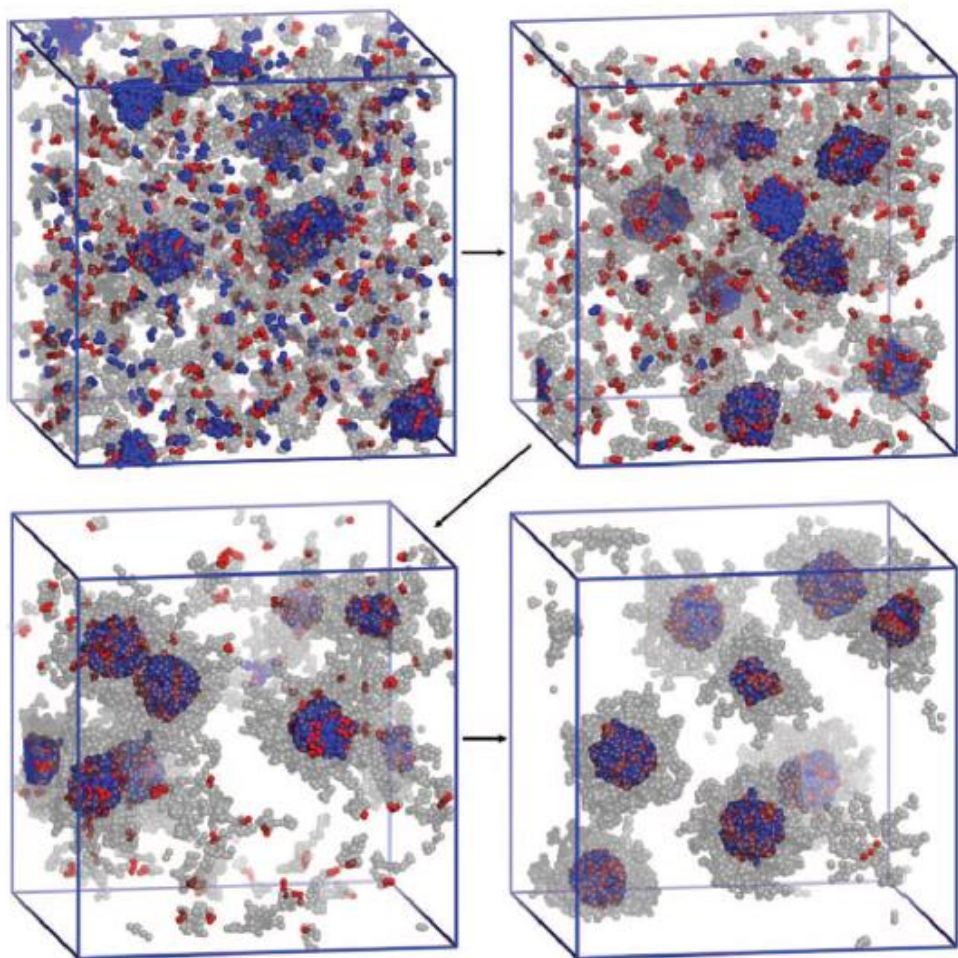


Figure 1.2 Snapshots taken from a system with favourable solute-polymer interaction at time points 12.5 μ s, 17.5 μ s, 25 μ s and 100 μ s. Solute bead (blue), PS block (red), PEG block (transparent grey). Taken from Ref¹⁹.

The authors conclude that their results should only serve as an indication of the Flash NanoPrecipitation of PS-PEG as the simulation conditions are not identical to experiment. Still, “a massive investment in

computing time” was required suggesting that a simulation at experimental concentrations is “still elusive”.

The only other computational study of nanoprecipitation is by Capretto et al. detailing the use of computational fluid dynamics (CFD) on nanoparticle formation through microfluidics²⁰. Microreactors are able to produce nanoparticles through nanoprecipitation of a narrow size range which is desirable for drug delivery purposes (Figure 1.3). As with the previous paper the aim of this study was to gain a better understanding of nanoparticle formation using computational modelling.

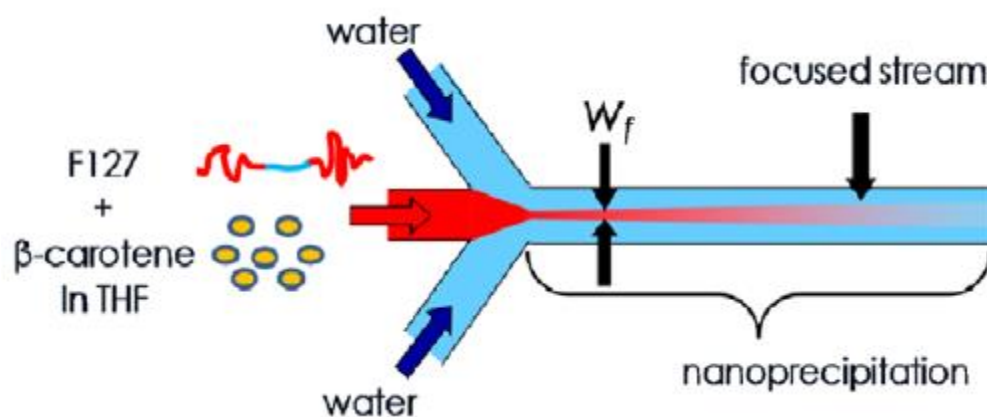


Figure 1.3 Schematic of a microreactor used for nanoprecipitation. Taken from Ref²⁰.

For this study the polymer used was Pluronic F127 ($\text{HO}(\text{C}_2\text{H}_4\text{O})_a(\text{C}_3\text{H}_6\text{O})_b(\text{C}_2\text{H}_4\text{O})_a\text{H}$) with the hydrophobic drug β -carotene. Microfluidics differs from “drop-wise” nanoprecipitation as the solvent and anti-solvent are mixed under continuous flow (1 ml/hour). For CFD a two dimensional model was used to simulate a polymer stream with adjacent water streams. This model has the benefit of being similar in scale to experimental conditions. The model was validated by comparison with experimental data using the width of the focused stream.

CFD was able to demonstrate how nanoparticles formed. First metastable micelles form separately from metastable β -carotene clusters. Further downstream the critical water concentration for β -carotene is reached and the insoluble portion of the polymer micelles act as a nucleation point causing their subsequent encapsulation. The time between β -carotene reaching its CWC and the polymer micelles reaching the CWC is defined as τ^* . Using CFD to obtain this parameter helps in forming stable nanoparticle batches without forming unwanted empty particle aggregates.

Both of these studies on nanoprecipitation have used models that lack atomistic detail of the molecules involved. This is understandable due to the computational demands of more accurate models. However, it is expected that in the future, advances in molecular dynamics and computational power will enable more accurate modelling of nanoprecipitation.

1.3.2 Nanoparticle Encapsulation Efficiency

Subashini et al. investigated drug uptake with various polymers using molecular dynamics²¹. Three drugs of varying water solubility were assessed with six polymers containing various functional groups. Nanoparticles were prepared by placing each drug adjacent to each polymer (decamers or hexamers). Topologies were generated by PRODRG whose accuracy has been questioned in the past²². Partial charges generated are often inaccurate and resulting in incorrect dynamics for small molecules. Simulations were carried out in periodic boxes solvated with water for 300 ps.

Molecular dynamics (MD) is one of the most common computational methods for simulating molecular interactions. Newton's equations of motion

are used to calculate forces between particles based on a force field. The force field dictates how attractive or repulsive the interactions are based on van der Waals and Coulombic forces. Compared with DPD, MD is more computational intensive but generally more accurate. However, MD is often limited to small systems due to the computational demand.

An interaction energy for the polymer and drug was calculated based on the difference in the total energy of a system containing the polymer and drug together and the polymer and drug separately. Hydrogen bonds were also calculated between the polymer and drug molecules. Hydrogen bonds showed a negative correlation with interaction energy and experimental drug uptake.

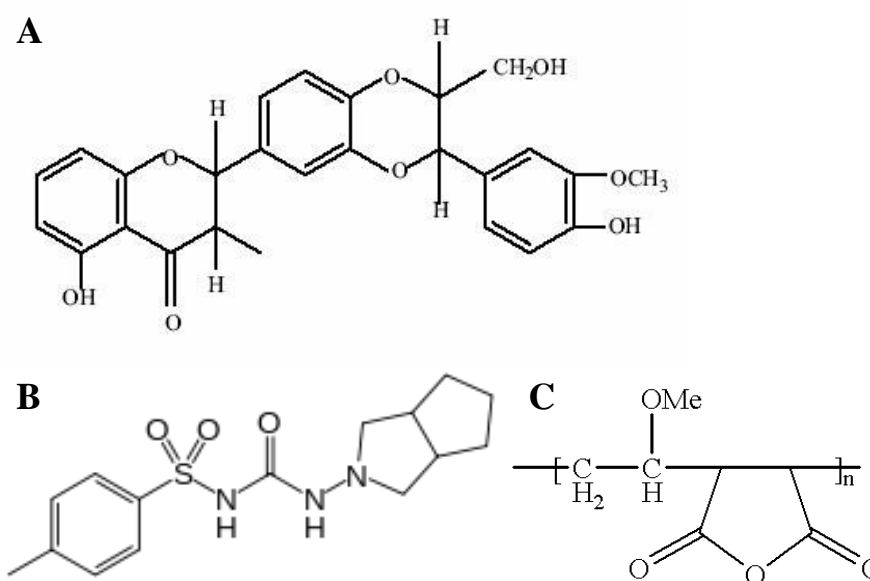


Figure 1.4 The chemical structure of Gantrez AN119 (A), Gliclazide (B) and Silymarin (C).

Gantrez AN119 (Figure 1.4A) formed no hydrogen bonds with gliclazide (Figure 1.4B) and silymarin (Figure 1.4C) yet achieved the highest drug uptake. For doxorubicin Gantrez AN119 had the second lowest amount of hydrogen bonds with the highest uptake indicating that hydrogen bonds do not influence drug uptake by the polymer.

The authors end by correlating drug uptake obtained experimentally with interaction energies from their simulations. A positive trend is observed indicating that interaction energies between a single drug and a single polymer could help predict the compatibility of a drug polymer pairing.

Luo et al. used MD and DPD to simulate drug loading and release of camptothecin (CPT) from a poly(β -amino ester) (PAE) poly(ethyl glycol) (PEG) copolymer²³ (Figure 1.5). PAE is protonated at low pH to trigger disassembly of PAE-PEG nanoparticles.

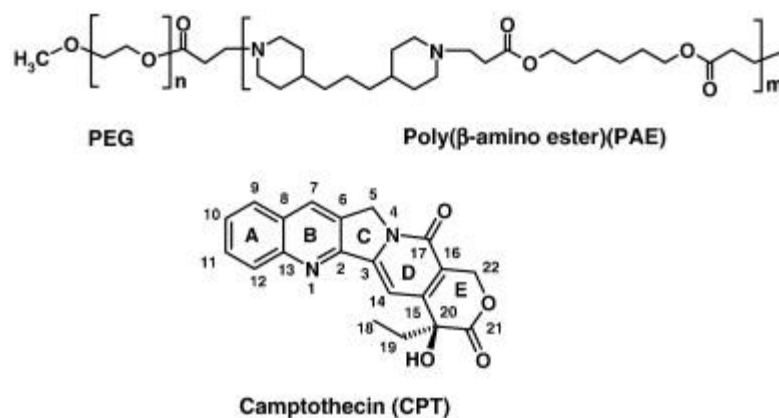


Figure 1.5 Chemical structures of the molecules involved in this study. Taken from Ref²³.

Molecular dynamics simulations were performed on separate binary mixtures of protonated and un-protonated PAE, PEG, CPT and water. Potential energies were generated from the last 1.5ns of a 5ns molecular dynamics simulation. Flory-Huggins parameters were calculated from the potential energies of each binary component mixture. The Flory-Huggins parameter gives an indication of the miscibility of two components and can be used to generate force constants for DPD simulations.

Mixtures of the polymer with CPT at 10 mg/ml and 1 mg/ml respectively were created and simulated in water for up to 1260ns at which

point stable polymeric micelles formed. Initially CPT is adsorbed on to polymer clusters but after 360ns these clusters grow into bigger micelles where CPT is found both in the core and on the surface. Encapsulation efficiencies obtained were different from experiment as there was no change in encapsulation with a change in drug concentration whilst experimentally a decrease was observed. The authors attribute this to the small size of this system which is not sufficiently large to directly compare with experimental results.

At an 8 times higher concentration the polymer forms a vesicle with CPT loaded into the hydrophobic layer (Figure 1.6). An increase in nanoparticle size is also seen experimentally with an increase in CPT concentration. However, the increase observed in the simulation is less pronounced. Again this is attributed to the insufficient box size which is limited due to computational resources.

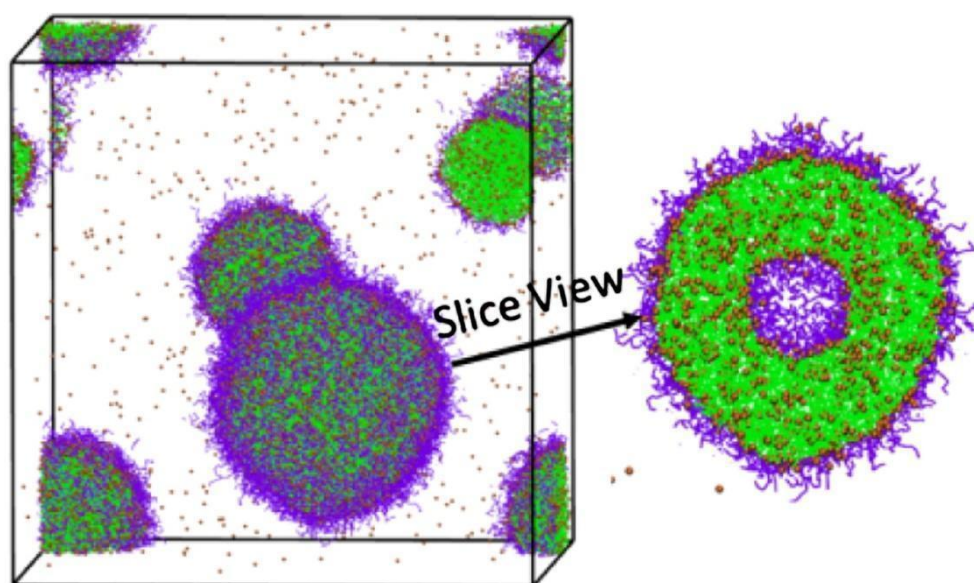


Figure 1.6 Snapshot taken at 900ns into a high concentration simulation of PAE-PEG with CPT. A vesicle forms with a hydrophobic layer of PAE (green) and hydrophilic PEG (purple). Orange spheres are camptothecin. Taken from Ref²³.

To simulate drug release the particle types for PAE were switched to those for its protonated form PAEH. In the simulation the micelles swell in size and the PAEH chains move out into the surrounding water. This causes release of CPT but the dynamics of DPD are accelerated as described previously and the 18ns time frame for CPT release observed is therefore not entirely accurate. However, DPD simulations still provide an insight into how CPT could be released from these particles.

DPD has also been used by Nie et al. to simulate a four-arm star triblock polymer encapsulating doxorubicin²⁴. A star shaped polymer is a dendritic polymer designed to improve the stability of micelles formed. The polymer (poly(ϵ -caprolactone)-b-poly(2-(diethylamino)ethyl methacrylate)-b-poly(poly-(ethylene glycol) methyl ether methacrylate) (4AS-PCL-b-PDEAE-

MA-b-PPEGMA)) is also pH sensitive enabling triggered drug release from micelles through the protonation of a diethyl amino moiety.

The polymer was coarse-grained using around 7-8 non-hydrogen atoms for each CG particle. Doxorubicin (DOX) was modelled as five separate particles of three different types. To simulate a change in pH a protonated version of the diethyl amino particle (DEAH) was also generated. The number of DEAH particles in the polymer correlated with the overall pH of the system. Beads had a volume of 18.2 nm^3 (1.63 nm diameter) and their interaction parameters were based on solubility parameters generated from molecular dynamics simulations.

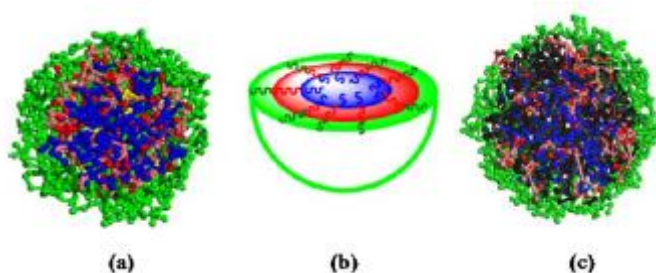


Figure 1.7 Cross-section views of (a) blank micelle, (b) schematic of blank micelle, (c) DOX loaded micelle. PCL (blue), DEA (pink/red), PEG (green). Taken from Ref²⁴.

Simulations in water revealed that the star polymer formed micelles after 20,000 steps of simulation. The micelle had a PCL hydrophobic core with hydrophilic PEG making up the shell and pH sensitive DEA in the core and shell of the micelle (Figure 1.7). When loaded with DOX, the drug is found in the PCL core and also in the “pH sensitive mesosphere”. This is useful as protonation of this region should cause rapid release of drug bound here. Simulations on blank micelles revealed that protonation of DEA causes this block of the polymer to move to the exterior of the micelle and interact with

surrounding water. At early stages of protonation i.e. weakly acidic environments, the movement of DEAH is less pronounced as the exterior PEG shell of the micelle resists. However, the movement of one block of DEAH causes a compound effect on the other protonated blocks causing a complete rearrangement of the micelle.

Whilst DEA protonation causes DOX to be exposed to water, none leave the micelle during the simulation. The authors claim this is due to a weak diffusion effect caused by the “still state” of the aqueous medium. The flow of water molecules found experimentally will promote drug release from protonated micelles. The release of drug from nanoparticles is typically over a much longer time frame than drug loading so this result is expected. Alternative techniques must be used in order to analyse drug release from nanoparticles such as umbrella sampling.

Ahmad et al. used coarse-grain molecular dynamics (CGMD) and DPD simulations for two separate systems²⁵. The encapsulation of prednisolone, paracetamol and isoniazid within poly(lactic acid) (PLA) was performed using DPD. Particle interactions for DPD were based on Flory-Huggins interaction parameters calculated using the additive group contribution technique. For this technique the structure of a molecule is split into simple functional groups and each group is assigned a parameter based on its chemistry. For multiple molecules in a system, this allows the calculation of thermodynamic properties such as solubility. The values obtained through this method were in reasonable agreement with existing literature values.

This study found that an increase in molecular weight of PLA increased the encapsulation of prednisolone; however values were different from

experimental data. With paracetamol, a less hydrophobic drug, data for an increase in drug concentration was in good agreement with experiment. For the hydrophilic drug isoniazid encapsulation was expected to be poor with hydrophobic PLA. However, the simulation reveals zero encapsulation of isoniazid in PLA at low drug concentrations. The authors argue that this may be because coarse-graining multiple molecules into single beads makes it difficult to observe extremely low drug loading.

To simulate isoniazid release from PLA the drugs were forced into the polymer nanoparticles by adjusting their interaction parameters. Upon switching the parameters back, release of the drug from the nanoparticle was rapid ~96ns; however experimentally this release occurs over a much longer time frame. The authors conclude that DPD is insufficient to model encapsulation of water soluble drugs such as isoniazid. Additionally DPD was unable to model the properties of their next polymer quaternary ammonium palmitoyl glycol chitosan (GCPQ) specifically an ionic functional group.

GCPQ was instead modelled using MD with the MARTINI CG force field. The MARTINI force field models four non-hydrogen atoms as a single coarse-grain (CG) bead. The mapping used for DPD is much larger than 4 to 1 so in theory CGMD is more accurate.

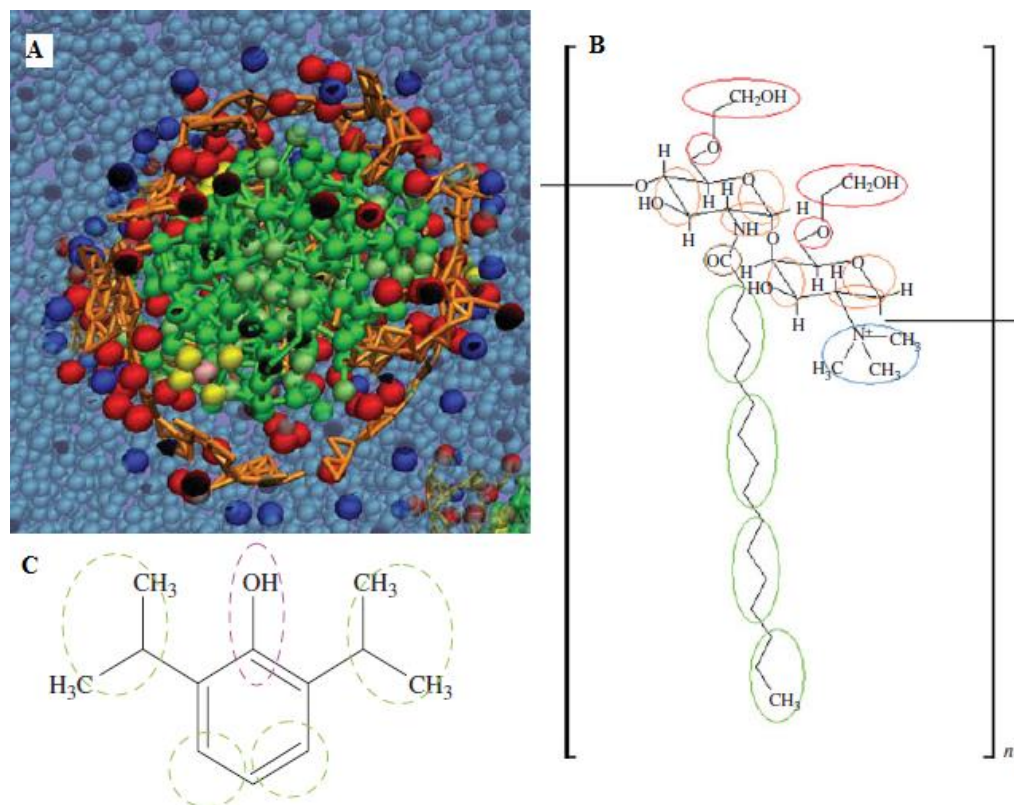


Figure 1.8 (A) Snapshot of propofol (yellow/pink) encapsulated within a GCPQ micelle. Chitosan (orange), glycol (red), quaternary ammonium (blue), palmitoyl (green). Structures of GCPQ (B) and propofol (C) with circles designating the atoms that make up the CG beads used in the model. Taken from Ref²⁵.

Micelles of eight GCPQ chains formed with a hydrophobic core of palmitoyl and ethylene glycol/quaternary ammonium groups at the surface. After the formation of the micelles, propofol molecules were introduced to the simulation to observe their encapsulation by the micelles. Experimentally encapsulation is done via probe sonication in water. Propofol partitions between the hydrophilic surface and hydrophobic core. This presumably due to hydrogen bonding between the hydroxyl group of propofol and the chitosan groups on GCPQ (Figure 1.8). A smaller micelle of GCPQ encapsulated more propofol than a larger one. Both of these findings and the encapsulation efficiency of the micelles was in agreement with experimental data.

This work shows that CGMD using the MARTINI force field is a more accurate technique for simulating polymer-based drug delivery systems than DPD. Whilst DPD showed disparity with experimental data, CGMD was able to confirm several experimental results. This could be due to the method of parameterisation (through the group contribution method) and/or a loss in accuracy due to modelling several molecules as a single bead with DPD.

Woodhead et al. used a different method to simulate drug encapsulation in block copolymers²⁶. Discontinuous molecular dynamics (DMD) involves modelling particle interactions using square-well potentials instead of Lennard-Jones potentials. This removes the need for discrete time steps and saves computational time, allowing the simulation of large systems over long time periods. The copolymer is divided into 12 spheres (4 solvent-phobic and 8 solvent-philic). Drug and solvent molecules were modelled as single spheres. As with previous studies on modelling polymer-drug encapsulation, the solute and polymer volume fraction used was higher than experimental values to save computational time. The authors claim that simulations with smaller volume fractions took too long to equilibrate presumably due to a lack of interactions between the molecules in the system.

An increase in polymer volume fraction was found to increase solute encapsulation efficiency due to an increase in the number of micelles in the system. By increasing the polymer-polymer interactions in the model the encapsulation efficiency decreased and in addition the number of surface bound solute particles increased. This is due to polymer-polymer interactions creating a barrier blocking solute entry into the core of the micelles.

In agreement with a study by Kumar and Prud-homme on the thermodynamics of drug encapsulation into micelles²⁷, the authors found that as drug loading increases, the free energy required to load a drug into the nanoparticle increases. This result explains why it is challenging to attain high levels of encapsulation efficiency into polymer nanoparticles.

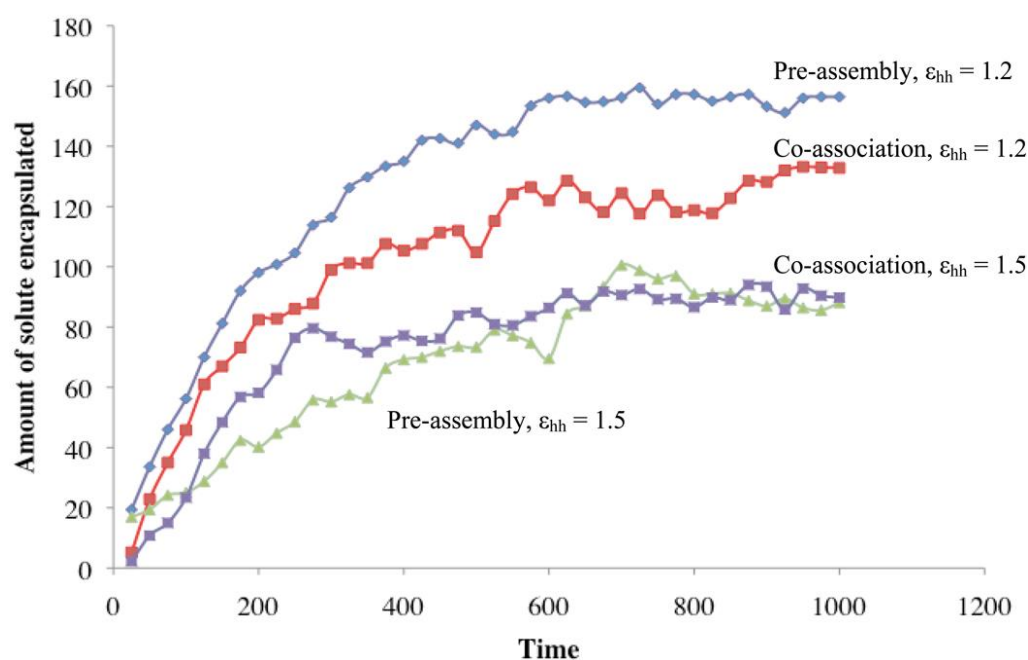


Figure 1.9 Solute encapsulation is measured over time for pre-assembled micelles and micelles that form in co-association with solute. The interaction between polymer solvent-phobic head particles (ϵ_{hh}) was set at 1.2 and 1.5 for comparison purposes. Taken from Ref²⁶.

Interestingly this study also explores differences in loading solute into micelles as they form as opposed to pre-formed micelles. Previous simulations were run on pre-formed micelles, when solute was introduced as the micelles formed there was no difference in the results obtained for encapsulation efficiency with an increase in polymer-polymer interactions. However, when solute encapsulation was measured over time at two different polymer-polymer

interaction values, pre-formed micelles were able to encapsulate more solute than micelles that formed in the presence of the solute (Figure 1.9).

With strong polymer-polymer interactions the barrier for solute entry into the micelles is high so solute encapsulation is low. With weaker polymer-polymer interactions the environment provided by the micelle is favourable for the solute and so encapsulation is high. When the micelles are still forming solute encapsulation is lower because this environment does not yet exist for the solute.

This result is very important when considering other literature in this field that does not consider the formation of polymer nanoparticles when analysing drug encapsulation efficiency^{23,24}. The formation of nanoparticles may play an important role in the encapsulation of a solute for a variety of reasons. By simulating drug encapsulation into pre-formed particles you may miss significant interactions between the solute and polymer.

In conclusion the authors suggest that to increase encapsulation efficiency within polymer nanoparticles a decrease in the polymer hydrophobicity may be required. Nanoparticles formed with drug mainly bound to the surface of the particle have poor release profiles and this may be due to strong hydrophobic interactions between polymer chains.

Loverde et al. explored the effects of nanoparticle shape on delivery using CGMD²⁸. Worm-like nanocarriers have been shown to increase the amount of drug delivered to tumours over spherical micelles. The aim of this study was to simulate the loading of Taxol (paclitaxel) into worm-like and spherical micelles.

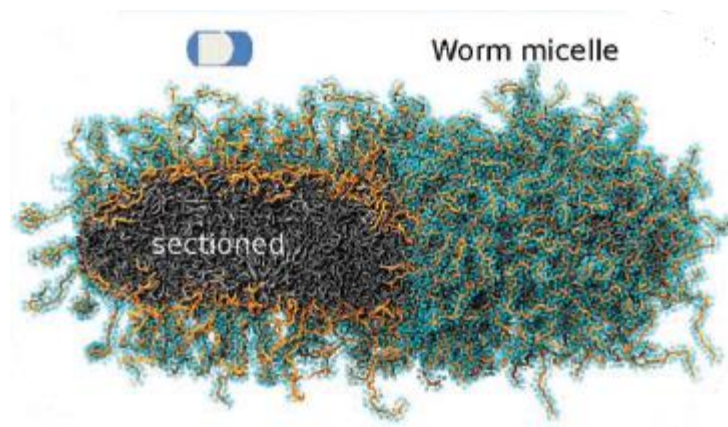


Figure 1.10 Snapshot of a worm-like micelle. Part of the micelle is sectioned to reveal the internal structure. Taken from Ref²⁸.

The CG topologies for the polymer and drug were based on atomistic simulations. Both worm and spherical micelles form in water, with Taxol encapsulated at the interface between the hydrophobic PCL core and hydrophilic PEG shell. The free energy profile for Taxol was calculated from the core of the micelle to the exterior. The free energy calculated was lower for the worm micelle compared with a spherical one. Taxol interacts strongly with the PEG chains of the micelle as a drop in the free energy profile occurs when Taxol enters the shell of the micelle.

The authors were also able to match an experimental phase diagram for the polymer nanostructures with their simulations. The transition from bilayer to worm to sphere is due to a change in the hydrophilic fraction of the copolymer.

Long simulations approaching μs were able to demonstrate that worm micelles, containing Taxol at experimental encapsulation levels, were stable. Whilst Taxol aggregates in water due to its insolubility, in the PCL core of the micelle it is more soluble. However, increases in the loading of Taxol shift the

drug to the interface between the PCL core and PEG shell increasing the burst release of drug from the micelle.

This is in agreement with the previous study as increased loading into these micelles appears to have a detrimental effect. Experimentally the goal is to achieve the highest loading possible, yet the results from modelling and thermodynamic calculations reveal that a) it may not be possible and b) it may not be desirable.

Tanis et al. were able to use fully atomistic MD to simulate ibuprofen interactions with a third-generation poly(amidoamine) dendrimer²⁹. Experimentally the maximum number of drug molecules per dendrimer did not exceed the number of primary amine groups on the dendrimer, 32. Models were created to replicate these experimental conditions including dendrimers with 4 different protonation states to mimic changes in pH.

At basic and neutral pH, density distributions from the centre of mass of the dendrimer show that ibuprofen binds throughout the dendrimer. In acidic conditions there is no stable drug/dendrimer complex formed, consistent with experimental data. When the drug is ionized it is predominately found at the surface of the dendrimer in contact with surrounding counter ions. The simulations also confirmed that the number of primary amines corresponds to the number of ibuprofen molecules bound at pH above the pKa of 4.9.

Analysis of hydrogen bonds via radial distribution function (RDF) revealed that ibuprofen forms H-bonds with the dendrimers amine/amide at basic/neutral pH respectively. This result is consistent with the previous observation that ibuprofen binds throughout the dendrimer at this pH range as amine/amide groups are present at all generation shells in the dendrimer. A

lack of H-bonds between the polymer and ionized ibuprofen suggests that an alternative interaction causes drug encapsulation at higher pH. Hydrophobic interactions were ruled out due the presence of drug at the exterior of the molecule not the hydrophobic interior. It is assumed that electrostatic pairing between the two molecules is a possible reason for drug encapsulation.

1.3.3 Single Drug Interactions

Patel et al. looked at nonpolar and polar interaction between PEO-b-PCL and the hydrophobic chemotherapeutic cucurbitacin³⁰. MD was used to calculate Flory-Huggins interaction parameters for binary mixtures of the drug with different ratio block copolymers. Simulations involved single drug molecules with single polymer chains (3750 Da in size).

With an increase in the PCL/PEO ratio the Flory-Huggins interaction parameter for the drug decreased. This indicates an increase in solubility of the drug with the polymer in agreement with experimental data. The total non-bonded energy for the drug decreases considerably when the PCL/PEO ratio increases indicating increased stability via non-bonded interactions. Additionally the number of hydrogen bonds increases as the PCL/PEO ratio increases. This is due to the majority of hydrogen bonds forming with the PCL block of the polymer.

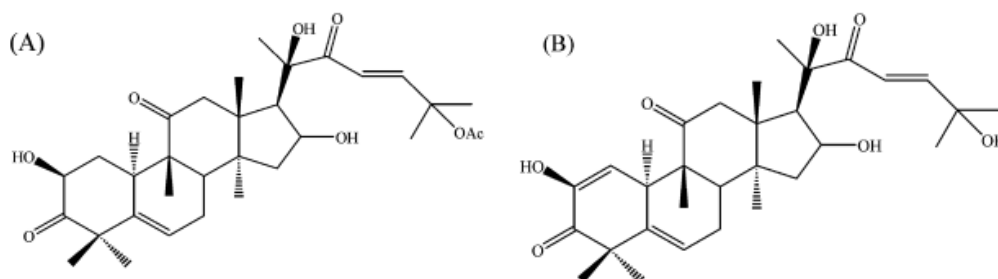


Figure 1.11 Chemical structures of (A) Curcubitacin B and (B) Curcubitacin I.

Experimentally the release rate of cucurbitacin B from PEO-b-PCL is slower than with curcubitacin I (Figure 1.11). H-bond analysis revealed that there is a more substantial increase in H-bonds for CuB with an increase in PCL/PEO ratio than for CuI. This may explain the experimental results.

However, this study is in contrast to the work described previously by Subashini et al. on Gantrez AN119. They found that hydrogen bonds had no role in increasing drug encapsulation with various polymers. On the contrary an increase in hydrogen bonds showed a decrease in encapsulation efficiency for the drugs tested. Both these results indicate that any data on H-bonds must be carefully construed and additional polymer-drug interactions must be considered before using H-bond analysis to interpret experimental data.

Costache et al. used a combination of MD and docking calculations to predict polymer-drug interactions in tyrosine derived triblock copolymer nanospheres³¹. Docking calculations normally used for small molecular interactions in protein binding sites are difficult to use for polymers due to their dynamic nature and lack of obvious binding sites.

The triblock polymer is of the ABA form with A-blocks of PEG at the exterior of the nanospheres and B-blocks of desaminotyrosyl-tyrosine octyl esters (DTO) in the core. Four drugs were analysed: curcumin, paclitaxel, vitamin D3 and camptothecin (CPT). CPT in particular showed poor loading with the nanospheres which the authors were interested in exploring computationally.

Polymers used were half the length of those used experimentally due to computational limitations. Nanospheres of four polymer chains were formed in water in the absence of drug molecules. Nanospheres formed were an order of

magnitude smaller than those formed experimentally. Chains of the polymer were placed close to each other and left to aggregate.

Only the hydrophobic DTO core of the nanospheres was used for docking to save computational time. It was assumed (and confirmed by simulation) that the hydrophobic B-blocks were mainly involved in drug interactions. Blind docking was applied to the entire core of the nanospheres as no specific binding site was known.

The most hydrophobic drug vitamin D3 showed the highest binding affinity. Overall the binding affinities generated for the three drug molecules were in agreement with an experimental trend in drug loading. Interestingly, the AlogP values for paclitaxel and curcumin were similar (3.2 and 3.6 respectively) but their binding affinities and drug loading differed. This suggests that for this drug polymer pairing, drug hydrophobicity is not indicative of its potential drug loading.

The increased binding affinity for curcumin over paclitaxel was explained through analysis of the lowest energy docking conformations. Curcumin's structure allows for ideal alignment with the DTO blocks in the polymer whilst paclitaxel formed less π - π stacking interactions and hydrogen bonds. Despite having no π - π interactions and a single hydrogen bond, vitamin D3 showed the highest binding affinity possibly due to its high flexibility allowing it to form multiple hydrophobic interactions with the polymer. Paclitaxel is far less flexible and this may also contribute to its low binding affinity (Figure 1.12).

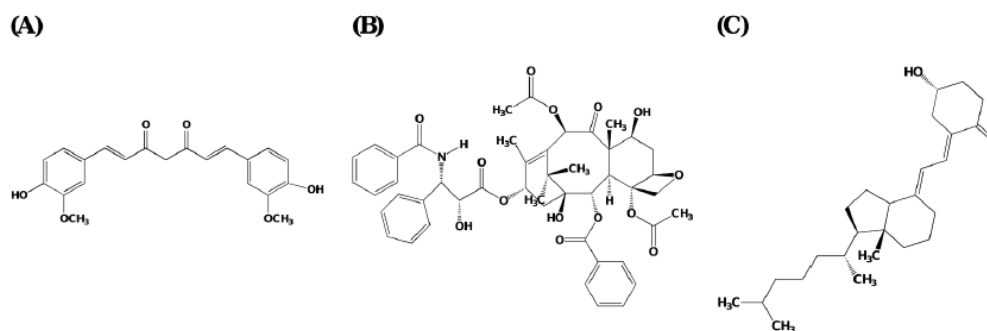


Figure 1.12 Chemical structures of curcumin (A), paclitaxel (B) and Vitamin D3 (C).

These results may help explain the previous dilemma with a correlation between hydrogen bonds and encapsulation efficiency. Whilst hydrogen bonds may not be necessary for encapsulation, the flexibility of a drug molecule appears to be an important factor.

Camptothecin (CPT), another rigid mildly hydrophobic drug, showed poor encapsulation experimentally yet the docking calculations showed high binding affinity. This result is explained in terms of how their methodology works. CPT preferred a particular “hot spot” on the DTO polymer and in this position affinity was high. The authors speculate that once this hot spot is occupied then the binding affinity for CPT would decrease drastically.

For this study docking studies were in good agreement with an experimental trend for three of the four drugs tested. The results for CPT revealed that simple binding affinities are not always indicative of experimental encapsulation efficiencies. To improve this docking technique a scoring function could improve its ability to screen multiple drug molecules. Refinement of the technique with a larger data set is suggested.

Maiti et al. also used docking in a study using a pH sensitive poly(amidoamine) (PAMAM) dendrimer³². The docking and release of four

drug molecules; salicylic acid (Sal), L-alanine (Ala), primidone (Prim) and phenylbutazone (Pbz) was investigated. Drugs were first blind docked into the centre of the dendrimers. The drug molecules were then pulled away from the centre of mass of the dendrimer using steered molecular dynamics. Steered MD involves applying a force to the drug molecule pulling it away from the polymer over a specified vector. Umbrella sampling is performed at several windows along this vector for each drug. The weighted histogram analysis method¹⁹ (WHAM) was used to calculate a potential of mean force (PMF) from the umbrella sampling simulations.

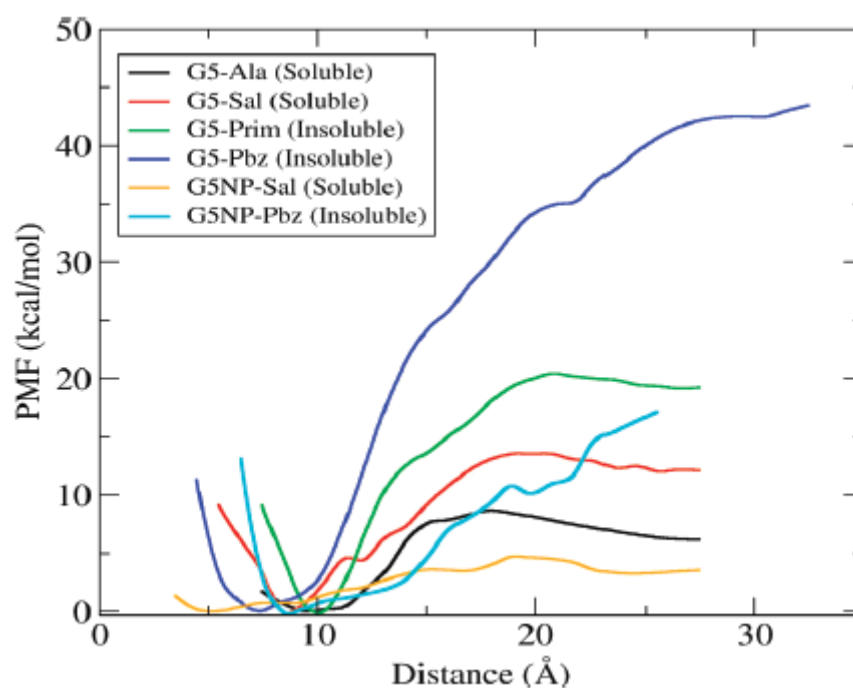


Figure 1.13 PMFs calculated over a distance from the dendrimer centre of mass. PAMAM dendrimer (G5), G5NP (PAMAM non-protonated). Taken from Ref³².

For the protonated dendrimers (G5), soluble Sal and Ala showed the lowest free energy barrier when compared with insoluble Pbz and Prim (Figure 1.13). Ala shows the lowest barrier indicating it will be released from the dendrimer with the most ease. Experimental data suggests that electrostatic

interactions drive encapsulation of drugs within the dendrimer core. For the hydrophobic drugs Pbz and Prim, Pbz has a negative charge forming electrostatic interactions with the dendrimer core. This results in Pbz having a significantly higher energy barrier than Prim although both are relatively hydrophobic.

The low free energy barrier for Ala and Sal not only suggests that drug is released easily from the dendrimer but also that drug loading would be relatively common in solution. However, experimentally there is low encapsulation efficiency with these drug molecules. This is due to a lack of nonpolar groups in their structures making fewer hydrophobic van der Waals interactions with the polymer. Stronger nonpolar interactions for Prim and Pbz increase their energy barrier and encapsulation within the dendrimer.

Hydrogen bonds between the drug and polymer were also calculated. There was no correlation between number of hydrogen bonds and an increase in the free energy barrier for release. Ala forms the most hydrogen bonds but has the lowest free energy barrier.

Non-protonated forms of the pH sensitive dendrimer were also tested (G5NP). A substantial decrease in the free energy barrier for both Sal and Pbz is seen when the dendrimer is non-protonated. This result suggests that release of Pbz can occur easily upon deprotonation of the dendrimer due to the decrease in the free energy barrier for release.

As this case is also true for salicylic acid the authors speculate that drug loading into dendrimers will be difficult at low pH values when the polymer is protonated. Protonation of the dendrimer decreases its electrostatic interactions with the ligands resulting in a decrease in the free energy barrier. Therefore the

authors suggest that encapsulation in PAMAM dendrimers should be carried out at high pH values. When the drug complex enters the blood stream the reduction in pH will cause strong binding between the polymer and drug causing controlled release of the drug.

This study reveals that both docking and umbrella sampling are valid methods to analyse polymer drug interactions. Drug release rates are often non-trivial to calculate through conventional molecular dynamics simulations due to the lengthy time scales required. Umbrella sampling allows fast and accurate analysis of free energy barriers which give an indication of drug release rates.

Samanta et al. analysed the interactions of a single curcumin molecule with a PEO-PPO-PEO block copolymer³³. The topology of curcumin was parameterised in water, methanol and 1-octanol. Curcumin was simulated in the presence of monomers of PEO and PPO (DME and DMP respectively). The drug formed stronger interactions with the more hydrophobic DMP monomer over DME. In the presence of a single polymer chain, again curcumin interacted favourably with the hydrophobic PPO section of the polymer.

Fluorescence emission spectra on PEO-PPO-PEO micelles indicated that curcumin is encapsulated within the hydrophobic core. In a simulation of a single curcumin molecule with eight polymer chains, curcumin is encapsulated within an aggregate of only four polymer chains. The spatial distribution of PEO and PPO around curcumin is shown in Figure 1.14. Hydrophobic PPO makes more contact with the drug molecule than hydrophilic PEO. Whilst these interactions are not in a micelle, the authors hypothesise that this drug-polymer aggregate could be the first step towards forming a larger micelle.

Whilst this work offers an insight into how these molecules interact, the simulation is far from experimental concentrations. Without including all the reagents at relevant concentrations that are present when preparing these delivery systems experimentally the results of these simulations may not be particularly relevant. However, computational resources are a big limitation to larger scale simulation as such fully atomistic simulations may not be ideal.

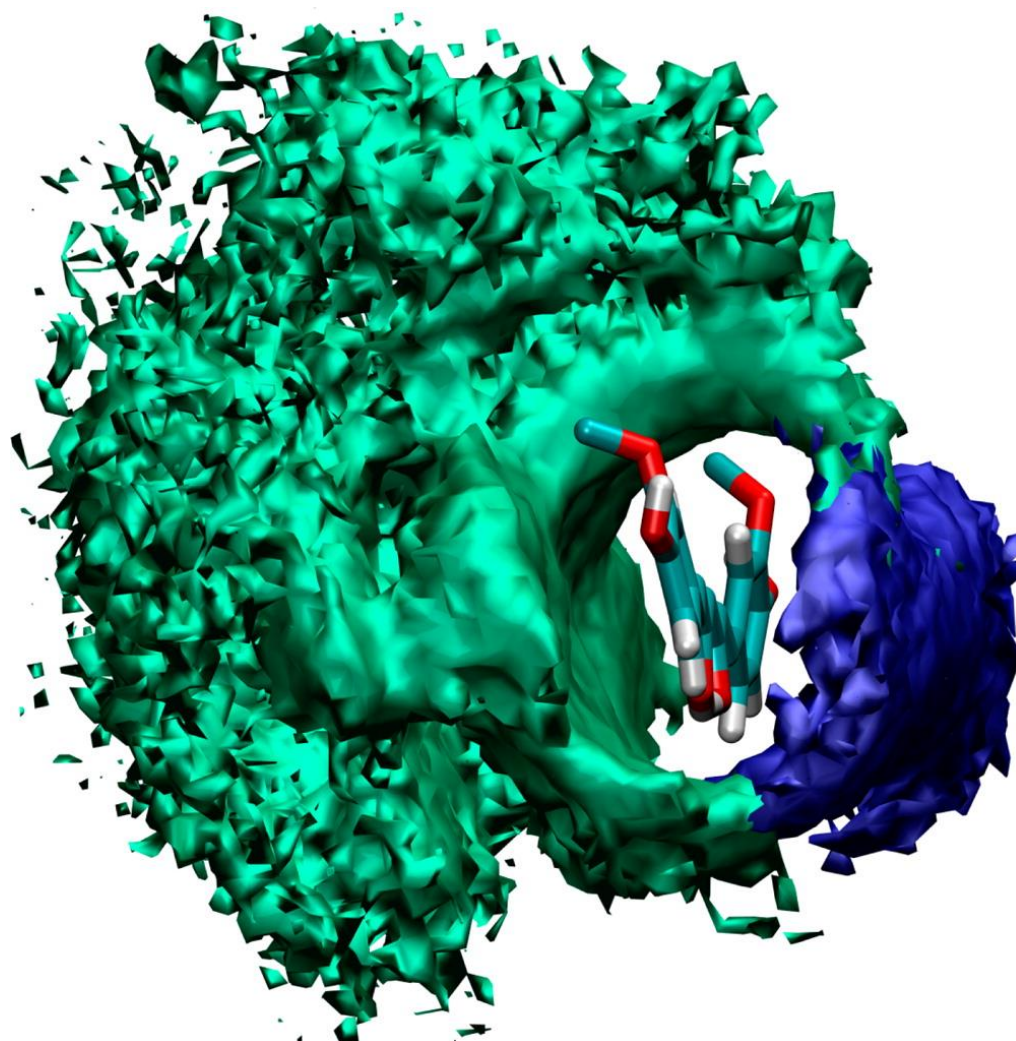


Figure 1.14 The spatial distribution of PEO (blue) and PPO (green) around curcumin is calculated. Taken from Ref³³.

1.4 Multiscale Modelling

When modelling polymer-based drug delivery systems the use of a mesoscale model is commonplace in addition to using concentrations that are greater than those used experimentally. To model even a single nanoparticle several simplifications must be made.

Rossi et al. described an atomic simulation of polymeric material alone requiring “simulations of tens or hundreds of microseconds and a length scale of tens of nanometers”³⁴. These simulations are only feasible on the most powerful supercomputers in the world. As such it is necessary to simplify a model whilst minimising the loss in accuracy of polymer-drug interactions.

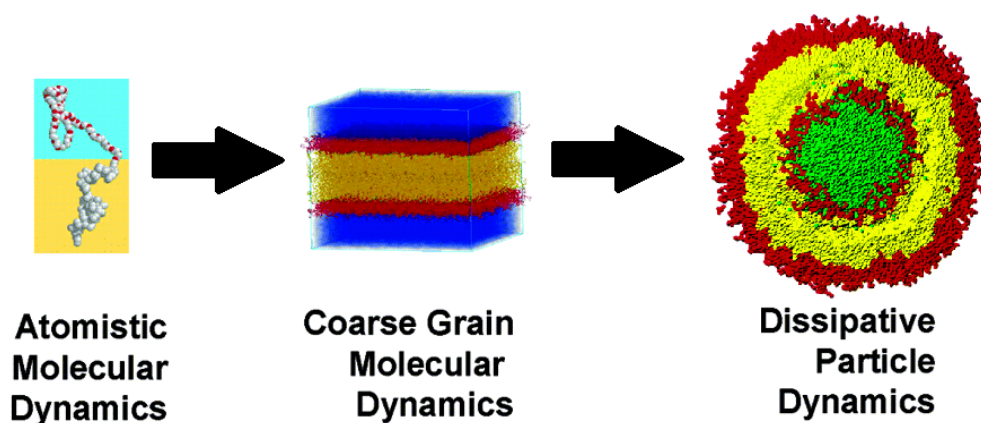


Figure 1.15 A summary of mesoscale simulations; atomistic being the most accurate and DPD the most simplistic yet fastest. Taken from Ref³⁵.

Mesoscale methods (Figure 1.15) allow the simulation of large systems of multiple polymer chains. This is useful as they come closer to simulating realistic events. However, coarse-grain (CG) models lack atomistic detail; as such they a) limit our ability to draw on our understanding of the basic chemistry of intermolecular interactions to explain and predict behaviour and b) limit the metrics that can be extracted from such simulations for comparison with experimental observables, such as spectroscopic properties.

Ideally a computational model will use an accurate all-atom (AA) force field for key interactions and sacrifice accuracy by using a CG force field for less important interactions in the simulation. For nanoparticle simulations this allows the simulation of larger systems with detailed interactions between the polymer and drug molecules.

One example of a multiscale model is the adaptive resolution scheme named AdResS from Kurt Kremer's group³⁶. This permits the use of two force fields by having a transition region whereby molecules passing through this region are converted from atomistic to coarse-grain molecules and vice versa. For example atomistic water can reside in the middle of a simulation box and water interacts using an atomistic force field. However, when a molecule drifts away from the centre of the box it passes through the transition region where its CG representation is gradually enabled and its AA representation is disabled. This allows it to interact with CG water already present in the periphery of the box (Figure 1.16).

Overall this allows the use of a CG model for the less significant parts of the system whilst retaining high accuracy atomistic interactions at the centre. This multiscale approach is not unlike the quantum mechanics/molecular mechanics (QM/MM) multiscale models originally developed by Warshel and Levitt in 1976³⁷ for which they won the Nobel Prize in 2013 with Martin Karplus¹⁷.

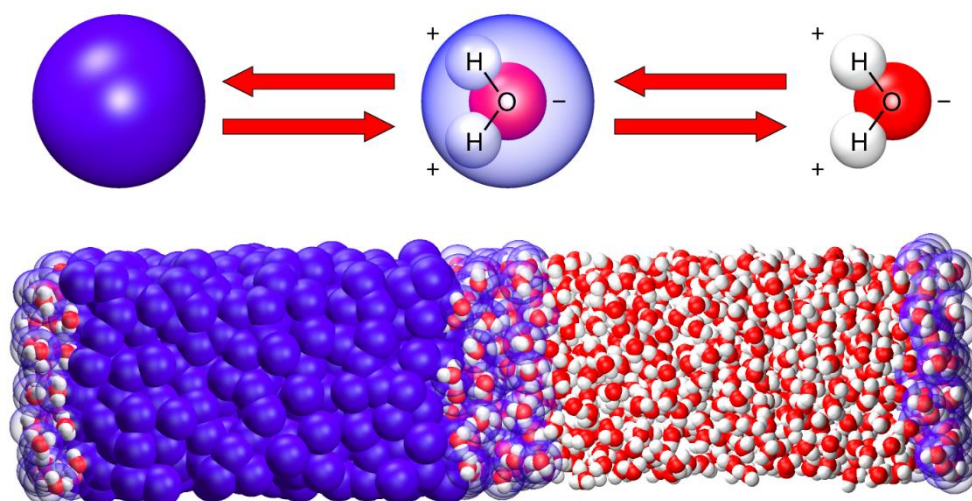


Figure 1.16 A diagram showing how AdResS (adaptive resolution scheme) works. Water is shown in its CG and AA representations at the top. In the middle and at the ends are transition regions where the CG and AA representations interchange. Taken from Ref³⁶.

The downside is that these schemes are tricky to implement and for water a 1:1 mapping is required for the AA to CG transition. As such the speed up obtained is not as significant as if a 4:1 water mapping was used such as in the MARTINI CG force field. However, a 4:1 mapping is not possible using AdResS as it would require constraining four water molecules to a single CG bead.

Another multiscale model was developed in 2011 by Rzepiela et al.³⁸ Their technique involved combining CG and AA force fields in the same simulation without using an adaptive scheme. Using GROMACS, CG virtual sites on atomistic molecules enable CG interactions with CG particles using a CG force field. AA molecules are still free to interact with each other using the GROMOS96 AA force field.

They assessed multiple CG force fields, some of which were based upon atomistic simulations using force matching and iterative Boltzmann

inversion. These techniques allow the conversion of atomistic dynamics into potentials for CG interactions. Overall the study found the MARTINI CG force field to be the superior force field for their system of liquid butane (Figure 1.17).

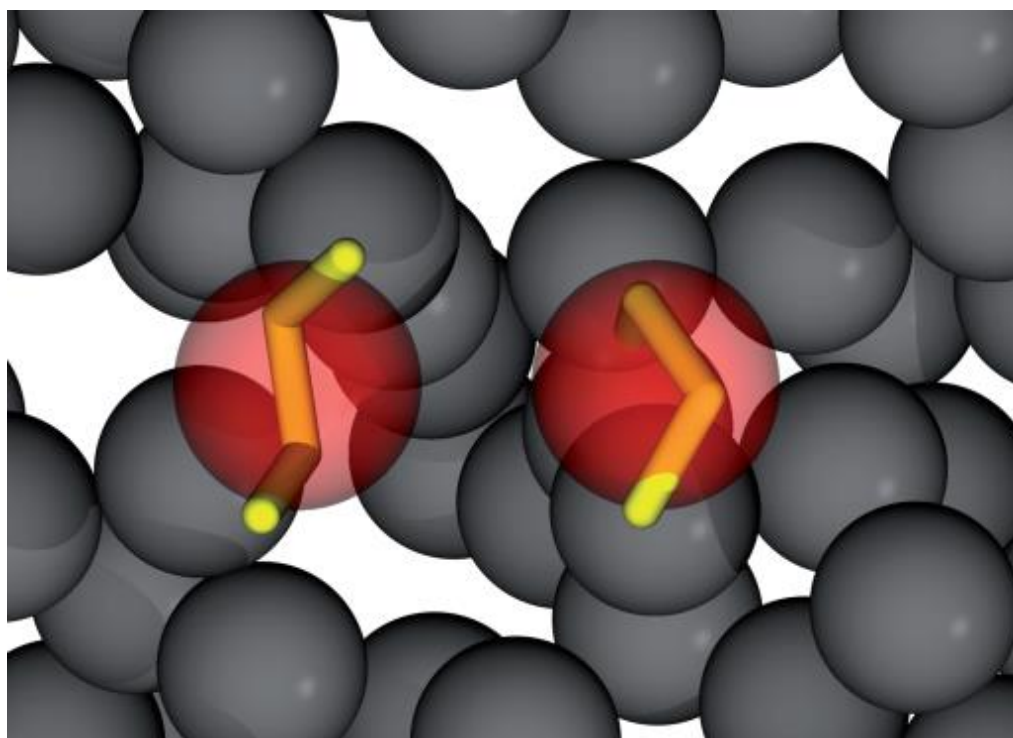


Figure 1.17 Atomistic butane (yellow) has CG virtual sites (red) to allow it to interact with the surrounding CG butane molecules (grey). Taken from Ref³⁸.

More recently this multiscale force field was used to simulate more complex molecules. Wassenaar et al. described the simulation of ubiquitin and a transmembrane α -helix using a mixture of the GROMOS and MARTINI force fields³⁹. They compared their multiscale simulations to atomistic simulations and found that the multiscale force field was acceptable for apolar side chains, more so than polar ones. This is due to a difficulty in simulating electrostatic interactions using a mixture of these two force fields. The CG force field lacks detailed polar interactions and as such was unable to

reproduce a potential of mean force similar to the one observed using that atomistic force field with single point charge water. They discuss how the relative dielectric permittivity in GROMACS must be adjusted to maintain the correct strength of electrostatic interactions for the molecules in the simulation.

For a polymer system these polar interactions found with protein side chains are often not present. Overall most polymer chains are often neutral making them more appropriate candidates for use with this multiscale force field.

1.5 Poly(glycerol adipate)

The theoretical work that will be explored in this thesis is based upon experimental work performed over the past ten years on poly(glycerol adipate) (PGA) and its derivatives. The data from this work has influenced the design of the computational models outlined in this thesis. Therefore it is prudent that this work is discussed in detail before the theoretical work is discussed.

In 2005 Kallinteri et al. published a method to synthesise poly(glycerol adipate) (PGA), a hydrolysable polyester containing pendant hydroxyl groups for functionalisation¹². The aim was to design a polymer that was non-toxic, did not require surfactants for nanoparticle formation and showed high drug incorporation levels. This polymer is also readily functionalised allowing a plethora of derivatives to be created with a variety of physicochemical properties and thus the potential to improve encapsulation efficiency and drug loading. These possibilities were investigated with the drug dexamethasone phosphate (DXMP). DXMP was chosen due to its multiple side effects that could be alleviated via targeted delivery in a nanoparticle. Additionally the

steroid ring on DXMP is lipophilic and could show strong interactions with a hydrophobic polymer.

Nanoprecipitation was used to prepare nanoparticles of size 150-250nm in the absence of surfactant. When prepared in the presence of DXMP the particle size increased up to 300nm. The zeta potential of the particles also increased indicating that the surface of the particles was more charged with drug bound.

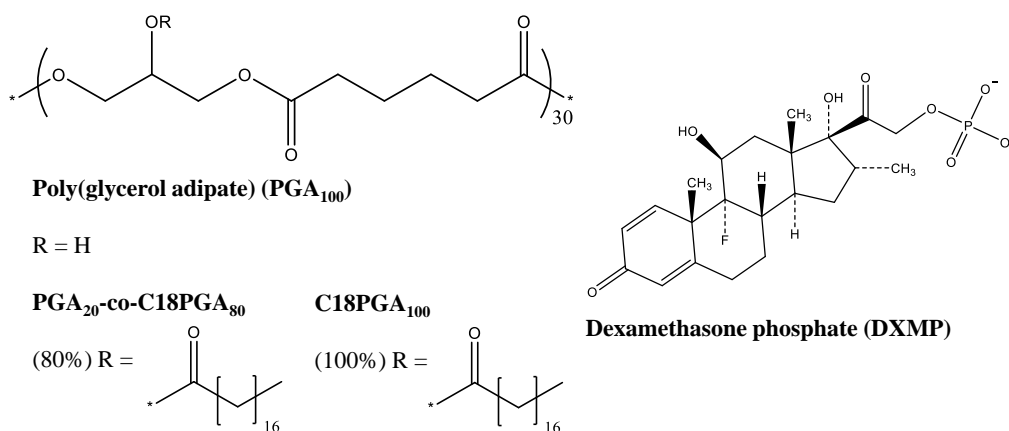


Figure 1.18 Chemical structures of PGA and two functionalised PGA polymers. The structure of the chemotherapeutic DXMP is also shown.

PGA was made in three sizes 2, 6 and 12 kDa and functionalised 40, 80 and 100% with a C8 or C18 acyl chain on the pendant hydroxyl group. A 6 kDa polymer corresponds to a degree of polymerisation of 30 for PGA (Figure 1.18). For both C8PGA and C18PGA an increase in molecular weight showed an increase in encapsulation efficiency. For C8-PGA as acylation was increased the encapsulation efficiency of DXMP also increased, with a large increase from 80 to 100% acylation. However, for C18-PGA, encapsulation efficiency increased until 80% acylation for 6 and 12 kDa polymers. At 100% acylation for C18-PGA a sharp decrease in encapsulation efficiency was seen (Figure 1.19). The authors suggested that this decrease was due to a lack of

aqueous space for the drug within the nanoparticles or decreased interactions with DXMP due to a lack of free hydroxyl groups on the 100% acylated polymer.

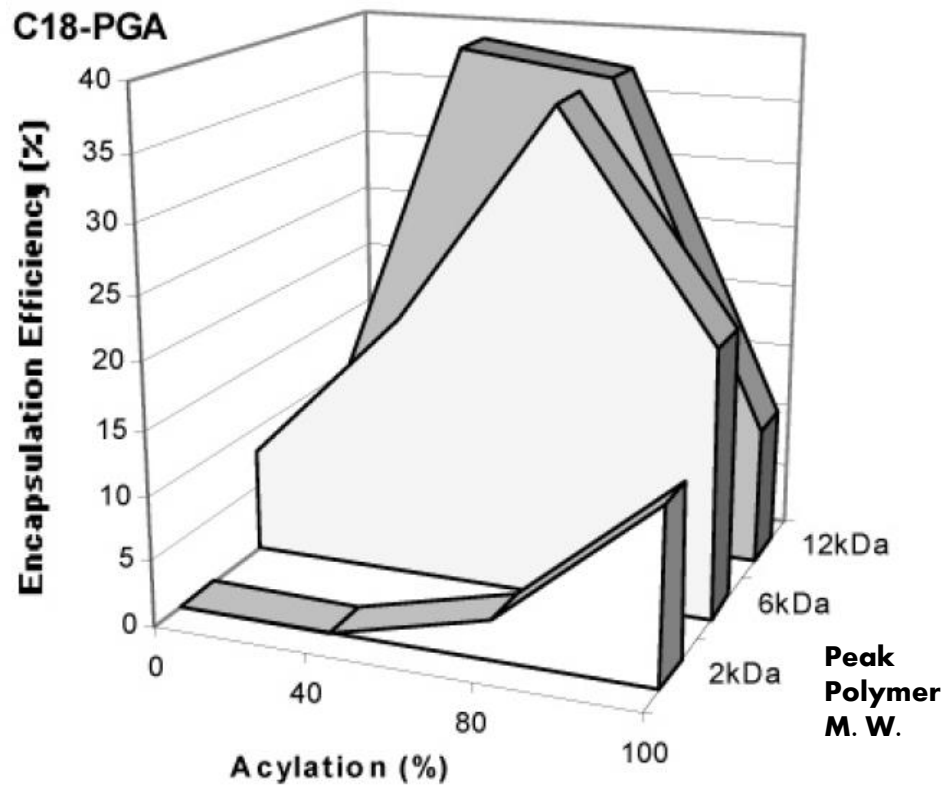


Figure 1.19 Effect of % acylation and PGA backbone molecular weight on DXMP encapsulation efficiency for a C18 acyl chain. Taken from Ref¹².

Whilst an increase in acylation increased the encapsulation efficiency of PGA it can impair its ability to form nanoparticles. For $\text{PGA}_{20}\text{-co-C8PGA}_{80}$ (2, 6 and 12 kDa) and C18PGA_{100} (2 kDa) polymers could not form particles and $\text{PGA}_{20}\text{-co-C18PGA}_{80}$ (12 kDa) was also unable to form particles instead forming an aggregate on the walls of the stirred vessel. The authors speculate that this is due to a lack of hydroxyl groups reducing the stabilization of the particles promoting aggregation. However, some of these polymers could form particles in the presence of DXMP. C18PGA_{100} was able to form particles with DXMP at all three molecular weights. This may be due to the high lipophilicity

of these polymers promoting particle formation with DXMP stabilising the structure.

They conclude that with PGA₂₀-co-C8PGA₈₀ (6kDa) they were able to achieve a high encapsulation efficiency compared with other polyesters in the literature.

Puri et al. published further work on PGA nanoparticles with DXMP and another water soluble chemotherapeutic, cytarabine (CYT)¹¹. Similar polymers were used to make particles as in the previous paper. A decrease in particle size was seen upon loading of either CYT or DXMP into PGA or C8PGA nanoparticles. It is hypothesised that this may be due to a change in the aggregation number of polymer molecules or an increased density due to the presence of drug in the particles.

Particles made with CYT were generally larger in diameter than those with DXMP which again could be attributed to stronger interactions with DXMP increasing the density of the particles. An increase of 6 mV in the zeta potential was observed only for DXMP not CYT presumably due to the negative charge on the phosphate group of DXMP.

The length of the acyl chain on PGA was varied to see its effect on drug incorporation. From C2 to C6 there was insufficient polymer hydrophobicity whilst C8 was sufficient. At C10 uncontrolled aggregation of the polymer occurred resulting in C8PGA being used for this study. Aggregation was also seen by Kallinteri et al. for some highly acylated polymers.

For C8PGA the drug loading and encapsulation efficiency was greater for DXMP than for CYT at all acylation percentages. However, with PGA backbone there was no difference between the two polymers. The authors

surmise that the increased hydrophobicity of C8PGA over PGA alone increases the drug loading with DXMP due to its lipophilic steroid ring. Highly polar CYT is unable to make strong interactions with the acyl chains on C8PGA as such shows low encapsulation efficiency. In agreement with the previous paper, an increase was seen in both loading and encapsulation efficiency for a 12 kDa polymer backbone over 2 and 6 kDa polymers.

Analysis of drug release revealed that for DXMP an increase in acylation decreased the release rate. For C8PGA₁₀₀ drug was steadily released over 15 days up to a cumulative release of ~70%. PGA backbone showed a burst release of the drug with ~40% release at a rate indicating that it was essentially unbound to the particles. (Figure 1.20).

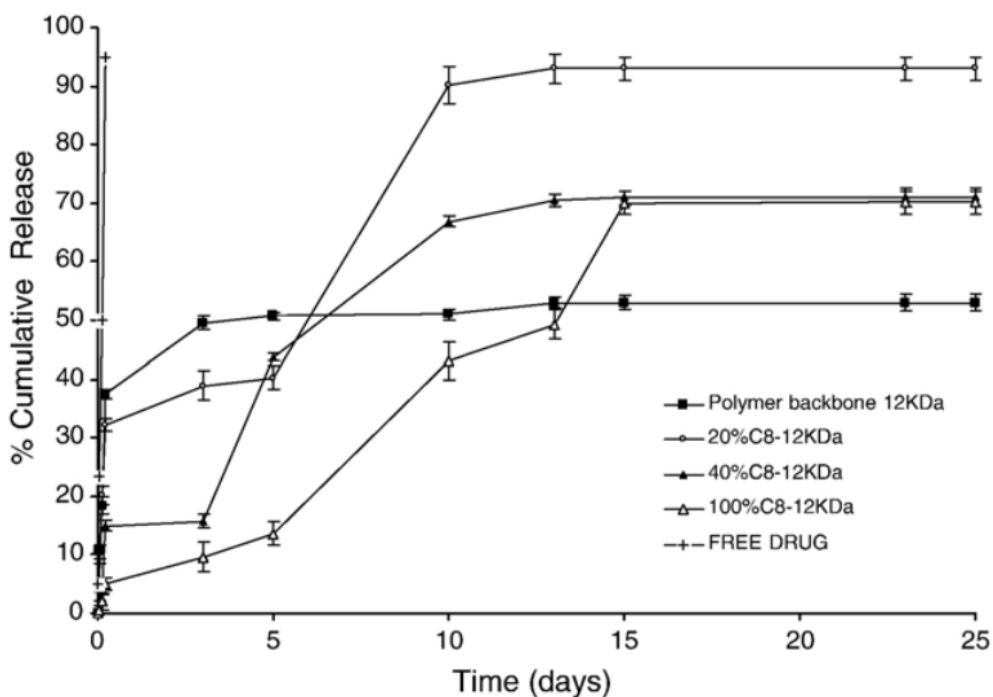


Figure 1.20 DXMP release from PGA polymers at various acylation % at 37°C in water over 25 days. Taken from Ref¹¹.

For CYT 100% acylation showed burst release comparable to free drug. PGA backbone and low acylation PGA showed a more controlled release of

CYTA over the 25 days tested. However, around 50% of the release occurred over the first few days for these polymers. The difference in loading and release for these two drugs is interesting given their water solubility at 300 mg/ml for CYT and 500 mg/ml for DXMP.

It is surmised that high drug loading can be indicative of a fast drug release rate due to drug predominately being bound at the surface of the particles. This is not the case for PGA with DXMP as high acylation % not only yielded high drug loading and encapsulation efficiency but also the superlative drug release profile. However, this result is likely unique to this drug-polymer combination.

Orafai et al. took a different approach to analysing the encapsulation efficiency of PGA using contact angles²⁹ (Figure 1.21). A polymer film is created on the surface of a microscope slide and liquids are dropped on to the surface. The contact angle the liquid makes with the surface enables surface free energies to be calculated. Contact angles have the advantage of being able to test several polymers in quick succession.

Surface free energy is the sum of several parameters including London dispersion forces and Keesom polar forces. Identical surface free energies may differ in their parameters. For this study diiodomethane and water were employed for their differences in polarity and potentially the parameters that make up their surface free energies.

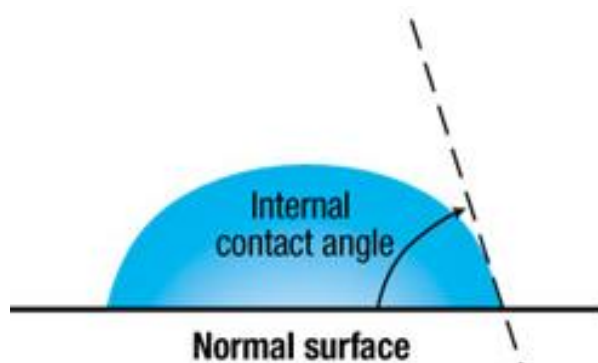


Figure 1.21 A contact angle can be measure for a drop of solvent on a surface coated with polymer. Taken from Ref⁴⁰.

For the polar solvent water, the contact angle increased with increasing acylation up to 40% presumably due to the increase in hydrophobicity. 100% acylation showed a decrease in contact angle from $\sim 70^\circ$ to $\sim 56^\circ$. For Diiodomethane contact angles were more varied but 40% acylation showed the largest contact angle. The total surface free energies calculated were lowest for $\text{PGA}_{60}\text{-co-C8PGA}_{40}$ leading them to conclude that it is the best candidate for nanoparticle formulations. $\text{PGA}_{60}\text{-co-C8PGA}_{40}$ also showed the lowest dispersion force around half of that calculated for the other polymers. Whilst its Keesom polar forces are comparable to C8PGA_{100} the low dispersion forces give $\text{PGA}_{60}\text{-co-C8PGA}_{40}$ the lowest total surface free energy.

Orafai's results are in agreement with previous work on PGA. Whilst an increase in acylation does increase the affinity of PGA for other molecules, full acylation of the polymer can have a detrimental effect on its interaction with other molecules. We will explore how acylation of PGA affects drug interactions using molecular dynamics later on in this thesis.

Tawfeek et al. synthesised PGA pentadecalactone (PGA-co-PDL) microparticles through spraydrying⁴¹. PGA-co-PDL is a block copolymer and differs from the structure of the PGA derivatives described previously as PDL

is added as a separate block not onto the pendant hydroxyl groups of PGA. However, the addition of PDL to PGA increases the polymers hydrophobicity in a similar way to the addition of acyl chains to PGA. Additionally arginine and leucine were incorporated into the microparticles to increase drug loading and encapsulation efficiency with the hydrophilic drug sodium fluorescein.

PGA-co-PDL with 1.5% arginine showed the highest encapsulation efficiency and loading. Although loading and encapsulation for all polymers tested was low presumably due to the hydrophilic nature of sodium fluorescein not being compatible with the hydrophobic polymer. However, PGA-co-PDL 1.5% Leu was chosen for release studies due to its optimal aerosolisation performance. When compared with PGA-co-PDL alone, the presence of leucine reduced the cumulative release of sodium fluorescein over time. When compared with PLGA, PGA-co-PDL showed a more controlled release of the drug over the first 10 hours tested.

It is unfortunate that this study did not consider variable sizes of the PDL block in the copolymer. However, they did reveal that the addition of the amino acid leucine or arginine increased the polymers affinity for a hydrophilic drug. There is potential to incorporate amino acids into PGA nanoparticles to also increase their encapsulation efficiency and drug loading for hydrophilic drugs such as cytarabine.

1.6 Thesis Aims

The main aim of this work is to recreate nanoprecipitation in a computer. A computational model has several advantages; a) changes to the polymer can be made with great precision, b) one gains atomistic detail of how

all of the molecules behave during nanoparticle formation, c) detailed metrics can be used to analyse these interactions in more detail.

As a test case the chemotherapeutic dexamethasone phosphate (DXMP) and polymers based on poly(glycerol adipate) (PGA) are used as there is a large amount of experimental data on these molecules^{11,12}. This experimental data will be used to check the accuracy of the simulations and will serve as a reference that the simulations will attempt to replicate. By keeping concentrations and simulation components as similar as possible to experimental conditions we hope to mimic the experimental data.

This thesis will be a story of the design and creation of a multiscale model to simulate polymer nanoprecipitation. Different models are described and the decision to use a multiscale model using CG virtual sites is explained.

To confirm the accuracy of the multiscale model, resolution transformation is used to generate atomistic reference simulations for comparison. Additionally a fully atomistic model of nanoprecipitation is analysed and this is used to further optimise the multiscale force field.

Once optimised, the multiscale nanoprecipitation simulations are analysed in detail to get a better understanding of the experimental results. These insights will aid in not only the design of future polymer-based drug delivery systems, but how functionalization of PGA affects its interaction with DXMP in general.

Chapter 2

Methodology

Whilst the results of this thesis are purely theoretical, polymer synthesis and nanoparticle preparation was also performed. The design and synthesis of PGA and its functionalised derivatives has relevance for understanding the overall approach to this work. PGA is a highly tuneable polymer, but we will only explore one type of functionalisation. Nevertheless, the modelling approach is in theory applicable to any type of polymer-based drug delivery system.

2.1 Experimental Work

2.1.1 Polymer Synthesis

Poly(glycerol adipate) (PGA) was prepared in batches as per Kallinteri et al.¹² The method is based on the enzyme-catalysed poly-condensation reaction between glycerol and divinyl adipate (Figure 2.22). A dry 250mL round bottomed flask was charged with divinyl adipate (9.91g, 0.05mol), glycerol (4.6g, 0.05mol) and 15 mL THF. The reactants were stirred for 30 minutes to equilibrate at 50°C. Novozyme 435 (1g) was then added to the

mixture and then stirred for 24 hours at 200rpm with a mechanical stirrer. An open top condenser was fitted to enable release of acetaldehyde during the reaction.

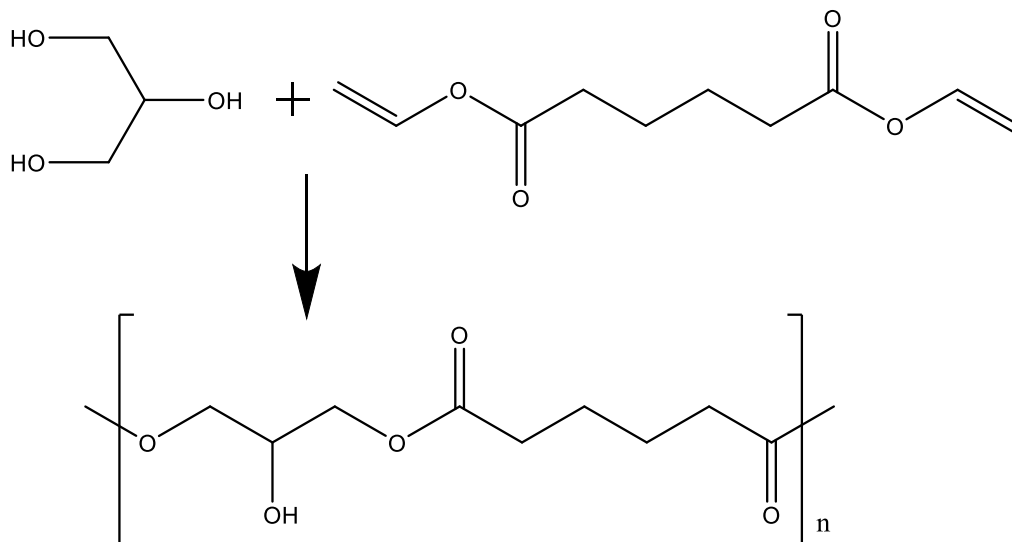


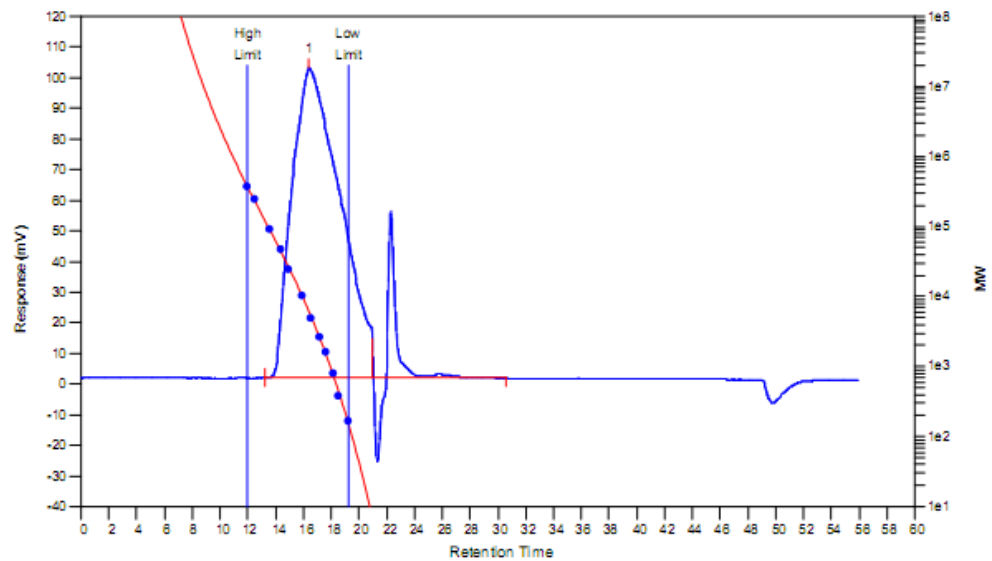
Figure 2.22 Synthesis of PGA by poly-condensation reaction of glycerol and divinyl adipate.

The product was filtered to remove the enzyme (which was fixed to a resin) and washed with more THF. A rotary evaporator (80 °C) and subsequently a vacuum oven (100 °C) were used to remove any excess solvent.

The polymer was analysed by GPC and it revealed a highly poly-disperse polymer (PD = 26.15). Whilst this value was large for this batch, subsequent batches made of PGA in the laboratory were closer to a PD of 4-6. The peak Mw measured by GPC was nearly 9kDa and this is roughly equivalent to a 45 unit polymer (or 45mer). This value varies between batches with the largest in length being 50-60mers.

PGA can be functionalised with various pendant groups. One example is the addition of a stearate chain via an acid chloride reaction (Figure 2.24).

Functionalisation occurs randomly throughout the polymer to form a random copolymer.



MW Averages

| Peak No | Mp | Mn | Mw | Mz | Mz+1 | Mv | PD |
|---------|------|-----|------|-------|-------|------|---------|
| 1 | 6246 | 339 | 8864 | 22608 | 33040 | 7148 | 26.1475 |

Figure 2.23 GPC plot showing a highly poly disperse polymer with a Mw of nearly 9kDa. This polymer was used for the nanoprecipitation experiments.

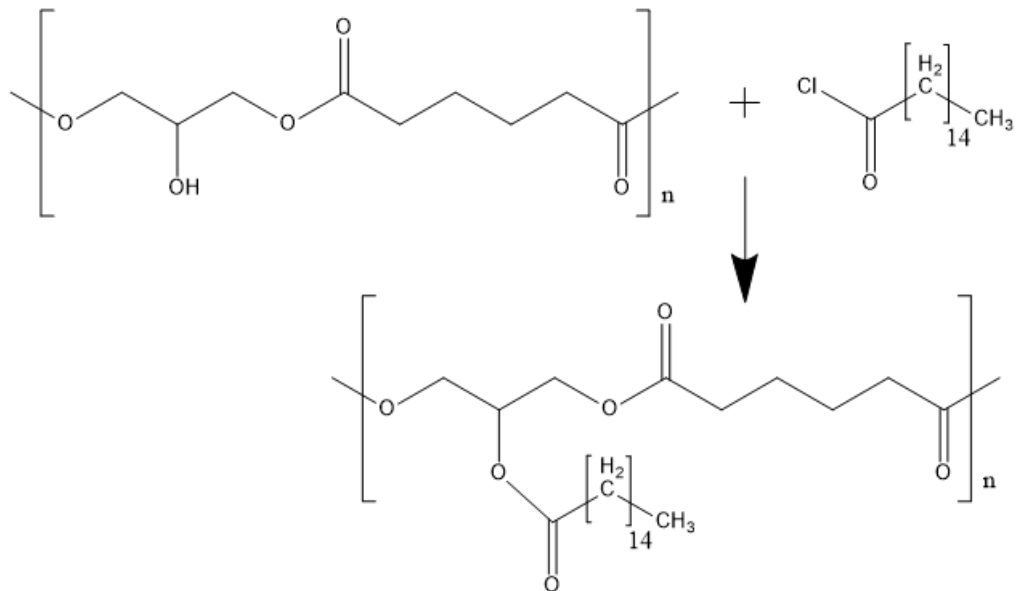


Figure 2.24 Functionalisation of PGA with a stearate chain via an acid chloride reaction.

Polymeric nanoparticles were prepared from the dry polymer using nanoprecipitation (interfacial deposition)¹. Polymer dissolved in acetone (10mg/mL) was added drop-wise to 7mL of water under constant stirring to obtain nanoparticles. To encapsulate DXMP in the nanoparticles, drug was dissolved in the water at 5mg/mL.

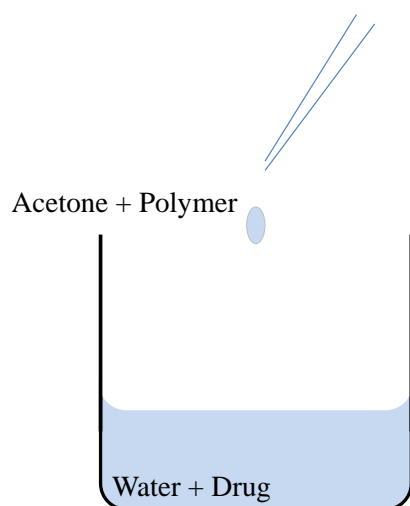


Figure 2.25 In nanoprecipitation polymer dissolved in acetone is added drop-wise to water containing hydrophilic drug molecules.

2.1.2 Polymer Designations

The unmodified polymer is designated simply as PGA_{100} . Acylation of the pendant hydroxyl group with stearyl moieties is designated by C18PGA with a subscript to denote the percentage of monomers modified. For example $\text{PGA}_{20}\text{-b-C18PGA}_{80}$ is PGA with 80% of the monomers modified with the C18 acyl chain.

2.2 Theoretical Work

2.2.1 Molecular Dynamics

Molecular dynamics (MD) is a technique used to simulate molecules and their interactions. A computer is used to solve Newton's equations of motion for a system of interacting atoms. Forces on a single atom are computed from the negative derivative of the interaction potential with every neighbouring atom (Equation 2.1). This process is iterative and forces are computed in time steps usually around 1-2 femtoseconds.

$$\mathbf{F} = -\nabla V(\mathbf{r}) \quad (2.1)$$

A leap-frog algorithm is used to accelerate the atoms by integrating equations of motion depending on the positions of the atoms at time t and velocities at time $t - \frac{1}{2}\Delta t$. This algorithm is time reversible meaning you can reverse the direction of the integration to arrive at the starting position of the atoms.

$$\mathbf{v}\left(t + \frac{1}{2}\Delta t\right) = \mathbf{v}\left(t - \frac{1}{2}\Delta t\right) + \frac{\Delta t}{m}\mathbf{F}(t) \quad (2.2)$$

$$\mathbf{r}(t + \Delta t) = \mathbf{r}(t) + \Delta t\mathbf{v}\left(t + \frac{1}{2}\Delta t\right) \quad (2.3)$$

At user-chosen time intervals, the position and velocity of the atoms are written to a trajectory file which can be read by the user to observe the dynamics of the molecules over the simulation. If the potential energy surface is accurate then this enables a detailed observation of how molecules interact.

The time taken to compute the forces at each time step is dependent on the size of the simulation. Larger simulations require more powerful computers and so currently molecular dynamics is limited based on the computational power available.

Whilst MD has been very fruitful in scientific research, it has several caveats. It is classical and as such cannot compute events such as reactions between molecules that require quantum mechanics. The potential energy surface of an atom is based on the force field chosen for the simulation. There are several force fields available and each of these are optimised for different molecules. A force field may require further optimisation depending on the molecules in the system.

To avoid computing long-range forces in a simulation, interactions are truncated at a specified distance called the cut-off. This reduces the amount of forces calculated speeding up the simulation. Van der Waals forces at long range are often very small so can be safely ignored. To prevent complete truncation of the forces at the cut-off a shift function can be used to generate continuous forces. This removes noise generated as the potential is shifted to 0 as it approaches the cut-off.

Whilst a cut-off can be used for coulomb interactions (Equation 2.4) it is not ideal as long-range electrostatics are required to prevent accumulation of charges at the cut-off boundary. The solution is to use Ewald summation to split Coulomb interactions into short-range and long-range contributions. Short-range contributions are calculated in real-space using standard cut-offs and a screening function to decay the charges to 0 at the cut-off. Long-range contributions are calculated in reciprocal space using Fourier transform to subtract the added screening functions. This allows two finite sums to calculate a potentially infinite sum.

$$V_c(r_{ij}) = \frac{1}{4\pi\epsilon_0} \left(\frac{q_i q_j}{\epsilon_r r_{ij}} \right) \quad (2.4)$$

A neighbour list is used to avoid calculating distances between all pairs of particles at every time step. This list denotes all the nearest neighbouring particles and only these particles are considered for the van der Waals and Coulomb interactions. The neighbour list is updated during the simulation just not at every time step.

Simulations are typically run within a box of specified size. To minimise edge effects in such a system periodic boundary conditions are used. The box is replicated in all dimensions such that there are effectively no boundaries to the system. Atoms that pass through a boundary are translocated to the opposing boundary. This gives the system bulk like properties as molecules are not confined to a specific space. The non-bonded cut-off of the simulation must be less than or equal to half the length of the simulation box to prevent molecules from interacting with multiple copies of other molecules.

Temperature and pressure during the system are maintained through a thermostat and barostat respectively. The thermostat is able couple the kinetics of the system to an external heat bath at a given temperature. Variations in temperature are slowly adjusted by rescaling the velocities of the particles. The barostat behaves in a similar way using a “pressure bath”. The coordinates and box size are adjusted at certain steps in the simulation to match the bath.

2.2.2 Interaction Potential

In all-atom (AA) molecular dynamics atoms are represented as single spherical particles with a van der Waals potential surrounding them. The 6-12 Lennard Jones potential models atoms as hard spheres (Figure 2.26). The

potential models the repulsive Pauli exclusion principle at short distances between atoms and attractive van der Waals forces at larger distances.

The shape of the potential can be changed by varying the epsilon (ϵ) and sigma (σ) values in Equation 2.5. These values are set based on the force field used and the atom types assigned to the molecules in a given system. When optimising a force field for a specific molecule the Lennard Jones potential can be altered to make atoms more attractive and repulsive based on the epsilon and sigma values used.

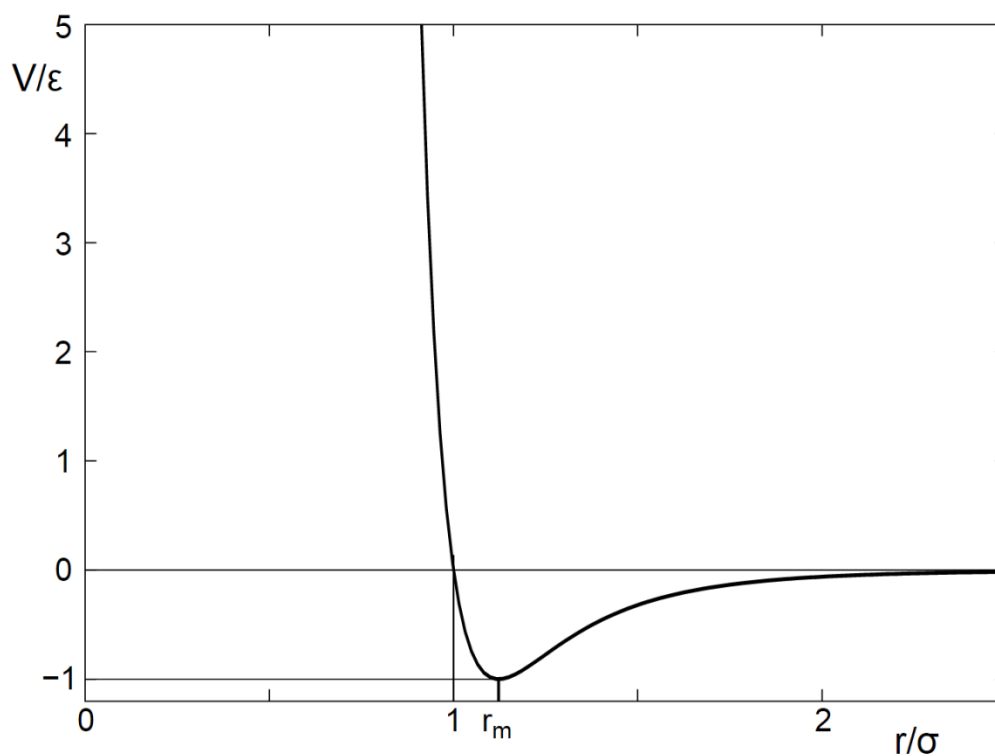


Figure 2.26 A plot of a 6-12 Lennard Jones potential.

$$V(r) = 4\epsilon \left[\left(\frac{\sigma}{r} \right)^{12} - \left(\frac{\sigma}{r} \right)^6 \right] \quad (2.5)$$

The partial charges on the atoms of a molecule are calculated through quantum mechanical (QM) methods. The distribution of charge is determined through QM calculations as a cloud around the molecule and partial charges

are assigned to the atoms based on their positions. In theory charge in a molecule would be dependent on the environment and conformation of the molecule but in molecular dynamics charges are fixed. Whilst it is possible to update the charges on a molecule during a simulation this is very computationally expensive and would significantly slow the simulation.

Bonds between the atoms are represented as harmonic oscillators. The minimum of the harmonic potential is assigned by the user based on the length of the bond (Figure 2.27). Angles, proper and improper dihedrals also use harmonic oscillators.

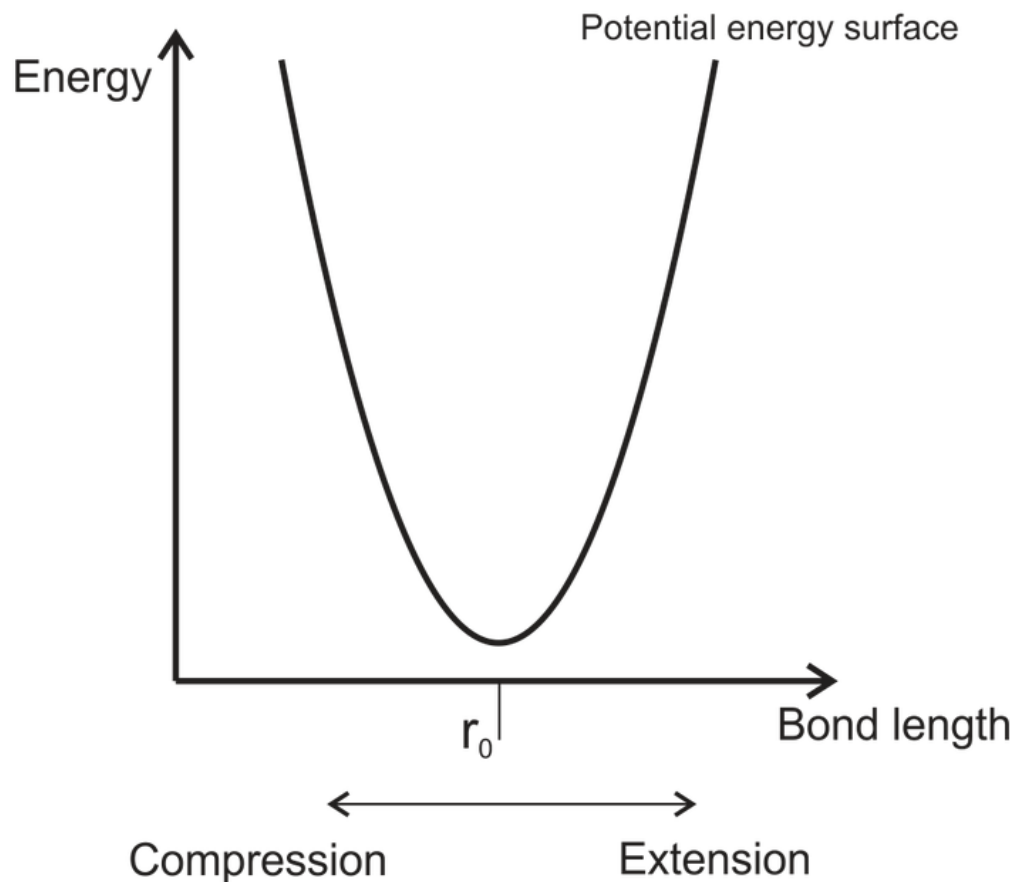


Figure 2.27 A graph of a harmonic oscillator used for bond lengths in molecular dynamics. The given bond length (r_0) is maintained due to the increase in potential energy upon bond compression or extension.

To avoid doubling of bonded and non-bonded forces for nearby atoms, a neighbour exclusion cut-off is set to three. This ensures that a given atom will not have non-bonded interactions with the nearest three atoms it is connected to through bonds.

2.2.3 Coarse-Grain Molecular Dynamics

Coarse-graining is a technique used to reduce the degrees of freedom in a simulation. By reducing the amount of forces computed at each time step the time taken for the simulation is reduced. To achieve this groups of atoms in a molecule are represented as single beads. This requires a specialised CG force field such as the MARTINI force field. The MARTINI force field was optimised using experimental water-octanol partition coefficients⁴².

A CG force field aims to reproduce the properties of a reference system. The MARTINI force field aims to conserve free energy but other techniques such as iterative Boltzmann inversion can reproduce the radial distribution of molecules in a system.

However it is difficult to match multiple aspects of a reference system, as such CG MD is often different to AA MD as the molecules are inherently different. Each CG molecule must be carefully parameterised for a given system.

2.2.4 Nanoprecipitation Model

Our aim was to model the time evolution of a system that began as a spherical drop of an acetone solution containing PGA polymer within a large box of water containing dexamethasone phosphate (DXMP). We calculated

that a suitable fully atomistic model, that contained all the relevant species at the experimental concentrations, would consist of a 12nm diameter droplet, containing ~16,000 molecules of acetone and two molecules of a PGA₁₀₀ 30mer (or one molecule of PGA₂₀-b-C18PGA₈₀ 30mer), at the centre of a 60 nm sided box of ~7 million molecules of water and ~1000 molecules of DXMP. In total this would be ~21 million atoms. This system is large for our computational resources and yet is at a concentration that contains just a single PGA₂₀-b-C18PGA₈₀ polymer. To include more polymer molecules we would need more solvent and a larger box of water to surround it.

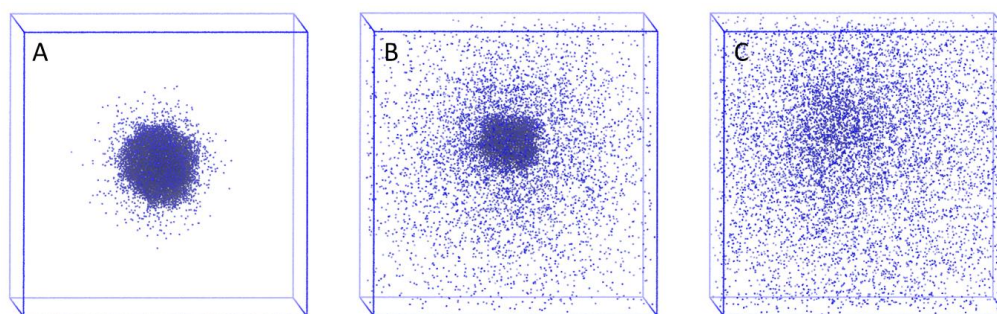


Figure 2.28 (A-C) The dispersion of acetone in a periodic box of water.

To address these issues we took advantage of the facility in the MD code GROMACS⁴³ to use multiscale, dual-resolution, modelling methods. Water and acetone were modelled purely coarse-grained, using the Martini model and parameters (Figure 2.28). PGA and DXMP were modelled at both atomistic and coarse-grained levels, using the virtual sites approach (explained later in the Methods). Thus in our simulations all solute-solute interactions were treated fully atomistically, but solute-solvent and solvent-solvent interactions were treated in a coarse grained way. We also decreased the amount of acetone present in the system whilst increasing the polymer concentration. This allows us to observe how multiple polymer chains interact

together to form a nanoparticle on a reasonable time scale (around 5 days using 192 MPI processes). The concentration of the drug in water is comparable to experiment at 3.22mg/ml. Overall, we were able to reduce the number of particles in the simulation system to ~1 million for two PGA₂₀-b-C18PGA₈₀, C18PGA₁₀₀ chains or three PGA₁₀₀ chains with 500 molecules of DXMP.

2.3 Simulation Setup

2.3.1 Molecular Dynamics

To run a simulation a coordinate file and topology file is required for each type of molecule in the system. The coordinate file describes the position of every atom within the molecule in 3D space. The topology file contains the atom types of every atom in the molecule, their charges and their bonded interactions. Atom types define the Lennard-Jones potential for the VDW forces in the simulation and are specific to the force field used.

For the polymer structures, first monomers of PGA and C18PGA were created in Avogadro⁴⁴. These files were converted into PREP files and combined into coordinate files for polymer chains containing 30 monomers using Ambergtools tleap⁴⁵. The topology files were created by submitting the PGA and C18PGA monomers to the Automated Topology Builder server (ATB)⁴⁶. The ATB uses quantum mechanics (QM) calculations to calculate the partial charges, atom types and bonded interactions for the molecule submitted. PM3 optimisation is used initially followed by B3LYP/6-31G* in implicit water. This generates partial charges for the atoms in the molecule. Bonded interactions are assigned based on atom types generated and the optimised bond lengths and angles from the QM calculation. The topology files for each

monomer were combined to form a whole topology for the 30mer polymer. PGA contained 30 PGA monomers, $\text{PGA}_{20}\text{-b-C18PGA}_{80}$ contained 4 PGA monomers with 26 C18-PGA monomers evenly distributed throughout the polymer and C18PGA_{100} contained 30 C18-PGA monomers. These atomistic models were compatible with the GROMOS 53a6 force field.

Dexamethasone phosphate's coordinate file was created in Avogadro. The resulting PDB was submitted to the ATB to generate its topology file compatible with GROMOS 53a6.

For atomistic solvent, a single point charge (spc) water model was used and a model for acetone was taken from the ATB which was also compatible with the GROMOS 53a6 force field. This acetone model was later adjusted based on the WS model⁴⁷ of acetone.

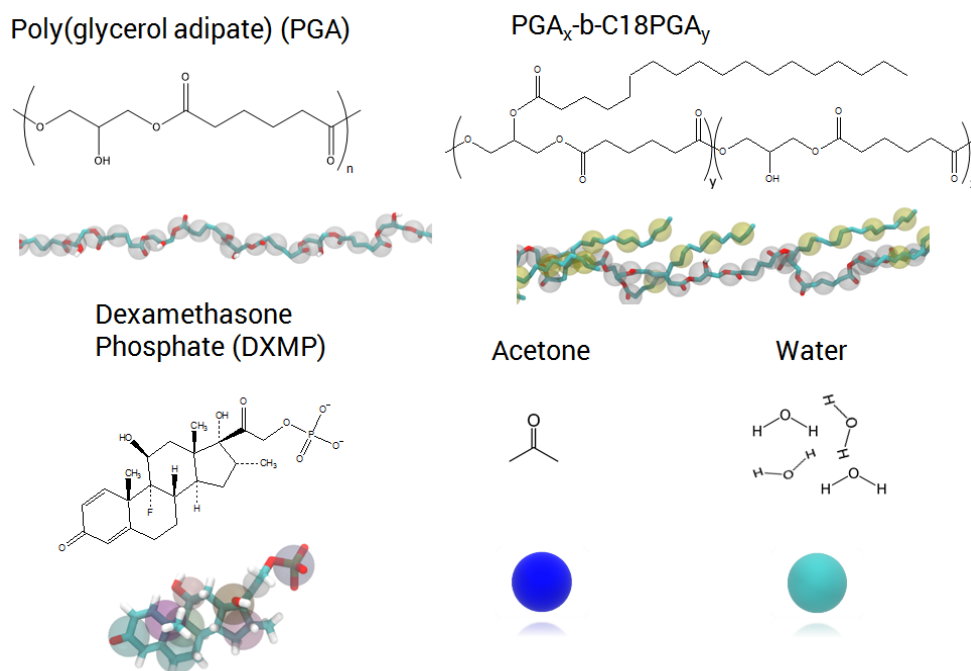


Figure 2.29 Molecules used in this work including their chemical structures and their in silico representations.

For the coarse-grained solvent two equilibrated boxes of water and acetone at 300 Kelvin and 1 bar pressure were used. As per the standard MARTINI approach, four water molecules were represented by a single water bead and a single acetone molecule was represented by a single acetone bead.

2.3.2 Multiscale Force Field

A multiscale representation containing both atomistic and coarse-grained structures was used for the polymer and drug molecules. The coarse-grain virtual sites on the atomistic molecules were created using VOTCA⁴⁸. A mapping file in .xml format was written which specifies the positions for the CG virtual sites at the centre of mass of the atoms they represent. Virtual sites are integrated into the topology file by specifying the atoms the CG virtual sites correspond to. During the simulation, forces on the CG virtual sites are imparted onto their corresponding atoms. As such the coarse-grain solvent can interact with the atomistic solute molecules.

For the force field file: atomistic non-bonded parameters and pair types from the GROMOS 53a6 force field were combined with CG non-bonded Lennard Jones potentials from the MARTINI force field v2.2. CG beads lack partial charges and therefore, unless fully charged, they interact solely through van der Waals forces. This allows one to adjust the Lennard Jones potential for these forces to optimise the multiscale force field. Whilst the atomistic parameters were untouched, the CG parameters were adjusted during the optimisation process by validation against a fully atomistic model.

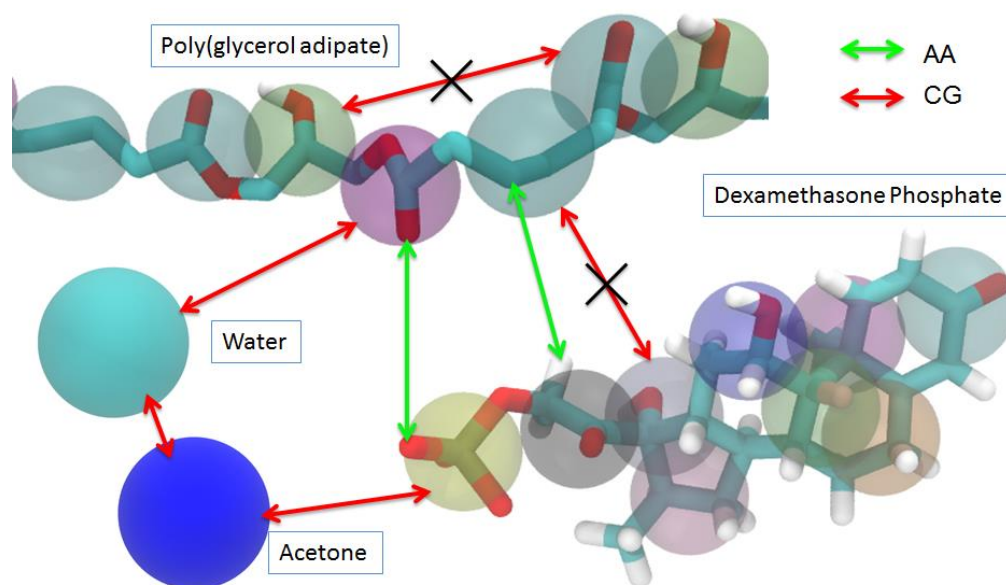


Figure 2.30 Interactions involved in the multiscale force field. AA interactions are labelled in green whilst CG interactions are in red. Note there are no CG interactions between the CG virtual sites on the AA molecules to prevent doubling with AA interactions already present.

2.3.3 Simulation Setup

First the acetone drop was created using the GROMACS *genbox* insert command to place polymer molecules (3 for PGA, 2 for PGA₂₀-b-C18PGA₈₀ and C18PGA₁₀₀) randomly within a 9nm sided periodic box. This box was solvated using *genbox* with a pre-equilibrated box of CG acetone. *genbox solvate* command fills the box with molecules and removes any that clash with the molecules already present in the box.

This acetone/polymer box was placed at the centre of a 50nm sided periodic box and 500 DXMP molecules were added randomly throughout using *genbox*. After solvation with CG water, 1000 sodium counter ions were introduced with *genion* by replacing random CG water beads in the box to keep the volume consistent.

Energy minimisation was performed for 10,000 steps using the steepest descents method. NVT equilibration was performed for 500ps with the v-rescale thermostat to achieve 310K temperature. Subsequent NPT equilibration for 2ns with the Berendsen barostat brought the system to 1 bar pressure.

Production MD was run in triplicate using a leap-frog integrator for 80ns with coordinates saved for the trajectory file every 100ps. Simulations used periodic boundary conditions with coulomb and VDW interactions shifted between 0 and the 1.2nm cut-off. Bonds were constrained using the LINCS algorithm to allow for a 2fs time step.

For fully atomistic simulations the same method was used but with atomistic solvent. Additionally the Particle Mesh Ewald method was used for coulomb interactions to preserve long range electrostatic interactions between partial charges in the atomistic molecules.

2.4 Analysis

2.4.1 Resolution Transformation

As part of the simulation validation procedure we wanted to sample the 80ns nanoprecipitation at three time points where we could convert the multiscale model to a fully atomistic model for a comparison between the two forcefields. At 30, 50 and 80ns, 11nm sided subsections of the 50nm sided box multiscale systems were converted back to fully atomistic representations. We used the “backward” python script⁴⁹ to reintroduce atomistic detail to our coarse-grain solvent. First atomistic molecules (one for acetone and four for water) are swapped for the coarse-grain beads. Steepest descent energy minimisation was run for 150 steps without non-bonded interactions followed

by another 150 steps with non-bonded interactions turned on. Next MD simulations were run at increasing time steps from 0.2fs to 2fs. The resulting atomistic coordinate file was combined with the polymer, drug molecules (without their coarse-grain virtual sites) and ions to create a fully atomistic subsystem.

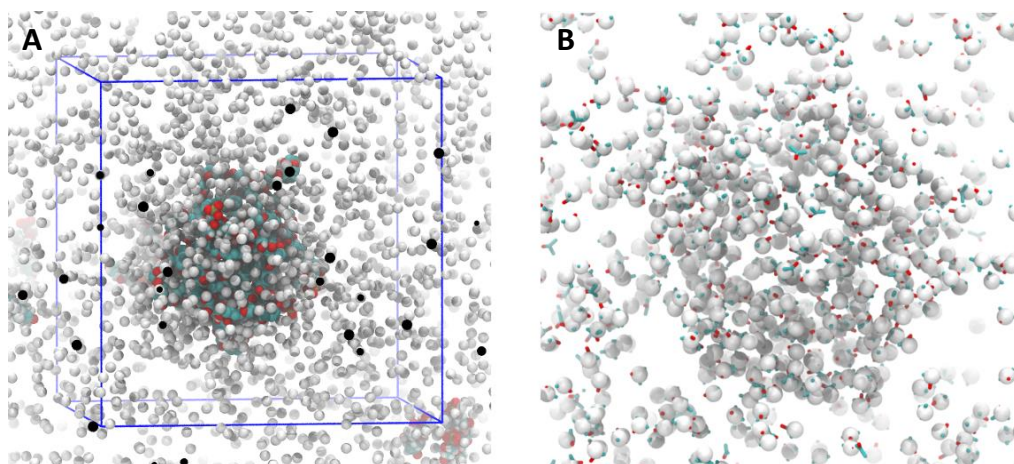


Figure 2.31 Resolution transformation procedure. (A) An 11nm sided

box is drawn around the polymer at a time point in the 80ns multiscale simulation. CG solvent in this box is subjected to resolution transformation. (B) During resolution transformation atomistic acetone (blue/red) is inserted in place of CG acetone beads (white).

2.4.2 Comparative Analysis of Multiscale and Atomistic Simulations

Subsystems from the resolution transformation were subjected to 5ns of production MD after minimisation and equilibration using the GROMOS 53a6 force field. For comparison, each 11nm sided subsection was also simulated for 5ns using the multiscale force field (simulations conditions identical to those described in 2.2.3).

The performance of the multiscale simulation vis-a-vis the atomistic “gold standard” MD was analysed with regard to two key parameters. Firstly

the time evolution of the total radius of gyration of the polymer clusters in the two simulations was compared using *g_gyrate*. Secondly the average orientation of the adsorbed DXMP molecules with respect to the polymer nanoparticle was evaluated. For this we measured the difference in the distance of the head phosphate and tail oxygen atoms of DXMP to the PGA centre of mass over the course of the simulation using *g_dist* (Figure 2.32). This was repeated for five different, randomly-chosen, drug molecules and averaged.

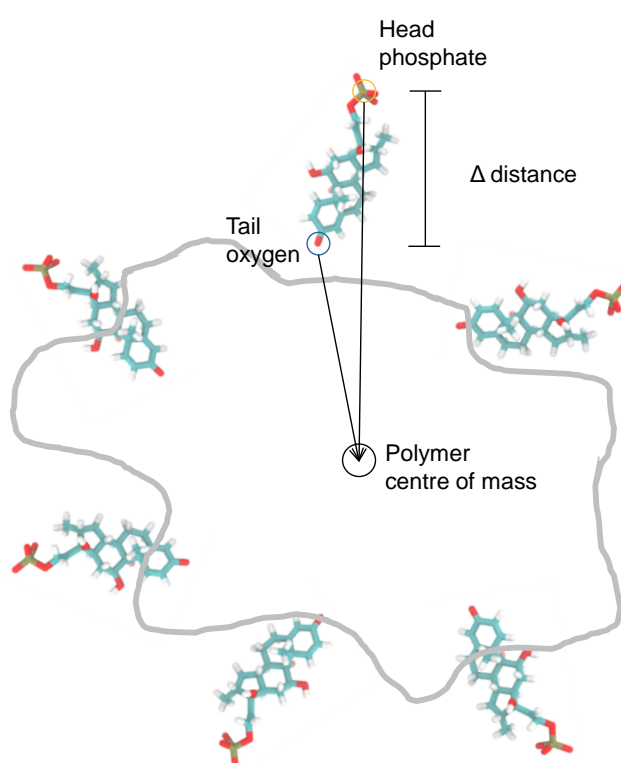


Figure 2.32 A cartoon depicting the calculation of the difference in the distance (Δ distance) from two atoms at opposite ends of DXMP to the centre of mass of the polymer nanoparticle.

2.4.3 Drug Loading and Encapsulation Efficiency

Experimentally, polymer-based drug delivery systems were analysed for their ability to encapsulate drug molecules. There are a variety of experimental techniques used to discern the amount of drug that is encapsulated. For our simulations we have the luxury of being able to see

exactly how many drug molecules are in contact with the polymer nanoparticle when it has formed.

The two most commonly used metrics for measuring drug encapsulation are encapsulation efficiency (EE) (Equation 2.6) and drug loading (DL) (Equation 2.7). Encapsulation efficiency will give an indication as to the amount of drug that was present in solution ends up encapsulated in the polymer nanoparticle. This value depends on the amount of drug present at the start of the simulation. If a small amount of drug was present in solution and it eventually all gets encapsulated on the surface of the polymer the EE is 100%. This value is equivalent to the reaction efficiency used in chemical synthesis and so is related more to the manufacturing cost of a formulation. It does not give an accurate indication of the encapsulation ability of a polymer.

The alternative parameter DL is an indication of the total capacity for a polymer nanoparticle to encapsulate drug molecules. Ideally this value should be as large as possible to get the optimal delivery of drug from the polymer nanoparticle. However, DL is often very low for polymer-based drug delivery systems. EE for a polymer could be 100% yet the DL may still be low depending on the amount of drug present in solution at the start.

$$\text{Encapsulation Efficiency} = \frac{\text{Mass of drug in nanoparticle}}{\text{Total mass of drug used}} \quad (2.6)$$

$$\text{Drug Loading} = \frac{\text{Mass of drug in nanoparticle}}{\text{Total mass of nanoparticle}} \quad (2.7)$$

A drug was considered bound to the nanoparticle if it made contact with the surface of the polymer nanoparticle. Although some drug molecules do not make full contact with the nanoparticle surface once simulated in pure water (to mimic a washing step) they become fully adsorbed to the nanoparticle surface.

Chapter 3

Designing a Model to Study Polymer Drug Interactions

The aim of this PhD was to analyse the interactions between drug and polymer molecules in a nanoparticle drug delivery system. Some initial questions were asked: What interactions cause the drug to be encapsulated in the polymer nanoparticle? Are drugs buried within or stuck on the surface? What functional groups on the drug or polymer are crucial to achieve high encapsulation efficiency of the drug within the nanoparticle? Molecular dynamics simulations provide an opportunity to answer these questions. The objective being that if it is possible to recreate nanoparticle formation in a computer, you can then analyse how the polymer and drugs interact in detail. From this you can begin to answer some of the questions listed above.

Initially the intention was to recreate existing data in an effort to ascertain if a computer simulation was capable of mimicking experimental conditions. If successful the system could be freely changed to explore the behaviour of new polymers and drugs.

An optimal simulation would involve using an accurate atomistic force field to model how thousands of drug and polymer molecules interact at concentrations relevant to the experimental conditions. However, molecular dynamics involves computing the interactions of every atom in a system, so as the number of atoms increases the speed of the simulation decreases. This problem is usually overcome by using more powerful resources for the simulations such as supercomputers and even specialised computers like Anton⁵⁰. An alternative is to use a simplified model that allows simulation of more basic molecules that behaves similarly to a fully atomistic model. Users must make compromises and adjustments to a system to ensure the most accurate simulation is run with the resources available.

3.1 An Acetone Drop Nanoprecipitation Model

The process of nanoprecipitation requires acetone to disperse within water therefore changing the solvent environment around the polymer chains causing them to aggregate into a nanoparticle.

Initially, the assumption was made that acetone was not critical to polymer aggregation and a simulation in pure water would be sufficient for assembling polymer nanoparticles. However, our simulations revealed that in pure water hydrophobic poly(glycerol adipate) chains collapse in on themselves over a few nanoseconds of simulation time. Small single polymer chain aggregates form first and these cluster into a larger nanoparticle when they collide with each other (Figure 3.33). In this case intramolecular polymer interactions take precedence over intermolecular polymer interactions.

When in acetone the polymer is soluble and does not aggregate. It was hypothesised that during nanoprecipitation the dispersion of acetone in water would create a gradient that would change over time, gradually exposing the polymer to the surrounding water. This would allow polymer chains to interact with each other before ultimately aggregating and forming a nanoparticle.

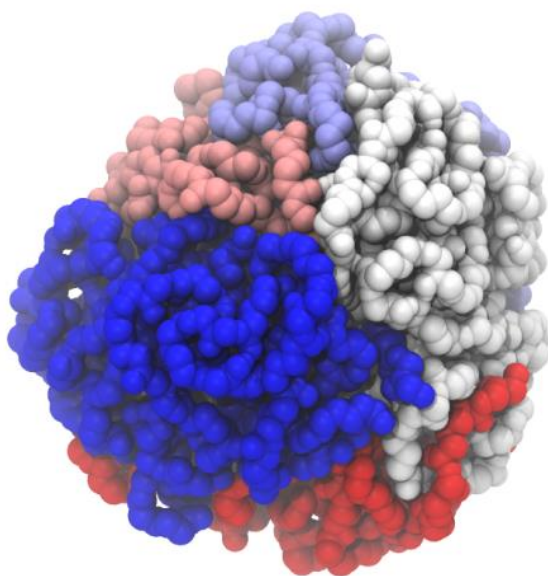


Figure 3.33 Snapshot taken from the end of a simulation of five 50mers of PGA_{100} in pure water. Each polymer chain is shown in a different colour to emphasize the lack of polymer chain entanglement.

A new simulation was performed this time including acetone. Polymer chains were modelled as dispersed within a small box of acetone and this was placed in a large box of water. As the simulation was run, water diffused into the polymer-containing region causing gradual formation of a nanoparticle. Whilst the polymer is slowly exposed to water in this simulation the speed of intramolecular polymer collapse is reduced and the amount of intermolecular

entanglement is increased. Overall this produced a more entangled polymer nanoparticle as hypothesised.

This acetone drop model was designed such that a single “drop” of acetone can fully disperse into a large box of water. Unfortunately, this simulation is far from optimal as a large amount of simulation time is spent on solvent interactions. For a simulation that was designed to analyse polymer drug interactions this is far from ideal. However, the dispersion of an acetone drop in water most closely resembles the experimental conditions for nanoprecipitation and it is for this reason we chose to pursue this system further.

A fully atomistic system, that contained all the relevant species at the experimental concentrations, consists of a 12nm diameter acetone drop containing ~16,000 molecules of acetone and two molecules of poly(glycerol adipate) (PGA₁₀₀) 30mer, one molecule of PGA₂₀-co-C18PGA₈₀ 30mer or C18PGA₁₀₀ 30mer. This droplet would be placed at the centre of a 60 nm sided box of ~7 million molecules of water and ~1000 molecules of dexamethasone phosphate (DXMP). In total this would be ~21 million atoms in order to simulate the formation of a nanoparticle of one or two polymer chains depending on the polymer used.

Simulating a system of this size using the resources available at the time of starting this PhD was not advisable as it would have taken several months to complete a single simulation. As stated previously it is common practice when dealing with such large systems to adopt a mesoscale modelling technique such as coarse-grained (CG) molecular dynamics or dissipative particle dynamics (DPD). A more simplified representation of the molecules in

the system reduces the computational requirements of the system and allows the simulation to be run.

For our system we initially chose a coarse-grained approach using the MARTINI force field. This involves converting every four non-hydrogen atoms in a molecule into a single CG bead. For water this involves converting four water molecules into a single bead; 4 to 1 mapping. The MARTINI force field is designed so that the interactions between these beads are based on the atoms they represent.

Overall for our acetone drop model this provides a four-fold reduction in the number of water molecules thus greatly reducing computational load. As our system is comprised predominately of water, coarse-graining is extremely favourable. Acetone can also be coarse-grained to provide an additional speed up.

However, coarse-graining has several caveats: the CG model lacks explicit electrostatic interactions present for the all-atom (AA) molecules. Instead these are implicitly included in the parameterisation of the van der Waals interactions between CG beads. Secondly the CG beads are much smoother than their AA counterparts. This speeds up their dynamics causing a timescale discrepancy between a CG and AA simulation. The MARTINI force field quotes a speed up of between 3-8 times⁴².

3.2 Coarse-Grained Solvent

For the dispersion of acetone in water during our nanoprecipitation simulation, our goal was to match the AA dynamics as closely as possible. AA dynamics are more likely to accurately mimic experimental conditions as all

the atoms of a molecule are represented. Thus, if the CG acetone dispersed at a faster rate than it does atomistically, we hypothesised this would have an adverse effect on the nanoprecipitation of the polymer chains during our simulation.

An initial step in optimising our system involved using AA simulations as a “gold-standard” reference to which we could match the dynamics using a CG force field. Two systems, one AA and one CG, were created of equal molar ratio containing a single drop of acetone molecules in a box of water.

The diffusion constant of acetone was measured over a 5ns simulation. The CG non-bonded parameters for acetone were adjusted such that the diffusion constant of acetone matched the AA acetone diffusion constant (Figure 3.34). The diffusion constant for CG acetone was adjusted from $1.367 \times 10^{-5} \text{ cm}^2/\text{s}$ to $2.213 \times 10^{-5} \text{ cm}^2/\text{s}$ (the AA diffusion constant was $2.113 \times 10^{-5} \text{ cm}^2/\text{s}$) for a 0.0357 molar ratio of acetone in water.

Mean squared displacement over time for the corrected force field is almost identical to atomistic simulation (Figure 3.34). Displacement over time will affect the speed of acetone dispersion from the acetone drop in water. By matching the atomistic simulation we ensure that the acetone dispersion in our acetone drop nanoprecipitation model is as close to experimental conditions as possible.

The dispersion of 512 molecules of acetone in water using an AA force field and a corrected CG force field is shown in Figure 3.35. A small box of acetone molecules disperses into a larger box of water. The dispersion rate of acetone in water is similar for both force fields used indicating that the new CG parameters match the AA acetone dispersion rate.

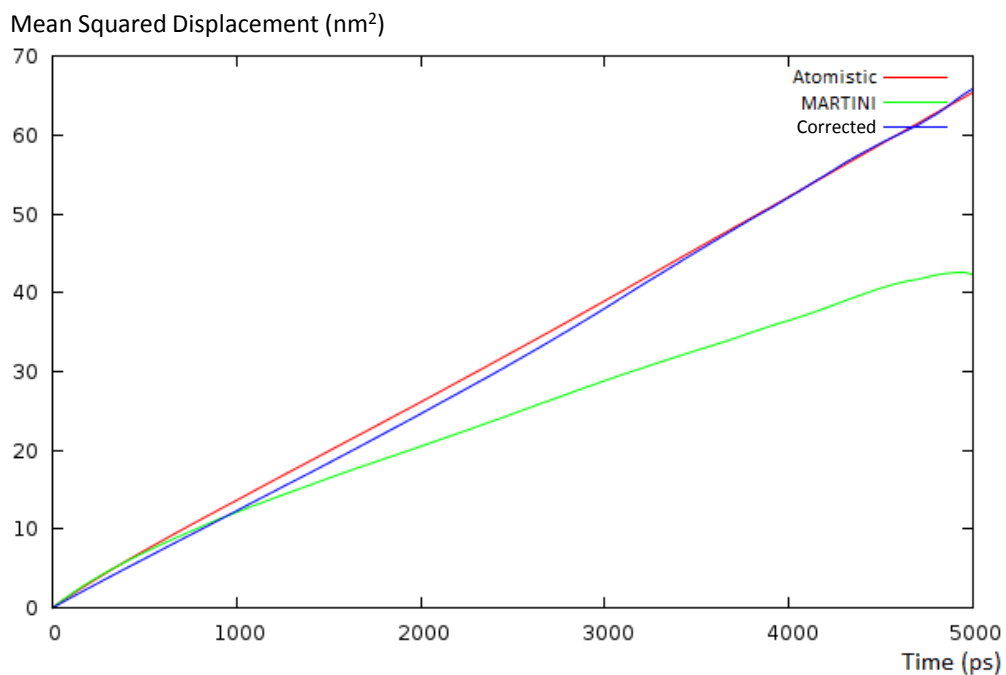


Figure 3.34 The mean square displacement of acetone in water over 5ns using the GROMOS 53a6 AA force field (red), MARTINI force field (green) and a corrected CG force field (blue).

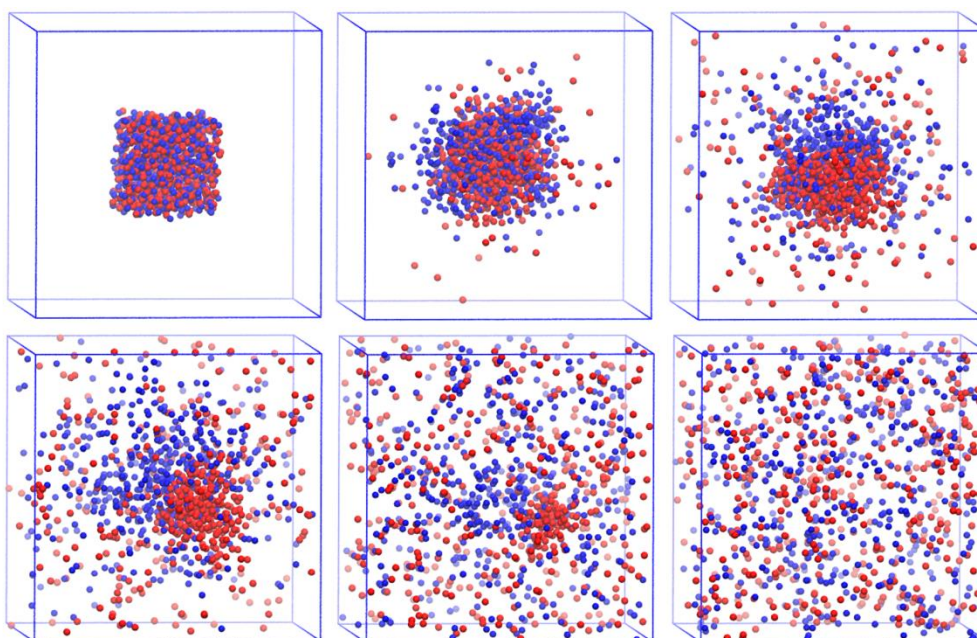


Figure 3.35 Two separate simulations of acetone dispersing in water using two different force fields: AA (red) and CG (blue). Water is not shown for clarity.

3.3 Coarse-Grained Polymer

To coarse-grain the polymer, the same 4 to 1 (AA to CG) mapping was used. The MARTINI force field has guidelines for allocating specific bead types to each CG bead in a molecule based on the atoms they represent. The mapping process is non-trivial and subject to user scrutiny. Mapping schemes can be very different but all try to represent the same molecule. Work by Kremer et al.⁵¹ has shown how small changes in the mapping scheme of a polymer can affect non-bonded and bonded interactions.

For bonded interactions the MARTINI force field recommends a 0.47nm bond length with a force constant of 1250 KJ mol⁻¹ for all CG bonds. Similarly angles are at 180° with a force constant of 25 KJ mol⁻¹. Using this topology, simulations of CG PGA₁₀₀ were run in pure CG water and pure CG acetone separately. In water the polymer formed an ordered crystalline structure and in acetone the polymer was insoluble. Both of these simulations differed from the AA reference simulations at the same concentrations where the polymer formed a more disordered spherical shape in water (Figure 3.36) and was soluble in acetone (not shown).

When using the MARTINI force field for a CG polymer the intramolecular interactions are too strong. This causes the polymer to adopt an ordered crystal-like structure as certain beads form tight interactions with each other. In contrast the atomistic force field generates a more disordered structure for the polymer aggregates. This difference in the CG representation could be due to the lack of detail in the CG structure or incorrect CG interaction parameters.

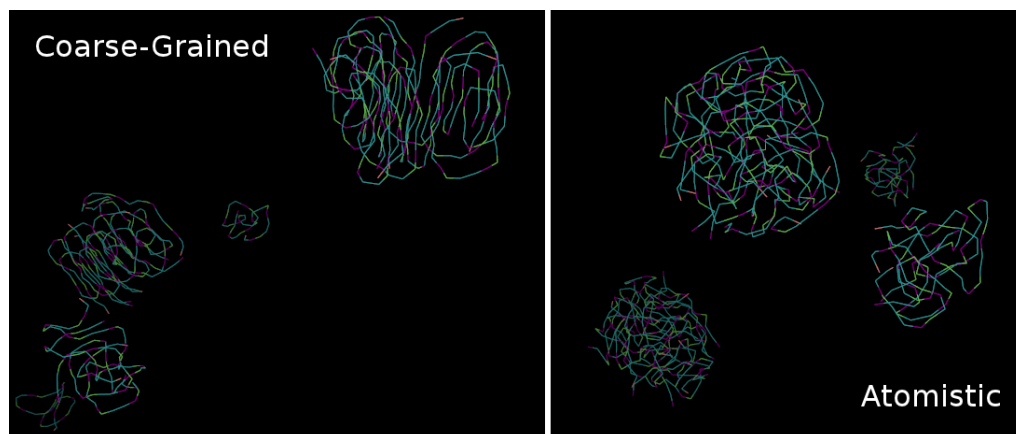


Figure 3.36 Snapshots taken from simulations of PGA_{100} in water. Polymers are represented as lines with different colours for the CG beads in the structure. The AA structures were mapped to CG representations at the end of the simulation for a clearer comparison.

3.3.1 Improving the CG interactions

The priority for this work was to ensure that polymer and drug interactions were as accurate as possible. It was important to ensure that CG interactions between these molecules resembled the AA interactions as closely as possible. One technique to improve coarse-grain models is to use AA simulations as a starting point for developing CG interaction potentials.

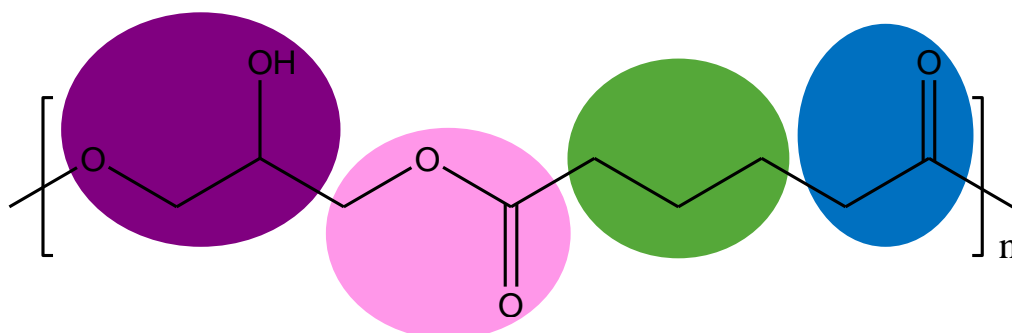


Figure 3.37 CG mapping scheme used for PGA_{100} . Every 3-4 non hydrogen atoms are mapped to a single CG bead.

This was done by using tabulated potentials for non-bonded interactions based on the dynamics of an AA reference simulation. For PGA_{100} in water an

AA simulation was run first and the resulting trajectory was mapped to a coarse-grain mapped trajectory using the mapping scheme shown in Figure 3.37.

The positions of the CG beads in the CG mapped trajectory are analysed by their radial distribution functions (RDF) (Figure 3.38). AA reference RDFs are generated for every non-bonded interaction in the system. The four beads in each monomer of the polymer were labelled A, B, C and D and RDFs generated were A-A, A-B, A-C, A-D, B-B, B-C etc. The aim was to match these AA reference RDFs using a CG force field made from tabulated potentials.

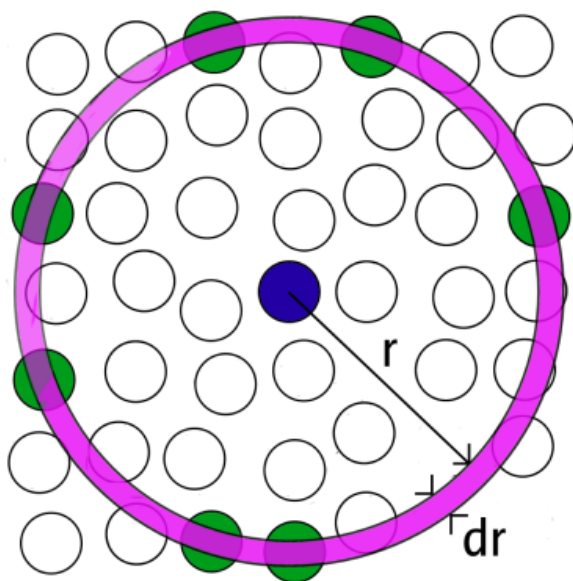


Figure 3.38 The RDF of a blue bead to green beads. Seven green beads are located at a distance r from the central blue bead.

To run the CG simulation, the first step was to create bonded interactions between the beads in the polymer. A short simulation was run of a PGA_{100} 20mer in a vacuum with all non-bonded interactions disabled. This allows the bonded interactions in the AA molecule to fully explore their entire

conformational space. The AA trajectory was converted to a CG mapped trajectory and a Boltzmann distribution was obtained for all the bonds and angles beads in the polymer. The versatile object orientated toolkit for coarse-graining applications (VOTCA) enabled the use of Boltzmann inversion to convert these distributions into bond and angle harmonic potentials for the CG molecule.

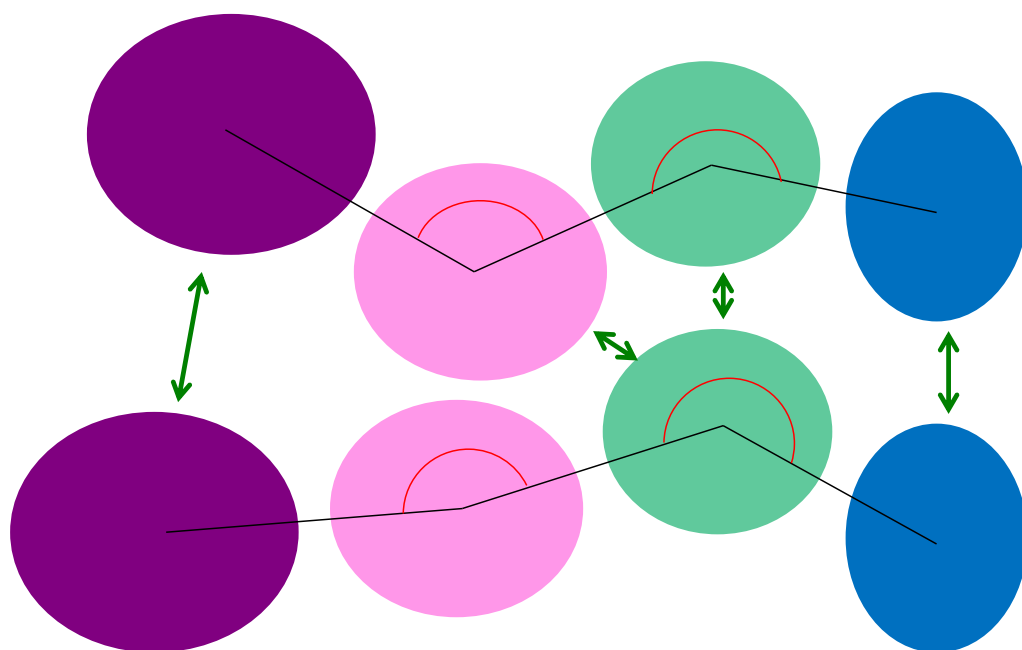


Figure 3.39 CG potentials required for PGA_{100} : Non-bonded (green), Bonds (black), Angles (red).

A similar technique was used to derive the non-bonded tabulated potentials for every bead pairing of the CG polymer. Using VOTCA again, RDFs from the AA reference simulation were subjected to Boltzmann inversion to generate an initial guess for the tabulated potentials. These potentials coupled with the bonded potentials allowed an initial CG simulation of PGA_{100} in CG water (Figure 3.39). When the simulation ended, RDFs were calculated from the simulation and compared with the original AA reference RDFs from the CG mapped trajectory of AA PGA_{100} in AA water.

A comparison was made and a new set of tabulated potentials were generated and tested with another CG simulation. In this way the non-bonded potentials were iteratively refined until the RDFs match. This is the process of iterative Boltzmann inversion (IBI) (Figure 3.40).

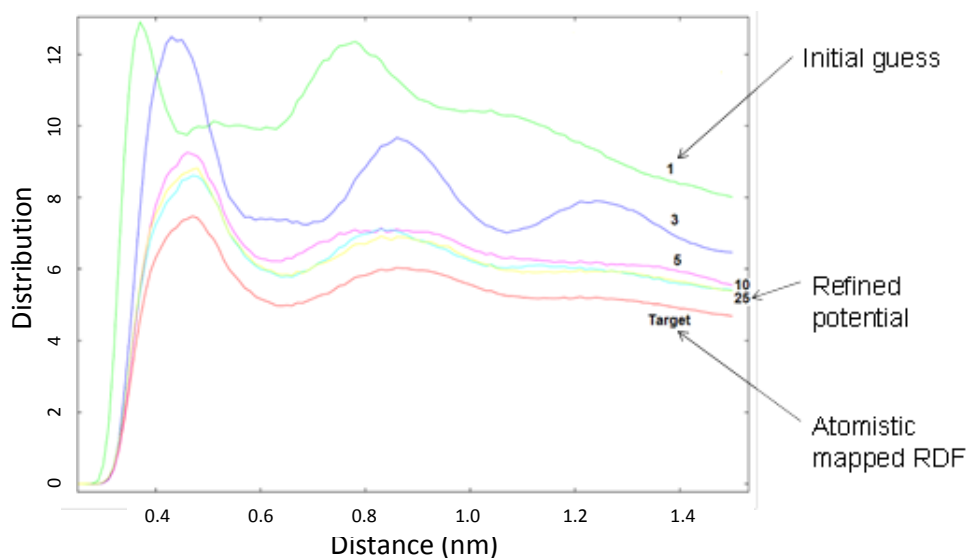


Figure 3.40 During iterative Boltzmann inversion RDFs from a CG simulation of PGA_{100} in water are plotted at different cycles during the process. The CG RDFs begin to converge to the AA reference RDF until a refined CG potential was obtained after 25 cycles.

Although the RDFs do not perfectly match, the potential is refined enough for the RDFs to be much closer than the initial guess. The inability to match the RDFs was due to the large amount of RDFs involved. Changing the tabulated potential for one interaction can have a knock on effect on the interactions of another bead pairing. The dynamic nature of the polymer nanoparticle used for IBI results in large fluctuations in the RDF during each cycle.

3.3.2 A new CG model

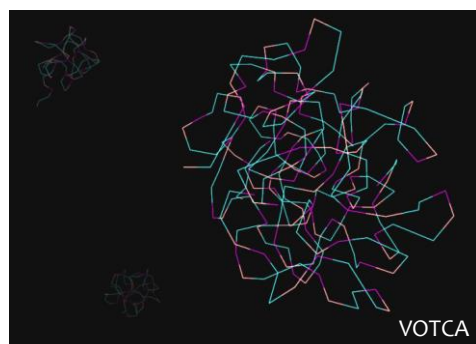


Figure 3.41 CG structure of a PGA_{100} nanoparticle in water using the CG potentials obtained with VOTCA. The structure more closely resembles the AA structure seen in Figure 3.36.

Upon repeating the CG simulation of PGA_{100} in water using the refined CG potentials, the nanoparticle structure is more disordered and less crystalline (Figure 3.41) more closely matching the AA structure shown in Figure 3.36.

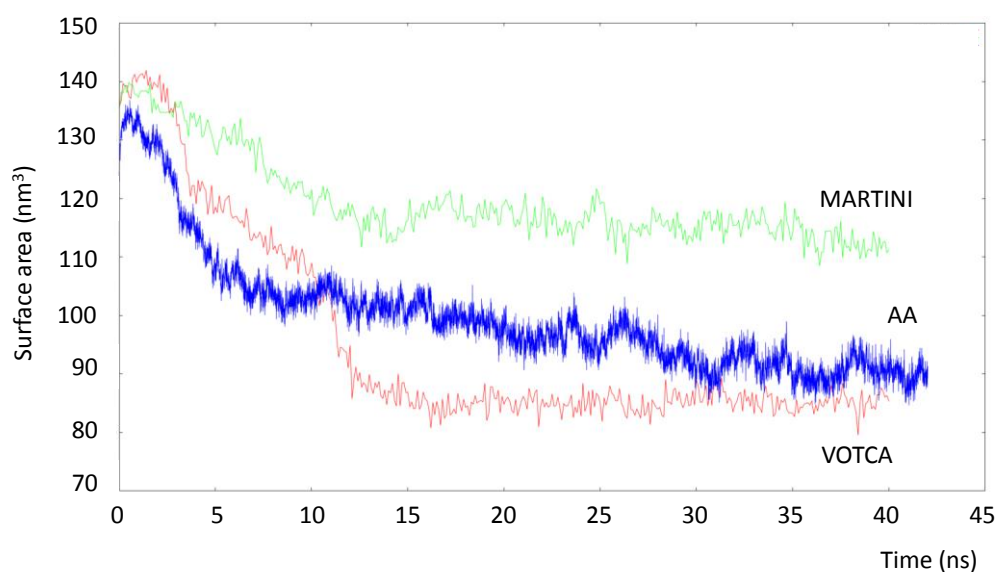


Figure 3.42 Plots for the solvent accessible surface area (SASA) of PGA_{100} over 40ns. The new CG tabulated potentials offered good agreement with the AA simulation compared with the MARTINI force field.

Figure 3.42 shows how the solvent accessible surface area (SASA) of the polymer changes over a 40ns simulation. A virtual probe was used to

measure the surface area of the polymer aggregates as they form in water during the simulation. The larger surface area found with the MARTINI force field was due to the crystalline aggregates formed. The aggregates formed using the refined CG potentials matched the SASA of the AA simulations more closely.

The improvements to the CG model are more clearly demonstrated in Figure 3.43 where the MARTINI force field caused 250 monomers of PGA₁₀₀ in water to aggregate into a bilayer. This again indicates that interactions between similar beads in the PGA₁₀₀ monomer are too strong. Using the new CG potentials from VOTCA a disordered aggregate formed in a similar manner to the polymer nanoparticles formed in water.

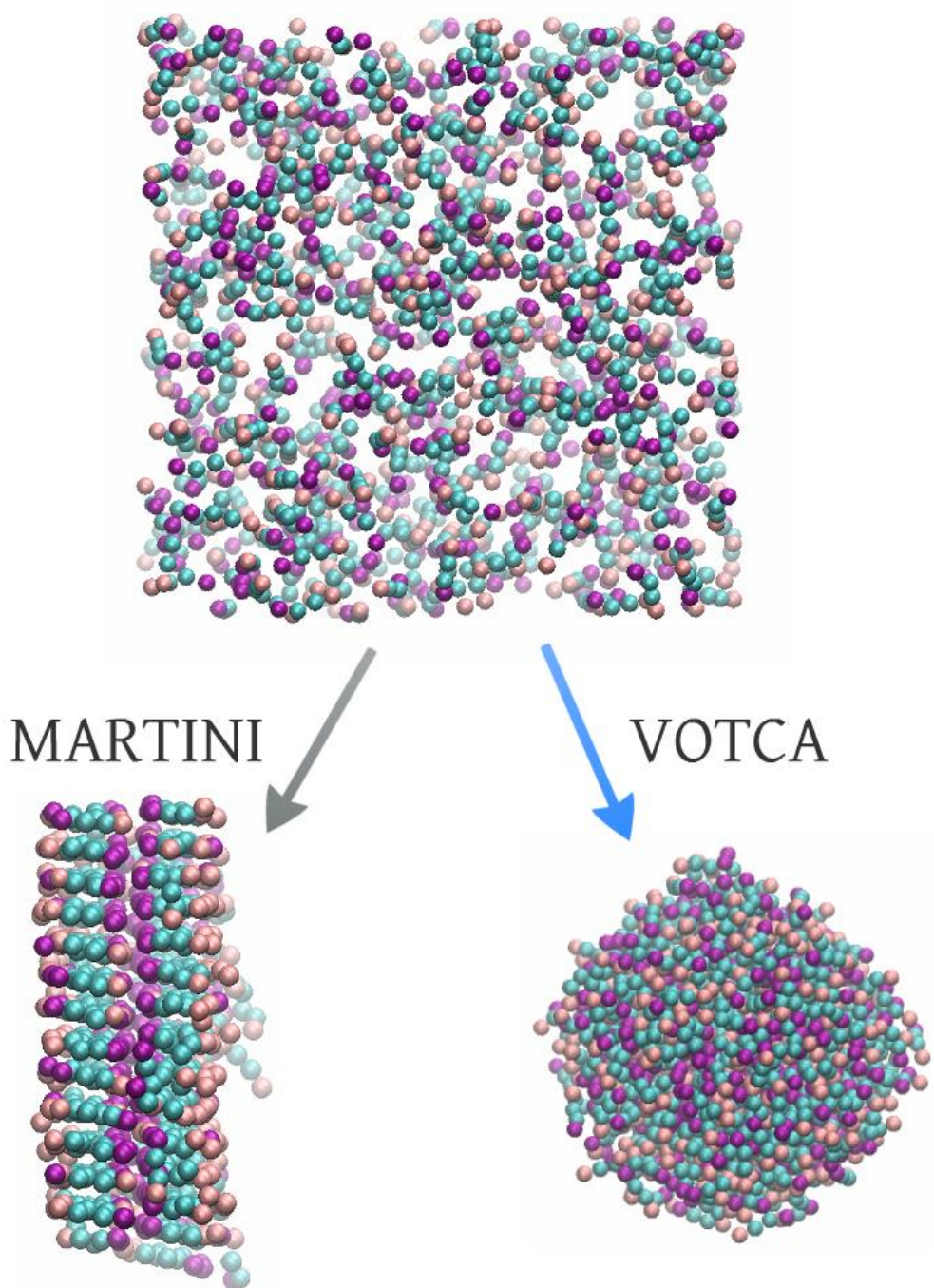


Figure 3.43 Two simulations of 250 monomers of PGA₁₀₀ in water using the MARTINI force field and the VOTCA refined CG force field. The MARTINI force field generates a bilayer like construct whereas the VOTCA force field generates a spherical nanoparticle.

3.4 Coarse-Grained Drug

For an aggregate such as the one formed by PGA_{100} in water, IBI is a good method to parameterise the CG model as the structure remains similar through each cycle allowing optimisation of the tabulated potentials. However, for a molecule that is soluble in water such as DXMP, IBI is not possible as the RDFs for the CG beads change drastically. Additionally for drug and polymer molecules there is no obvious reference AA simulation that will enable IBI to work. One idea is to simulate melts of polymer and drug molecules. However, these simulations do not represent the conditions which will be used for the acetone drop nanoprecipitation simulation.

Additionally, the number of RDFs required to converge is increased as CG DXMP contains nine beads. 36 tabulated potentials must be simultaneously refined to try and match the same number of AA reference RDFs.

This is also a problem for drug polymer interactions. Therefore other techniques were attempted to obtain tabulated potentials such as umbrella sampling. However, it is difficult to obtain accurate potentials for a single drug molecule with a large polymer chain which contains multiple conformations and functional groups.

For these reasons a fully CG model for nanoprecipitation is extremely difficult to create. There is potential to modify the MARTINI force field such that it matches small scale AA simulations, but this is a non-trivial empirical process that would create a force field specific to one polymer and drug combination. Ideally the force field used in this work should be compatible with any polymer and drug combination with minimal optimisation required.

3.5 Multiscale Modelling

As CG simulations are inaccurate for our needs and AA simulations are unfeasible, a force field that uses aspects from both scales should have the correct balance between accuracy and speed required.

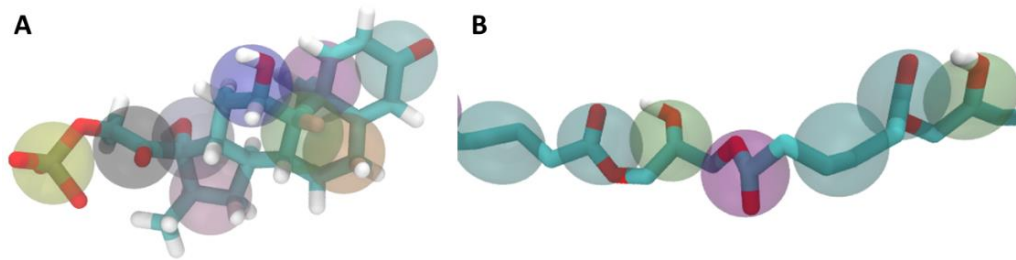


Figure 3.44 Multiscale model used for DXMP (A) and PGA (B). The transparent CG beads are virtual sites that are positioned at the centre of mass of the atoms they represent. The atomistic molecules interact with surrounding CG solvent molecules through these virtual sites using the MARTINI CG force field.

A multiscale or hybrid CG/AA model involves the mixing of two force fields. This enables some molecules in a system to be at an AA level of detail whilst other molecules are coarse-grained. AA molecules interact with themselves and other AA molecules through an AA force field like a standard simulation. In a similar vein CG molecules also interact with themselves and other CG molecules using the MARTINI force field. However, in order for AA molecules to interact with CG molecules, CG virtual sites are created on all of the AA molecules in the system (Figure 3.44).

CG virtual sites are mapped onto the AA molecules in the same way an AA molecule is converted to a CG molecule. The CG virtual sites are linked to the atoms they are mapped from. Forces acting on the CG virtual sites from other CG molecules are passed onto the underlying atoms in the AA molecule. In this way CG molecules can interact with AA molecules in the system and vice versa.

For our nanoprecipitation simulation, multiscale modelling allows the use of CG solvent with AA polymer and drug molecules. As the majority of the system consists of solvent molecules, coarse-graining the solvent provides an increase in the speed of the simulation due to a decrease in degrees of freedom for the solvent molecules. Solute molecules (drug and polymer) are kept atomistic to preserve the accurate interactions obtained through the use of an AA force field.

The interactions between the solute molecules in the system are the most important and so these need to be kept at the highest resolution possible. Conversely, the solvent interactions are less important, specifically the intermolecular interactions in bulk water. Using a CG force field for these interactions provides a large speed up to the simulation whilst hopefully having a minor effect on the solute interactions.

3.6 Multiscale Model Optimisations

Combining two force fields that have been separately parameterised over several years is a non-trivial exercise. It is critical that any multiscale simulation is fully optimised to ensure that the dynamics are as accurate as possible. Again fully AA reference simulations can be used to determine the optimal dynamics of a system. From these reference simulations the multiscale force field can be optimised.

3.6.1 Polymer-Drug Interactions

In GROMACS the relative dielectric constant, ϵ_r , sets the screening for the electrostatic interactions in the system. Electrostatic forces play a vital role

in the interaction between AA molecules in the system. However, the CG molecules and CG virtual sites on the AA molecules have no electrostatic interactions. At low values of ϵ_r there is little screening of electrostatic interactions and vice versa.

GROMOS96 v53a6 uses an ϵ_r of 1 (the default value) as the force field does not require screening of electrostatics. The MARTINI force field uses an ϵ_r of 15 as its basic electrostatics are only integer charges (+1, -1, 0 etc.). CG beads are only charged if the underlying atoms would collectively have an integer charge. To balance these large charges with the van der Waals forces in the system a large dielectric screening constant is used.

For our system a major problem is that CG water has no electrostatic interactions with the highly charged DXMP molecules. It should be noted that the CG virtual sites on DXMP carry no charge but the atoms themselves are charged. Therefore the double negative charge on the phosphate group of DXMP interacts through the AA force field. This charge has strong electrostatic interactions to nearby positive charges.

Whilst AA water is polar and contains a partial positive charge on its hydrogen atoms, CG water is a representation of four whole water molecules whose overall charge is neutral. In a multiscale simulation, CG water is unable to partially neutralise the negatively charged DXMP phosphate group. With low values of ϵ_r , negatively charged DXMP molecules are strongly drawn to positive charges in the system. They either tightly bind to sodium counter ions or bury themselves in the AA polymer molecules (Figure 3.45).

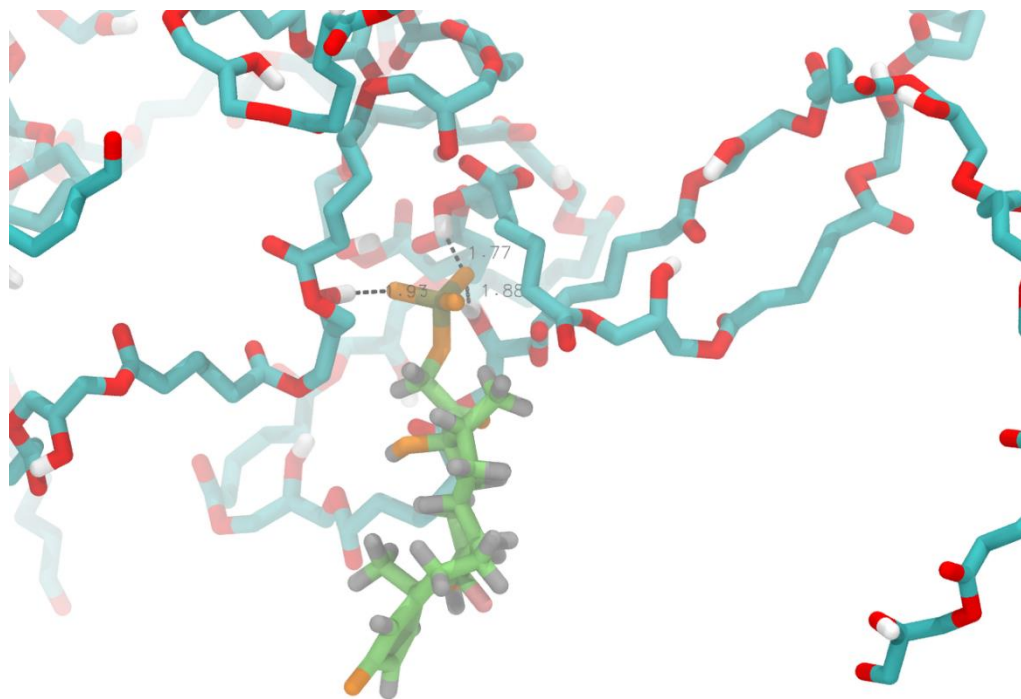


Figure 3.45 Snapshot taken during a 20ns multiscale simulation of DXMP (green/orange) with PGA₁₀₀ (blue/red) in CG water. Black dashed lines show the distance between charged oxygen atoms on the phosphate of DXMP to hydroxyl groups on PGA₁₀₀. The CG water molecules are not shown for clarity.

Using an AA force field polar water molecules provide counter charge to the DXMP phosphate groups. For the multiscale force field we increased the ϵ_r , to reduce the strength of electrostatic interactions, referencing the orientation of DXMP. This matches the AA reference simulation in which the relatively hydrophobic steroid portion interacts with the polymer while the phosphate group remains exposed to the solvent (Figure 3.46).

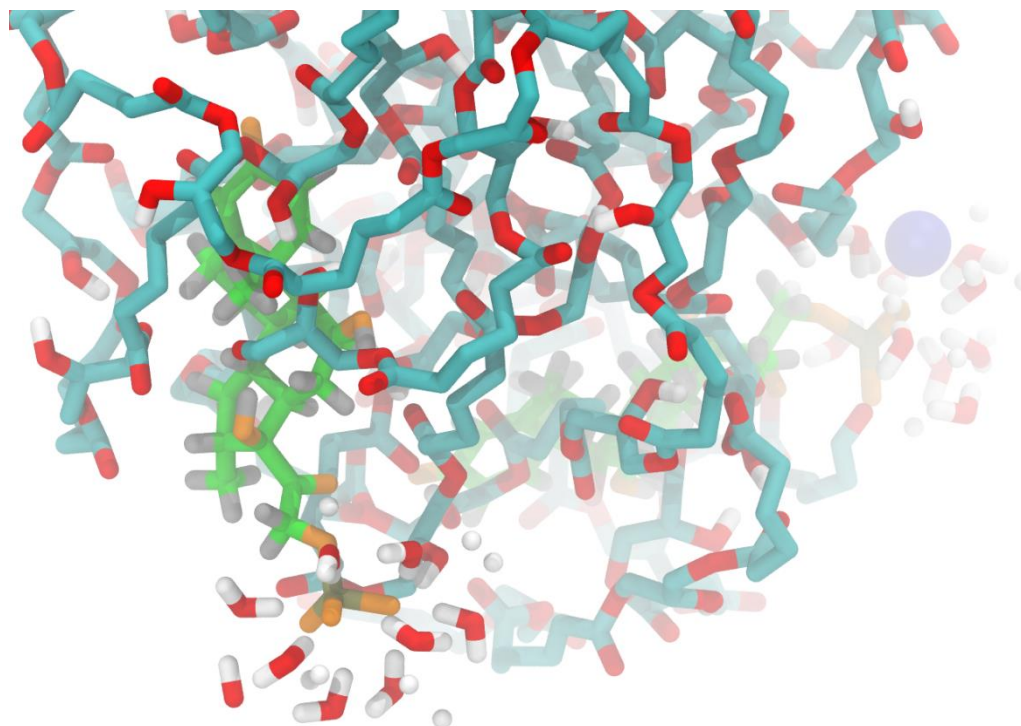


Figure 3.46 Snapshot taken at the end of a 20ns multiscale simulation of DXMP with PGA₁₀₀ in AA water. There is counter charge present for the DXMP molecule and so it adopts a different orientation with respect to the polymer. Only water atoms in close proximity to the DXMP phosphate group are shown for clarity.

An ϵ_r of 6 was found to be optimal for DXMP with PGA₁₀₀. Ideally the ϵ_r should be kept as low as possible to ensure that the AA interactions in the system are not affected as they are initially optimised to a value of 1. An ϵ_r of 6 is quite high due the large charge present on DXMP. For a system with uncharged drug molecules it is hypothesised that a lower value of ϵ_r could be used.

Whilst an ϵ_r of 6 is required to reduce the electrostatic interactions of DXMP's phosphate group, this value is not compatible for the polymer or solvent molecules which are initially parameterised to different values for ϵ_r . As such, adjustments to the CG interactions in the force field were required.

At $\epsilon_r = 6$, the electrostatic interactions that keep the polymer aggregated in water are weakened as they are optimised for a lower value of ϵ_r . To address this, the interaction between the CG water molecules and the CG virtual sites on the polymer was made more repulsive by adjusting their Lennard Jones potentials within the force field. The radius of gyration of the polymer nanoparticle is used to compare with the AA reference simulation (Figure 3.47).

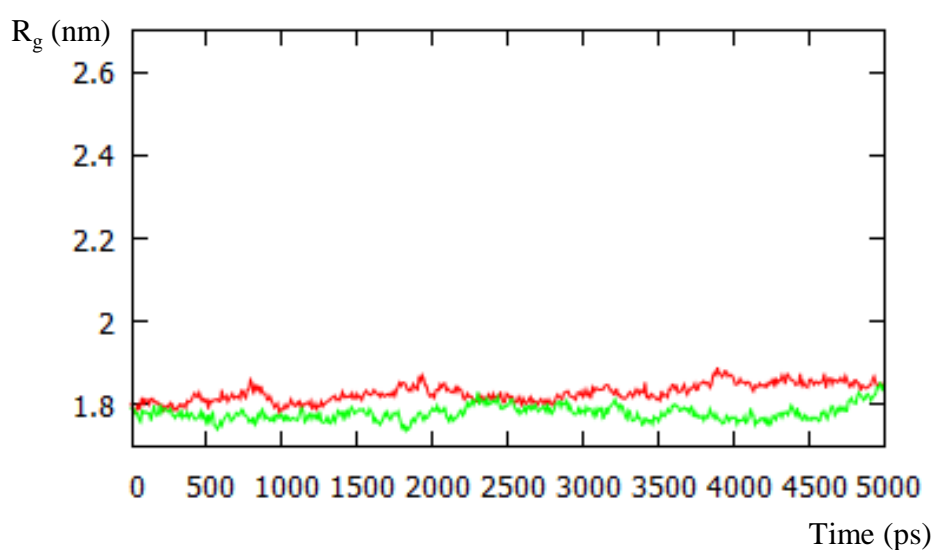


Figure 3.47 The radius of gyration for PGA_{100} in water using an AA force field (red) is compared with the multiscale force field at $\epsilon_r = 6$ (green).

Simulations in pure water for 20ns comparing both force fields reveals the orientation of the drug molecules and the aggregation of the polymer chains are in good agreement (Figure 3.48).

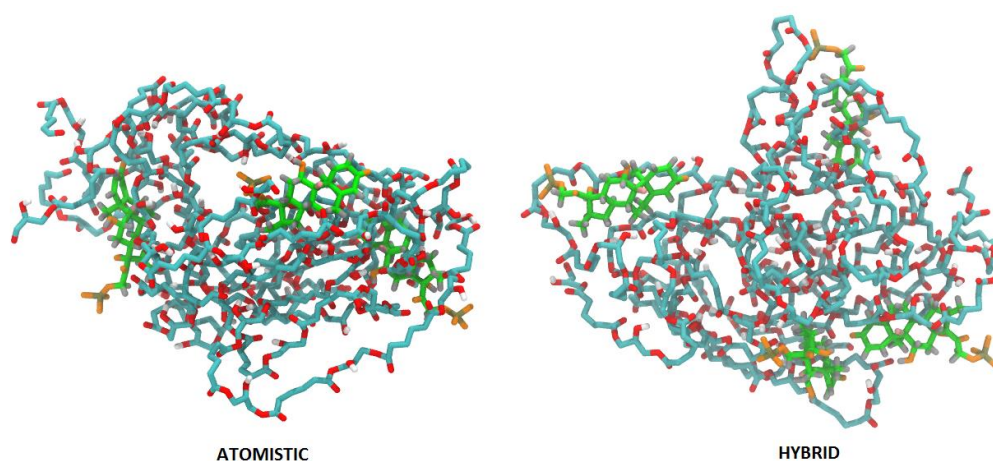


Figure 3.48 Snapshots comparing the final atomistic structure with a corrected multiscale (hybrid) force field. Water is not shown for clarity. PGA₁₀₀ (blue/red), DXMP (green/orange).

3.6.2 DXMP Orientation

To further analyse the effect of the relative dielectric constant, the orientation of DXMP was analysed over a short 5ns simulation using different values of ϵ_r (Figure 3.49).

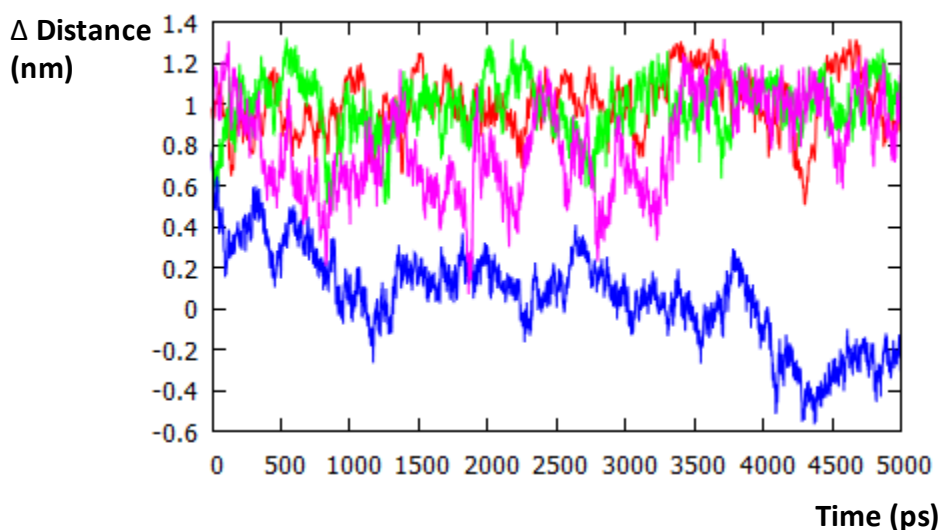


Figure 3.49 The orientation of DXMP in relation to a PGA nanoparticle in water was analysed over four different 5ns simulations. AA (red), multiscale ($\epsilon_r = 6$) (green), multiscale ($\epsilon_r = 1$) (blue), multiscale ($\epsilon_r = 15$) (pink).

The difference in the distances (Δ distance) of the phosphorus atom and the oxygen atom attached to the steroid A ring of DXMP to the centre of mass of the polymer nanoparticle was analysed over a 5ns simulation in water (see Methods).

In the AA reference simulation (Figure 3.49 red line) the phosphate end of DXMP interacted favourably with counter ions and polar water molecules surrounding the polymer nanoparticle. This resulted in the phosphate end of DXMP being further from the centre of mass of the polymer than its opposite oxygen end. The oxygen end of the molecule is more hydrophobic and was associated with the surface of the polymer nanoparticle. In this orientation the Δ distance is a positive value. For the AA reference the Δ distance averaged around 1nm for five DXMP molecules during a 5ns simulation.

For an ϵ_r of 1 (Figure 3.49 blue line) the electrostatic interactions are not screened, therefore the phosphate end of DXMP turned from its initial position to face in towards the polymer surface (as is seen in Figure 3.45) decreasing the Δ distance. By the end of the simulation the Δ distance was negative indicating that the orientation of DXMP had almost fully reversed.

At $\epsilon_r = 15$ (Figure 3.49 pink line) the electrostatic interaction are too weak and the interactions AA interactions the system were affected. Although the Δ distance remains positive, the value fluctuated due to a change in the aggregation of the polymer. With decreased electrostatic interactions the polymer was no longer able to maintain its aggregated state and began to unravel. This affected the metric as the centre of mass of the polymer nanoparticle changed and fluctuated during the simulation. As the polymer

unravelling its interactions with DXMP also changed affecting the Δ distance metric.

For $\epsilon_r = 6$ (Figure 3.49 green line) the correct balance of electrostatic and van der Waals forces was seen such that the Δ distance remained close to 1nm matching the reference AA simulation.

3.6.3 Drug Solvent Interactions

To parameterise the interaction between DXMP and the two types of solvent molecule involved in our nanoprecipitation model, a partition simulation was created. A single molecule of DXMP was placed at the interface between acetone and water solvent in a cuboid box. Simulations of 10ns were run to analyse the partitioning of DXMP in the two solvents before they fully mixed.

An AA reference simulation revealed that the phosphate group on DXMP stayed in the aqueous phase whilst the rest of the molecule was in the acetone phase. This was presumably due to the charged phosphate group having strong electrostatic interactions with the polar water molecules. The rest of DXMP is steroidal and hydrophobic so it had stronger interactions with the acetone phase and did not enter into the aqueous phase.

A multiscale simulation was run of the same system using CG solvent. With an ϵ_r of 6 the solvent interactions with DXMP were adjusted such that it partitioned in the two solvents similarly to the AA reference simulation (Figure 3.50).

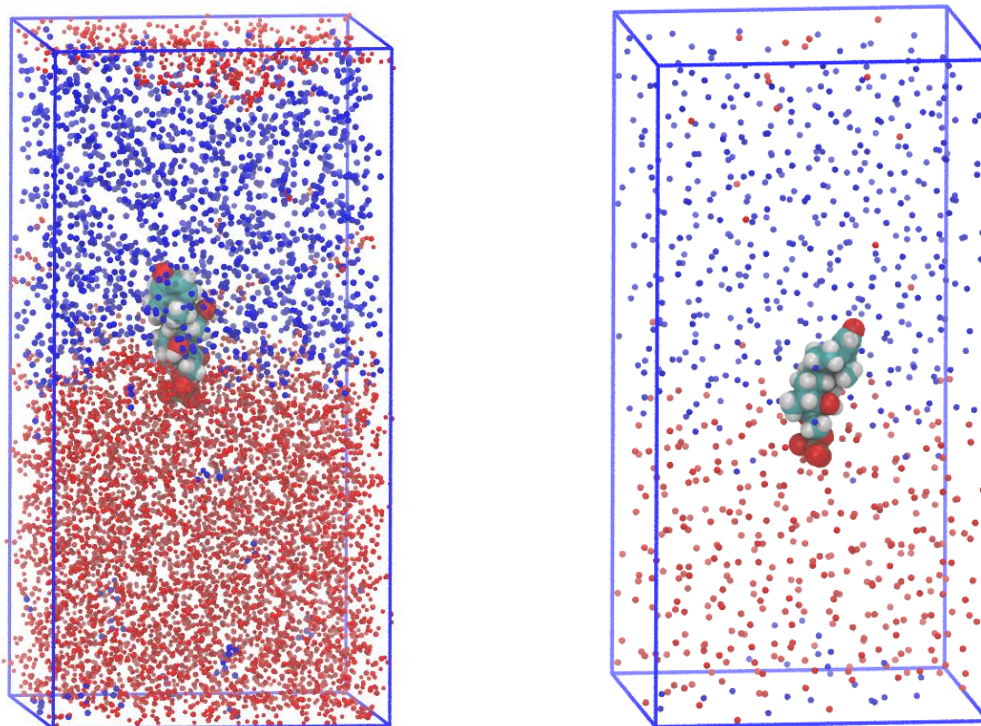


Figure 3.50 Snapshots taken at the end of 10ns simulations showing the partitioning of DXMP in acetone/water. With an AA force field (left) and multiscale (right). Water (red dots), acetone (blue dots).

3.7 Conclusion

This chapter serves as an overview of a number of techniques that can be used to simulate drug polymer interactions. There are of course many other methods that have not been attempted such as simulating only part of the polymer nanoparticle or using coarser dynamics such as DPD.

The choice of a multiscale model for simulating polymer nanoprecipitation was driven by the ability to choose the levels of resolution for separate molecules in the simulation. Our focus is on the polymer drug interactions and a multiscale model provides a method to marry accurate AA interactions with coarser solvent interactions.

By using small scale AA simulations as references it is possible to optimise a multiscale force field for any given molecule with relative ease. DXMP is a tricky case as its large charge presents some major problems when combining two force fields. However, we have shown that it is possible to overcome these problems through the design of metrics and analytical techniques to ensure the multiscale dynamics closely resemble AA reference simulations.

It is hypothesised that uncharged drug molecules would be easier to optimise for this multiscale force field. Additionally a low value of ϵ_r could be used such that there would be less optimisation necessary for AA interactions. Nevertheless, DXMP is an interesting case example and demonstrates that with efficient optimisation a multiscale force field can be used to simulate polymer drug interactions.

Chapter 4

Incorporation of DXMP into PGA Nanoparticles: Multiscale Model

The aim of this chapter was to simulate the process of DXMP being incorporated into PGA nanoparticles using a multiscale force field. Simulating polymers and drugs which have been used experimentally allows us to verify the accuracy of our model. Experimental data has shown that encapsulation efficiency of DXMP into PGA nanoparticles is highest for PGA₂₀-co-C18PGA₈₀ when compared with PGA₁₀₀ and C18PGA₁₀₀. Our model should be able to reproduce this experimental trend if it is an accurate representation of how these molecules behave. If the experimental data correlates with the simulations then we can analyse the reason for the experimental trend at the molecular level. By revealing key interactions between the molecules we will gain a better understanding of drug-polymer compatibility and help create better polymer-based drug delivery systems in the future.

The multiscale force field detailed in the previous chapter involves using CG solvent molecules in place of AA molecules to decrease the degrees of freedom in the simulation. As molecular dynamics involves the calculation of interactions between every particle in a given system, reducing the number of particles decreases the time taken to simulate nanoprecipitation. By using CG solvent in place of AA solvent the total amount of interacting particles in the system decreases from over 21 million to ~2 million. However, this is still a significantly large number of molecules to simulate.

One major drawback from using the multiscale force field is that the time step of the simulation is low (2 fs) as atomistic molecules are still present in the simulation. Although the majority of our simulation is single CG particles (water and acetone) we must accommodate the small part of our simulation that is atomistic. Simulating nearly 2 million molecules at this time step on our computational resources was still too slow. Additionally the simulation still only contained a single molecule of PGA₂₀-co-C18PGA₈₀ 30mer.

To better observe the formation of a nanoparticle containing multiple polymer chains the concentration of the polymer molecules was doubled. In addition the number of acetone molecules was halved to allow for a smaller box with substantially less water. Although the polymer concentration in our system is now not identical to the experimental conditions, the aim was to observe differences between the polymers in our simulations not compare directly with experimental data. As was seen in Chapter 1, changing the concentrations of components in a simulation is common practice due to computational limitations. In the future with more computational resources

there will be the potential to run larger scale simulations at the correct concentrations.

The modelled concentration of drug in water was kept comparable to experiment at 3.22mg/ml. Overall; we were able to reduce the number of particles in the simulation system to 1,054,063 for two PGA₂₀-co-C18PGA₈₀ or C18PGA₁₀₀ chains and 1,053,653 for three PGA₁₀₀ chains with 500 molecules of DXMP.

4.1 Simulation of PGA₁₀₀ nanoprecipitation in the presence of DXMP

We first explored the nanoprecipitation of the parent, un-substituted, PGA₁₀₀ over an 80ns multiscale simulation. This simulation time ensured full dispersion of the acetone into the surrounding water and that the aggregation of the polymer nanoparticle was complete (the metrics used to confirm this are discussed later). The polymer molecules in the acetone drop at the beginning of the simulation were initially well dispersed and in chain-extended conformations (Figure 4.51B). As the acetone dispersed into the surrounding water, the relatively hydrophobic polymer chains moved towards the centre of the shrinking drop. Because the rate of diffusion of the polymer chains was slower than that of the solvents, they experienced an increasingly polar environment and polymer-polymer interactions became more pronounced. This produced both intramolecular collapse of individual polymer chains and stronger, more entangled, intermolecular interactions.

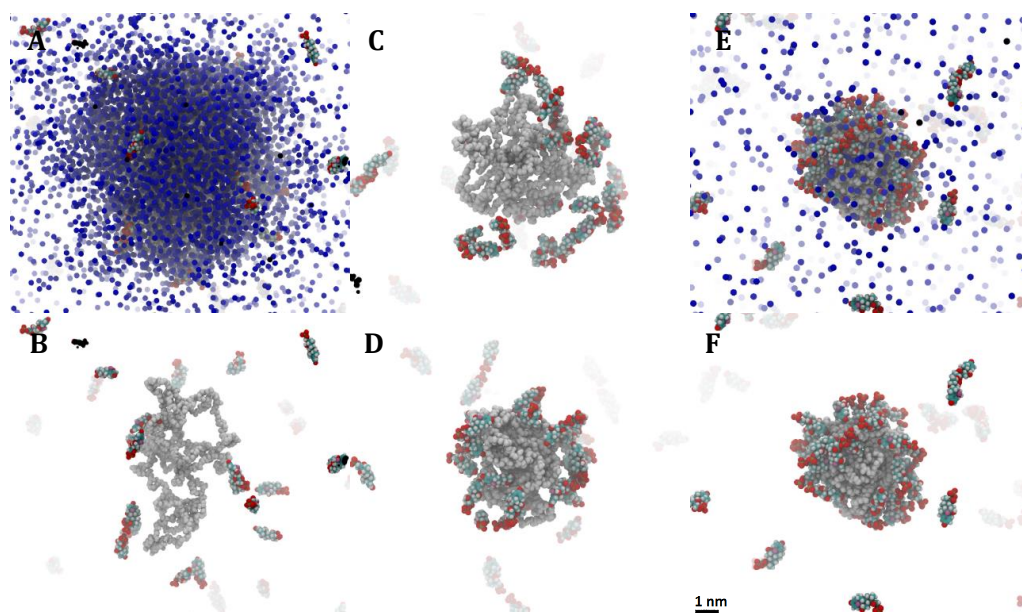


Figure 4.51 Snapshots taken during the 80ns multiscale simulation of PGA₁₀₀ with DXMP. A: 5ns (with acetone shown), B: 5ns, C: 30ns, D: 50ns, E: 80ns (with acetone shown), F: 80ns. DXMP (red/blue), PGA (white), acetone (blue). Water and CG virtual sites not shown for clarity.

DXMP is soluble in water and diffused around the simulation box. The acetone drop shrank in size during the simulation yet remained relatively spherical. DXMP has amphiphilic properties so preferentially interacted at the acetone water interphase.

The more hydrophobic region of DXMP is its steroid nucleus that prefers to reside inside in the acetone drop rather than in water. The more hydrophilic part of the molecule, the phosphate head group, remains in the aqueous phase due to interactions with polar water and ions. This amphiphilic nature of DXMP was also seen in Chapter 3 when optimising the drug solvent interactions.

Some DXMP molecules that are in close proximity to the acetone drop at the start of the simulation were able to interact quickly with the polymer chains (Figure 4.51B). During the rest of the simulation other DXMP

molecules positioned at the surface of the shrinking acetone drop were pulled onto the surface of the polymer nanoparticle as it assembled. Eventually enough acetone dispersed to cause full aggregation of the polymer chains; at this point a proportion of DXMP molecules become encapsulated in the nascent nanoparticle (Figure 4.51).

During the simulation DXMP molecules orientated in a favourable position as the most hydrophobic part of the molecule was positioned to interact with the surface of the relatively hydrophobic polymer nanoparticle. This left the phosphate head group of DXMP to interact preferentially with surrounding water and counter ions (Figure 4.52).

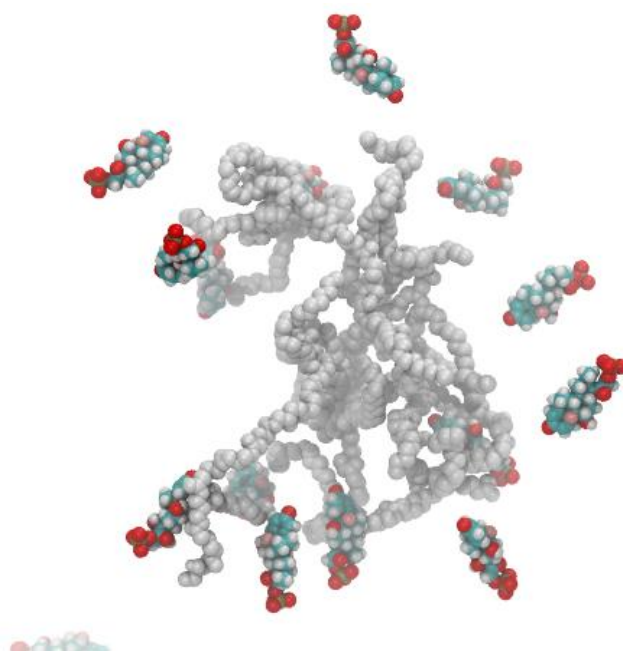


Figure 4.52 Snapshot taken from a simulation of PGA₁₀₀ with DXMP. DXMP molecules position themselves at the surface of the acetone drop in a specific orientation.

Whilst the polymer chains are in an extended conformation in the acetone drop they have interactions with DXMP molecules at the surface of the acetone drop. This could help draw more drug molecules onto the surface of

the acetone drop also increasing the amount of drug encapsulated in the assembling nanoparticle. These interactions could be specific to this drug-polymer combination as the amphiphilic nature of DXMP and the solubility of PGA₁₀₀ both enable this to happen.

In practical formulation experiments, DXMP-loaded nanoparticles were found to display a 20% larger zeta potential than non-loaded polymer nanoparticles⁵. This finding is one indication that the simulation is consistent with experimental data and suggests the orientation of DXMP seen in these simulations – i.e. with the exposed phosphate groups at the surface of the nanoparticles, is a plausible explanation for the experimentally observed negative zeta potentials for DXMP containing nanoparticles.

Once the acetone is fully dispersed a few acetone molecules are still present at the surface of the nascent nanoparticle next to the DXMP molecules also present at the surface (Figure 4.51E-F). Experimentally acetone is allowed to evaporate and it is assumed that all of the acetone evaporates from the water eventually. We are limited to simulating only short time frames so it is not known if these acetone molecules remain on the surface of the particles or not.

This simulation emphasizes the importance of having acetone present in the model. Modelling a single solvent type whose characteristics were ‘morphed’ from acetone to water over the course of the simulation, in a manner similar to Spaeth *et al.*, produced structures similar to those seen in simulations of pure water (see Chapter 3). The dispersion and subsequent shrinkage of acetone drop brings polymer chains together and promotes their entanglement into a nanoparticle.

Furthermore DXMP behaves differently in the presence of a shrinking acetone drop as already described. With a single solvent particle there is no opportunity for DXMP to interact with the surface of an acetone drop. DXMP interaction with acetone drop may drive its encapsulation into PGA_{100} due to the shrinkage of the acetone drop. Without acetone, drug molecules would have to drift into the vicinity of the aggregating polymer nanoparticle.

4.2 Simulation of $\text{PGA}_{20}\text{-co-C18PGA}_{80}$ nanoprecipitation in the presence of DXMP

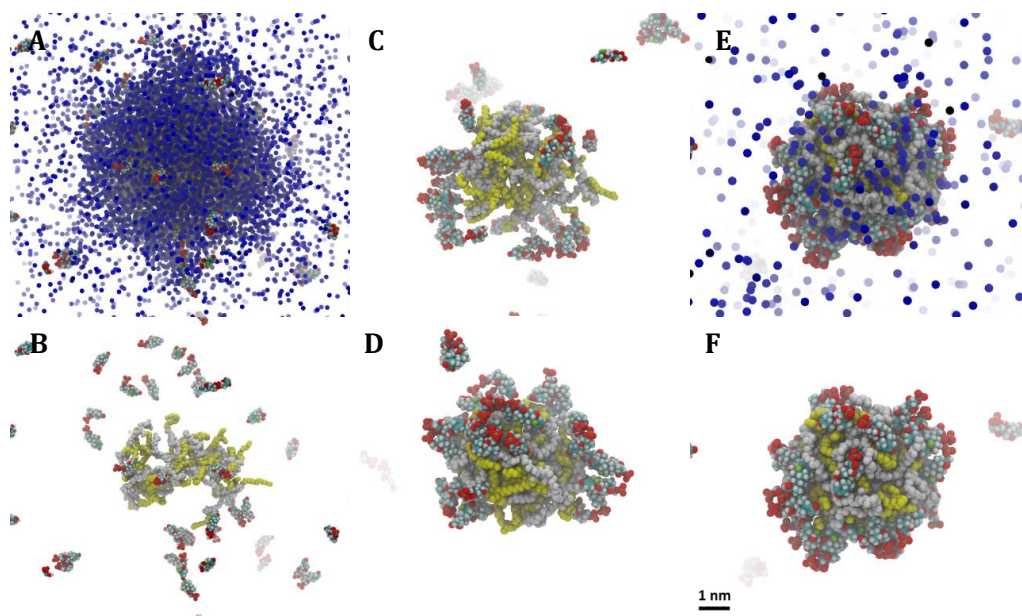


Figure 4.53 Snapshots taken during the 80ns multiscale simulation of $\text{PGA}_{20}\text{-co-C18PGA}_{80}$ with DXMP. A: 5ns (with acetone shown), B: 5ns, C: 30ns, D: 50ns, E: 80ns (with acetone shown), F: 80ns. DXMP (red/blue/white), PGA (white), C18 chains (yellow), acetone (blue). Water and CG virtual sites not shown for clarity.

Experimental data suggests that at this specific degree of polymerisation (30mer) $\text{PGA}_{20}\text{-co-C18PGA}_{80}$ should display the best encapsulation efficiency when compared with PGA_{100} and C18PGA_{100} . Our aim was to test if our multiscale simulations could also match this experimental

trend. PGA_{20-co-C18}PGA₈₀ was simulated in exactly the same conditions as PGA₁₀₀ except two polymer chains were used instead of three inside the acetone drop.

PGA_{20-co-C18}PGA₈₀ differs from PGA₁₀₀ by having less hydroxyl groups and long hydrophobic acyl chains that extended away from the polymer in acetone (Figure 4.53C). The polymer is less soluble in water and the result is that the C18 chains on the polymer were able to interact with DXMP molecules near the surface of the shrinking acetone drop. More drugs ended up positioned at the surface of the shrinking acetone drop and so this polymer was able to encapsulate more DXMP molecules in total when compared with PGA₁₀₀.

Towards the end of the simulation the polymer chains were more exposed to the surrounding water and so the C18 chains become more buried in the emerging nanoparticle (Figure 4.53D-F). However, due to the degree of side-chain functionalisation of this polymer there was insufficient PGA backbone to shield the hydrophobic C18 chains fully from the surrounding water. This left some C18 chains exposed to interact with DXMP molecules at the surface (Figure 4.53F). Considering the orientation of the DXMP molecules was such that the hydrophobic steroid part of the molecule faces the nanoparticle surface, these C18 chains can now make strong interactions with DXMP as it is drawn onto the nanoparticle surface. These strong interactions could affect the release of DXMP from these nanoparticles.

4.3 Simulation of C18PGA₁₀₀ nanoprecipitation in the presence of DXMP

The experimental data on C18 functionalised PGA with DXMP shows that PGA₂₀-co-C18PGA₈₀ is the optimal polymer. The reasons for this are unclear but the most striking result from the experiments studies on PGA is that C18PGA₁₀₀ displays a marked decrease in encapsulation efficiency when compared with PGA₂₀-co-C18PGA₈₀. This result suggests that the increase in hydrophobicity and elimination of free hydroxyl groups from the polymer influences its ability to encapsulate DXMP. Our aim here was to simulate C18PGA₁₀₀ nanoprecipitation to gain an insight into this experimental trend.

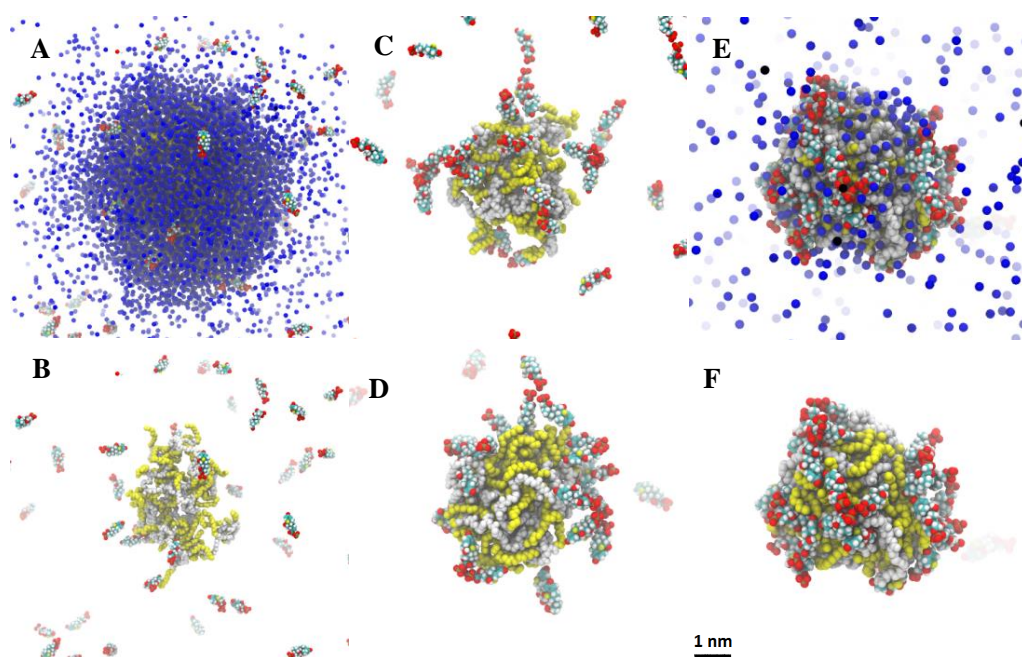


Figure 4.54 Snapshots taken during the 80ns multiscale simulation of C18PGA₁₀₀ with DXMP. A: 5ns (with acetone shown), B: 5ns, C: 30ns, D: 50ns, E: 80ns (with acetone shown), F: 80ns. DXMP (red/blue/white), PGA (white), C18 chains (yellow), acetone (blue). Water and CG virtual sites not shown for clarity.

The simulations for C18PGA₁₀₀ were similar to the simulations with PGA₂₀-co-C18PGA₈₀. DXMP maintains a similar orientation at the surface of

the acetone drop and the final aggregated nanoparticle had C18 chains exposed that interact with DXMP (Figure 4.54). This was expected as C18PGA₁₀₀ is a very similar polymer to PGA₂₀-co-C18PGA₈₀.

The surface of the nascent nanoparticle (Figure 4.54F) appeared to contain more exposed C18 chains. Compared with PGA₂₀-co-C18PGA₈₀ there are more C18 chains, but as only the same number can be buried, into the core of the nanoparticle upon aggregation there were a greater number of exposed chains. These exposed C18 chains could play a role in increasing interactions with DXMP's hydrophobic steroid rings. Increasing the acylation of PGA changes the packing of the chains in the nanoparticle and could change its ability to interact with DXMP. A more hydrophobic polymer should pack its C18 chains tighter in the nanoparticle reducing interactions with drug molecules.

4.4 Model validation through resolution transformation

To assess the accuracy of our multiscale simulations it would be desirable to compare with equivalent simulations run with a fully atomistic force field. By converting the CG solvent to atomistic solvent and removing the CG virtual sites, we created fully atomistic systems for a pure AAMD simulation.

Our aim was to perform AA simulations on snapshots from the 80ns multiscale simulation. This would allow comparison of the multiscale force field with an atomistic force field. The full simulation system is too large to be studied at the atomistic level, therefore subsections from the 80ns multiscale

nanoprecipitation simulation, centred on the nascent nanoparticle, were extracted at three time points (30, 50, and 80ns). These subsections were simulated using an atomistic and multiscale force field separately and the behaviour of the polymer and drug molecules was examined.

These subsections are still in an active state of acetone dispersion. As such the comparison simulations were limited to 5ns of molecular dynamics. This is because we only wanted to analyse the behaviour of the molecules at this time point and not the dynamics of the system over time. Longer simulations would result in dispersion of the acetone drop especially at the 30ns time point.

Our goal was that the dynamics in both simulations should be as similar as possible. Two particular features of the simulations that seemed to be important for influencing encapsulation efficiency were the degree of compaction of the emerging nascent nanoparticle, and the orientational preferences of the drug molecules. We evaluated the former by comparing the total radius of gyration (R_g) of the polymer cluster in atomistic versus multiscale representations, and the latter using the orientational metric described in the Methods.

Our analysis (Figure 4.55) showed that we were able to replicate both features very well using the multiscale force field. For the compaction of the nanoparticle the greatest variation in the polymer R_g was seen at the 30ns timepoint when the acetone drop is largest. This is due to the solubility of the polymer in acetone causing variations in the cluster size. Whilst the fluctuation of the R_g was large it is similar for both force fields used. Notably for PGA₂₀-co-C18PGA₈₀ at the 30ns time point a decrease in R_g was seen. This is

presumably due to the dispersion of acetone during the 5ns simulation that effects the compaction of the nanoparticle. However, the changes in R_g that were seen in the atomistic simulation are matched with the multiscale representation.

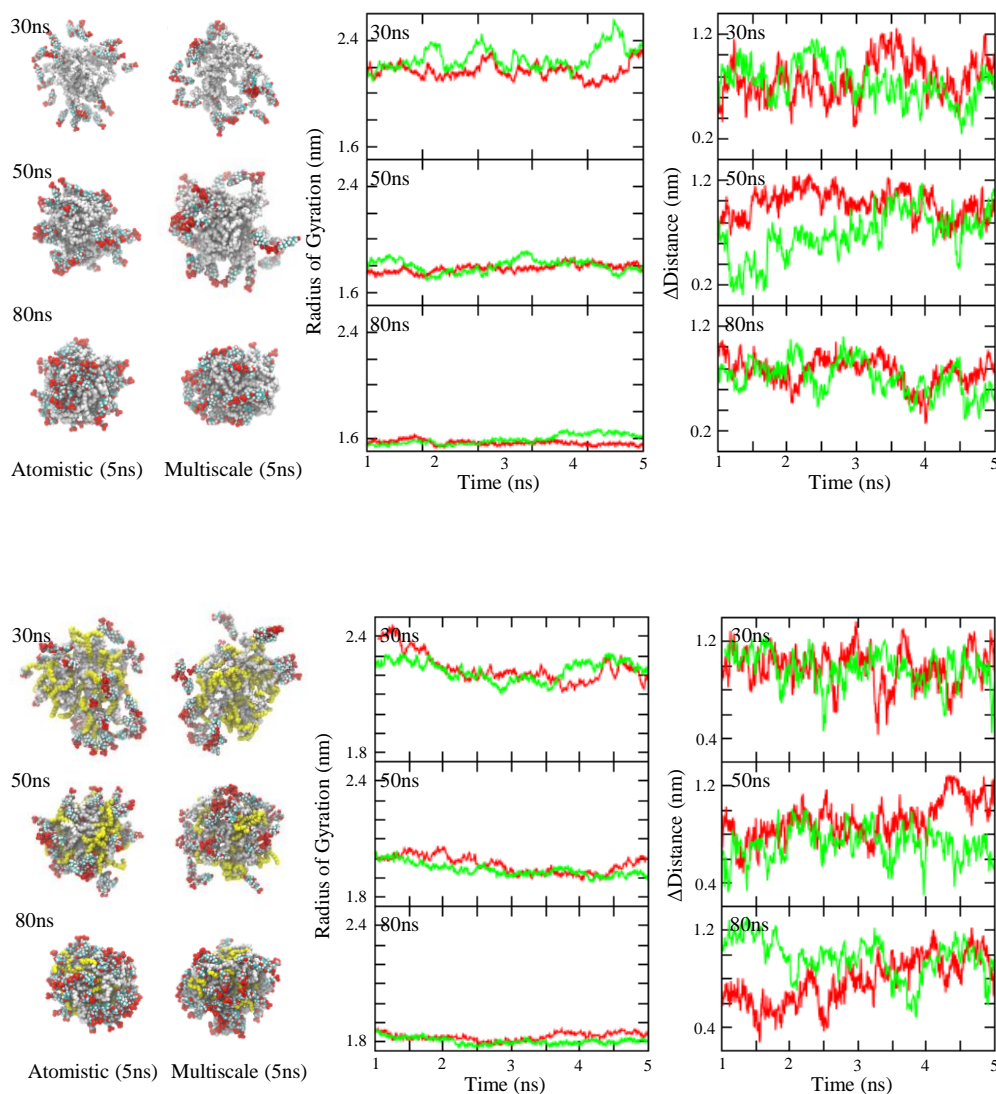


Figure 4.55 Analysis for PGA_{100} (top) $PGA_{20-co-C18PGA_{80}}$ (bottom) with DXMP. Left: Two snapshots from the end of the 5ns simulations. DXMP (multi), PGA (white with C18 chains yellow). Graphs for the total radius of gyration of the polymer cluster (middle) and the orientation of DXMP in relation to the centre of mass of the polymer chains (right). Atomistic (red), multiscale (green).

The orientation of DXMP also fluctuates during the 5ns simulations. This was mostly seen at the 50ns and 80ns time points. As DXMP begins to interact with the surface of the polymer cluster its orientation can change more drastically than when it is positioned at the surface of the acetone drop. Drug molecules can lay flat on the surface of the nanoparticle and this will reduce the Δ distance observed. However, whilst changes are seen they were similar with both force fields used.

The greatest differences between the simulations was seen at the start of the simulations when the simulation is still equilibrating to the resolution transformation of the solvent. Replacing large spheres with small atomistic molecules requires the solute molecules to reorientate around the atomistic solvent. Whilst the CG molecules lack any polarity the atomistic molecules they were replaced with do. The interactions with the atomistic solute can be different depending on the orientation of the atomistic solvent molecules close by. With this in mind it is important to consider the orientation of DXMP towards the end of the simulations and it is at this point the two simulations are predominately in good agreement.

Resolution transformation of the C18PGA₁₀₀ simulation was not performed due to the polymer's similarity to PGA_{20-co-C18PGA}₈₀. Both of these polymers have the same CG interactions with the CG solvent as they possess the same virtual sites.

4.5 Encapsulation Efficiency and Drug Loading

Experimentally, PGA_{20-co-C18PGA}₈₀ nanoparticles have shown the highest DXMP loading (DL) and encapsulation efficiency (EE)¹¹. With PGA₁₀₀

and C18PGA₁₀₀ showing similar lower values for DL and EE. Our simulation results were in qualitative agreement with this trend: after running triplicates of both simulations we found an increase in EE and DL for PGA₂₀-co-C18PGA₈₀ over the other two polymers simulated (Table 4.1).

| Acylation (%) | Encapsulation Efficiency (%) | Drug Loading (%) |
|----------------------|-------------------------------------|-------------------------|
| 0 | 5.93 +/- 0.25 | 44.76 +/- 1.05 |
| 80 | 8.73 +/- 0.25 | 46.60 +/- 0.71 |
| 100 | 6.07 +/- 0.09 | 34.16 +/- 0.35 |

$$\text{Encapsulation Efficiency} = \frac{\text{Mass of drug in nanoparticle}}{\text{Total mass of drug used}}$$

$$\text{Drug Loading} = \frac{\text{Mass of drug in nanoparticle}}{\text{Total mass of nanoparticle}}$$

Table 4.1 Encapsulation efficiency and drug loading for the three polymer systems is calculated for triplicate repeats. Data is obtained from the final snapshot of the simulation.

A direct comparison of these values to the experimental data, whilst possible, was not considered due to multiple reasons. The size of our nanoprecipitation simulation is incredibly small compared to real life experiment. Experimentally nanoparticles formed are roughly 150 nm in diameter. The nanoparticles produced by simulation are ~4 nm in diameter, roughly 30 times smaller than those made experimentally. Therefore the addition a single drug molecule has a much more profound effect on the drug loading as this is based on the total weight of the nanoparticle.

Additionally the volume of water in the simulation has to be fixed. Experimentally the volume ratio between acetone and water is much larger. This affects the encapsulation efficiency because it is dependent on the total mass of drug present in the solvent. As such the drug loading values are likely a better metric for comparison with experimental values.

We found the simulation values for EE were lower than those found experimentally. EE is dependent on the total drug that the nanoparticle can hold. In our simulations a large majority of the nanoparticle surface was covered in drug molecules. Additionally the simulations were only run for 80ns and additional drug may bind to the nanoparticles if the simulations were longer. A much larger particle with a larger surface area should be able to bind more drug at the same concentration as there is more room for drug to interact with the surface of the nanoparticle. Whilst the EE for PGA₁₀₀ is quite similar to experimental data (5.93% vs. ~8% from experiment), the other polymers show large differences from experimental values.

DL is the opposite, simulation values are larger than those found experimentally. Again this could be due to the size of the simulated nanoparticle. DL is dependent on the mass of drugs present in the nanoparticle and the mass of the nanoparticle itself. If the majority of DXMP binds to the surface of the polymer nanoparticle then for a small nanoparticle the drug loading is large. However, for a large polymer size with predominately surface bound DXMP the drug loading decreases as the weight of the polymer has increased significantly over the amount of drug encapsulated. A larger sized particle has a lower surface area to volume ratio so for an equivalent amount of polymer there would be less drug binding for a larger particle.

For these reasons it is difficult to compare our small scale simulations directly with experimental data. We decided instead to focus on the comparison of the EE and DL between different polymers which is in good agreement.

4.6 Testing Drug Binding Affinity

As discussed in the Methods, some DXMP molecules do not strongly interact with the surface of the polymer nanoparticle. However, these drugs were still counted as encapsulated by the nanoparticle based on a subsequent simulation in pure water.

The polymer nanoparticle, including DXMP and acetone molecules near the surface of the particle, was placed in a new periodic box filled with water. Experimentally once the particles are formed they are eventually washed in pure water to remove any drug that is not fully encapsulated. This simulation attempts to mimic this process in order to ascertain how DXMP interact with the nanoparticle during washing (Figure 4.56).

For PGA₁₀₀ a drug was chosen that made minimal contacts with the polymer nanoparticle at the end of the 80ns nanoprecipitation simulation. During the subsequent 20ns “washing” simulation the drug quickly brings its hydrophobic steroidal backbone in greater contact with the polymer whilst keeping its hydrophilic phosphate group exposed to the surrounding water. Additionally the polymer appears to cluster around the drug molecule to make stronger contact.

The same was true for PGA_{20-co-C18}PGA₈₀ with DXMP. Figure 4.56F shows that C18 chains in yellow move to make interactions with the hydrophobic steroid part of DXMP. The hydrophobic C18 chains of this polymer appeared to make stronger interactions with the drug when compared with PGA₁₀₀. This could result in a better drug release profile for this polymer over PGA₁₀₀ as drugs are held more tightly by the nanoparticle.

A drug delivery system aims to release drug over a prolonged period of time rather than burst release. From this simulation it was seen that PGA₁₀₀ is more likely to show a burst release of DXMP as it made less interaction with the drug than PGA_{20-co-C18PGA}₈₀. With PGA_{20-co-C18PGA}₈₀ the polymer moved to make strong hydrophobic interactions with the drug whilst the more hydrophilic parts of the polymer were still interacting with the hydrophilic part of the drug.

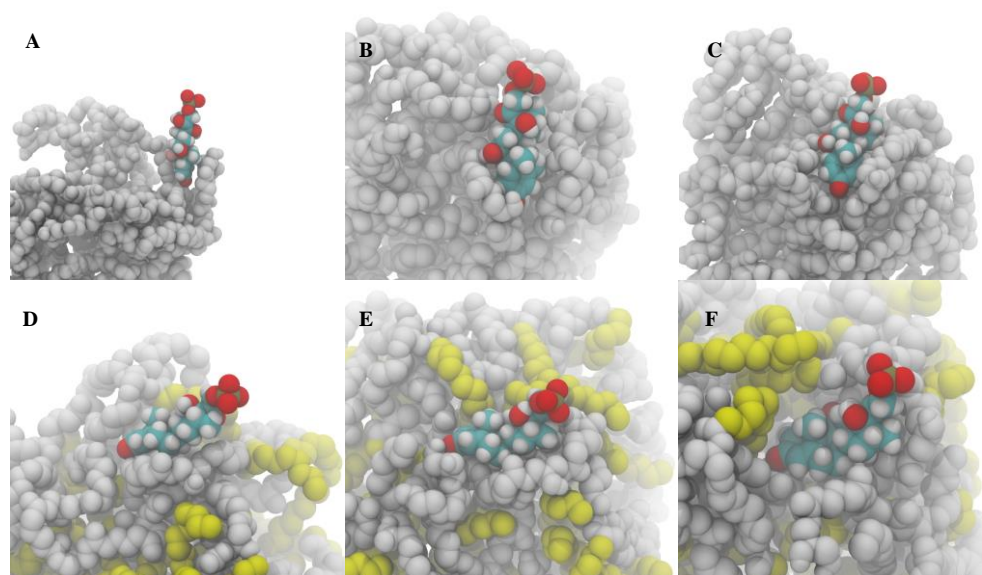


Figure 4.56 Snapshots taken during a 20ns pure water simulation of the final nascent nanoparticles from the 80ns nanoprecipitation simulation of PGA₁₀₀ (A,B,C) and PGA_{20-co-C18PGA}₈₀ (D,E,F) with A and D being the start, B and E middle and C and F the end of the simulation. PGA (white), C18 chains (yellow) and DXMP (multi). For clarity only a single drug molecule with no CG solvent or virtual sites are shown.

4.7 The Importance of Acetone Dispersion

The general fit of the experimental trends observed for drug incorporation by the simulations provides mechanistic insight as to why PGA_{20-co-C18PGA}₈₀ is the most effective polymer at encapsulating DXMP.

From our simulations we observed that DXMP preferentially interacts with the acetone water interface, resulting in multiple molecules positioning at the surface of the shrinking acetone drop. As the drop reduces in size this brings the drug molecules towards the surface of the aggregating polymer chains. This drives the interaction of DXMP with the polymer nanoparticle.

One advantage of using a computational model is that it can be quickly adjusted to test new hypotheses. To further assess the effect of acetone dispersion on drug loading and encapsulation efficiency we ran two simulations. The first involved PGA₂₀-co-C18PGA₈₀ with DXMP in pure water without acetone. The polymer and drug molar ratios were kept the same as in the original multiscale simulation with acetone and the polymer chains started in a similar configuration as they did for the 80ns nanoprecipitation simulation. We found a 23% reduction in DL and 43% decrease in EE when compared to the original simulations using an acetone droplet.

The second simulation tested the effect of the rate of acetone dispersion by adjusting the diffusion constant of acetone in water. When acetone disperses at a faster rate we found a 47% reduction in drug loading and a 69% reduction in encapsulation efficiency when compared with the original simulations.

These results, albeit difficult to reproduce experimentally, confirm our initial findings that acetone plays a major role in bringing drug molecules close to the surface of the polymer. When the dispersion of an acetone drop is not present or artificially sped up, the encapsulation of drug within the polymer nanoparticle is reduced. DXMP benefits from having interactions with both the acetone and water and this allows drug molecules to be drawn towards the polymer as the acetone drop shrinks, increasing encapsulation efficiency and

loading. This behaviour may be unique to DXMP and when using nanoprecipitation to form a drug delivery system it is important to not only consider the drug-polymer interactions involved but the drug's solubility in both solvents used.

The positioning of DXMP at the acetone drop surface could also explain why this drug is encapsulated better than cytarabine by PGA and its derivatives experimentally¹¹. DXMP is amphiphilic ($\log P = 1.56$) and can interact favourably with both the organic and aqueous phases in the system. However, cytarabine is neutral with a $\log P$ of -2.8 and as such may not be able to adopt this orientation on the acetone surface and hence will not be pulled into the surface of the aggregating nanoparticle.

An 80ns nanoprecipitation simulation of PGA₁₀₀ with cytarabine confirmed this hypothesis. Using experimental conditions similar to simulations with DXMP, PGA₁₀₀ had low EE and DL with cytarabine. Our simulations also showed that cytarabine does not interact with the acetone drop as hypothesised reducing its encapsulation within PGA₁₀₀. For cytarabine, drug encapsulation is reliant on drug diffusing towards the surface of the polymer nanoparticle (Figure 4.57).

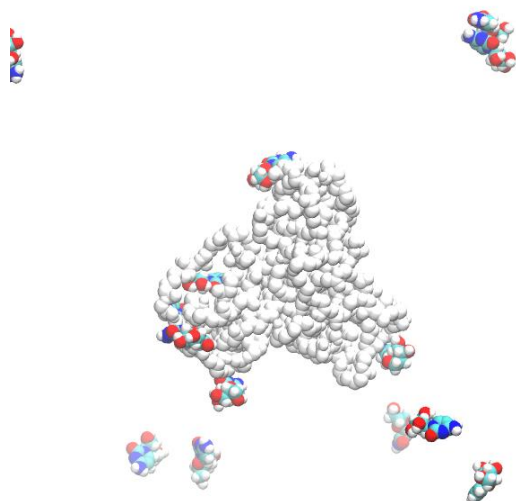


Figure 4.57 Snapshot taken at the end of a simulation containing three chains of PGA₁₀₀ with cytarabine. PGA₁₀₀ (white), cytarabine (multi). CG solvent and virtual sites are not shown for clarity.

When designing future drug delivery systems it is important to consider the interactions between the drug and solvent. For acetone in water an amphiphilic drug that interacts with both solvents appears to exhibit increased EE and DL. This phenomenon appears to be independent of the polymer used.

4.8 Explanation for the Experimental Trend

The dispersion of acetone is consistent in all three systems yet we see differences in encapsulation efficiency i.e. the amount of drug that reaches the surface of the polymer nanoparticle. We analysed the interaction of the polymer chains with DXMP over the course of the 80ns simulations (Figure 4.58). Specifically we looked within the 1.2 nm cut-off for intermolecular interactions used in the simulations. This ensured we only consider drug molecules that are interacting specifically with the polymer.

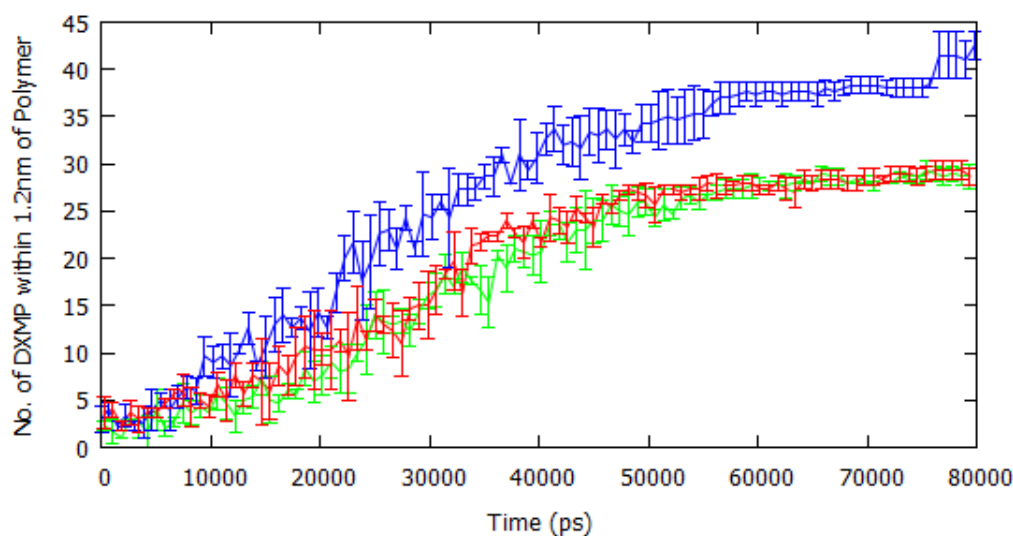


Figure 4.58 Number of DXMP molecules within 1.2 nm of the polymer chains is analysed for all three polymers over the 80ns simulations. Error bars are included for the standard error of the mean from triplicate repeats. PGA₁₀₀ (red), PGA_{20-co-C18PGA₈₀} (blue), C18PGA₁₀₀ (green).

As the acetone drop dispersed during the simulation, DXMP molecules were brought within the 1.2 nm cut-off as they interacted with the polymer chains inside. At first there was a consistent increase for all three polymers over the first 20ns. However after 20ns PGA_{20-co-C18PGA₈₀} was able to interact with more drug molecules than the other two polymers. More DXMP molecules are present at the acetone drop surface when it contains PGA_{20-co-C18PGA₈₀} polymer chains, indicating an increased affinity for the drug. By 50ns acetone had dispersed enough to allow all the DXMP molecules that were present at the acetone drop surface to interact with the polymer nanoparticle. For the rest of the simulation there was little change in the number of DXMP within the 1.2nm cut-off.

However, it is noteworthy that for PGA_{20-co-C18PGA₈₀} there was a sharp rise in the number of drug molecules interacting with the nanoparticle.

This is due to a cluster of drug molecules binding to the surface of the nanoparticle (Figure 4.59).

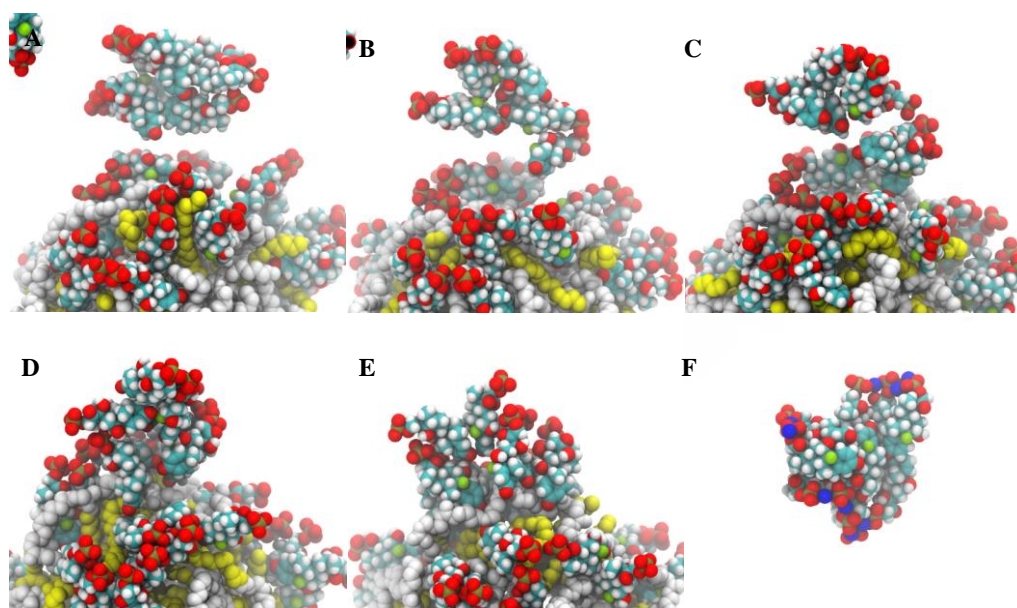


Figure 4.59 Snapshots taken from a $\text{PGA}_{20}\text{-co-C18PGA}_{80}$ multiscale simulation with DXMP. (A-E) A drug cluster binds to the surface of the polymer nanoparticle. (F) A drug cluster in solution formed during the 80ns simulation.

Visual analysis revealed the cluster interacts initially with other drug molecules on the surface. Interaction with the C18 chains of the polymer was only observed after the drug molecules re-orientate across the surface of the particle. Whilst this may be a chance occurrence it was not observed for the other two polymers.

This result suggests that the number of drugs encapsulated within these polymers may potentially increase during longer simulations. Drug molecules diffusing in the surrounding water may collide with the formed nanoparticle and become encapsulated. It is not realistic to test these events with the model due to the slow speed of the simulation. As the total simulation time is kept constant for all the polymers tested, the comparison between them is still fair.

The difference in the number of DXMP interacting with the three different polymer chains occurred during the 20-50ns time frame. This is a key point in nanoprecipitation where acetone begins to disperse revealing the aggregating polymer chains inside the acetone drop.

A number of factors are involved in how many drugs reach the surface of the acetone drop and were subsequently encapsulated in the polymer nanoparticle. The solubility of the polymer chains in both solvents affected the rate of polymer aggregation. A more aggregated polymer had fewer interactions with DXMP molecules surrounding the acetone drop.

Additionally, the functional groups on the polymer played a role as the C18 chains on $\text{PGA}_{20}\text{-co-C18PGA}_{80}$ and C18PGA_{100} made stronger hydrophobic interactions with DXMP. These C18 chains were in an extended conformation in acetone but when exposed to water they became buried into the nanoparticle. When buried, the interactions with surrounding DXMP molecules were decreased resulting in less DXMP bound to the nascent nanoparticle (Figure 4.60).

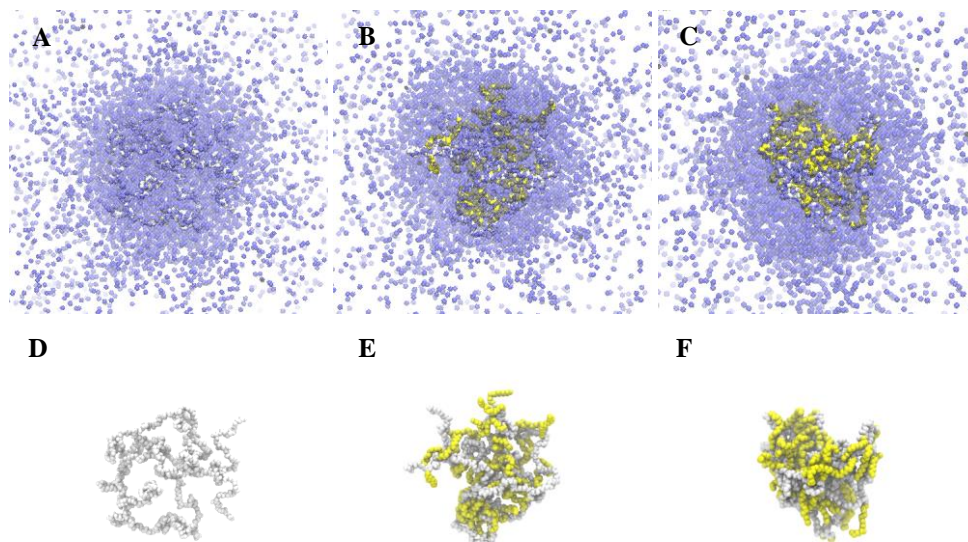


Figure 4.60 Snapshots taken at the around the 20ns time point of the nanoprecipitation simulations. PGA₁₀₀ (A,D), PGA_{20-co-C18PGA}₈₀ (B,E), C18PGA₁₀₀ (C,F). Acetone is shown on the top row of snapshots to indicate the size of the acetone drop. PGA (white) and C18 chains (yellow). Water is not shown for clarity.

A polymer needs to maintain good solubility in both solvents to ensure it is in an extended, un-aggregated state for as long as possible. This guarantees maximum interaction with surrounding DXMP molecules before the polymer fully aggregates into a nanoparticle. However, hydrophobic moieties that reduce the solubility of the polymer are still required. C18 chains formed stronger interactions with DXMP than the PGA backbone in the simulation. Whilst hydroxyl groups may be necessary for the solubility of the polymer they do not seem to form strong interactions with the drug molecules. A balance of hydrophobic and hydrophilic moieties is required to ensure optimal interactions with surrounding DXMP molecules.

To analyse this further the total radius of gyration (R_g) for the polymer clusters was calculated during the 10-50ns time period where acetone disperses and water begins to interact with the polymer chains (Figure 4.61).

In acetone the polymers were relatively soluble and so the total R_g was large and fluctuated. However, as acetone dispersed, the polymer was exposed to water and this triggered the aggregation of the polymer chains. PGA_{100} was the most soluble of the three polymers in both acetone and water and so maintained a large total R_g during this time period. The total R_g for $\text{PGA}_{20}\text{-co-C18PGA}_{80}$ and C18PGA_{100} was lower due a decrease in solubility arising from the acylation of PGA. However, the total R_g was higher for $\text{PGA}_{20}\text{-co-C18PGA}_{80}$ as it contains 20% more hydrophilic hydroxyl groups than C18PGA_{100} . This allowed $\text{PGA}_{20}\text{-co-C18PGA}_{80}$ to maintain a more extended conformation during the simulation than C18PGA_{100} during this crucial time period.

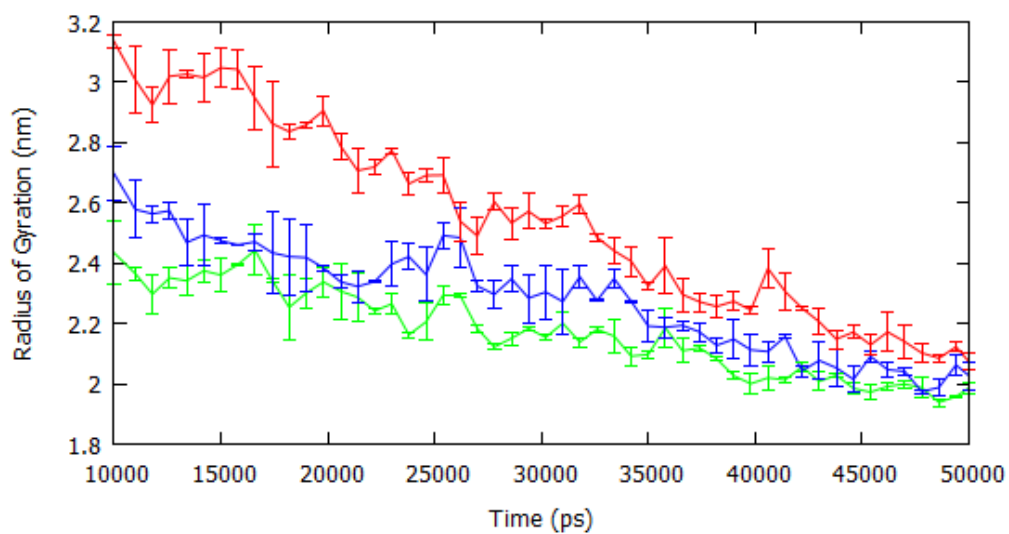


Figure 4.61 The radius of gyration of the all the polymers in each system over the 10-50ns time period of the 80ns multiscale simulation. Error bars are included for the standard error of the mean from triplicate repeats. PGA_{100} (red), $\text{PGA}_{20}\text{-co-C18PGA}_{80}$ (blue), C18PGA_{100} (green).

Overall $\text{PGA}_{20}\text{-co-C18PGA}_{80}$ was able to interact with more DXMP molecules in the surrounding water. This pulled more DXMP onto the acetone

drop surface which subsequently increased drug loading with this particular polymer.

Whilst PGA₁₀₀ had the largest total R_g , indicating it interacted the most with surrounding DXMP molecules, it lacks the hydrophobic C18 chains that are required for strong interactions with DXMP.

4.9 Conclusion

The results from this chapter on polymer drug compatibility are in agreement with contact angle measurements on similar PGA polymers by Orafai et al.⁴⁰ A PGA₆₀-co-C8PGA₄₀ polymer showed the lowest surface free energy when compared with PGA₁₀₀ and C8PGA₁₀₀ polymers. It was hypothesised that this due to a balance of polar and nonpolar components in the polymer.

The balance of polymer polarity/hydrophilicity was also proposed from experimental data by Kallinteri et al.¹² However, they suggested that hydroxyl groups on PGA may play a role in interacting with the DXMP's phosphate groups forming hydrogen bonds. This is an assumption that drug-polymer interactions drive encapsulation. Our simulations revealed that whilst DXMP may form hydrogen bonds with PGA's hydroxyl groups it is the solubilities of the drug and polymer molecules in the two solvents used that affects the encapsulation efficiency of this particular polymer-based drug delivery system.

Our simulations have revealed intricate processes that affect drug encapsulation. Molecular dynamics has provided a unique insight into nanoprecipitation. Whilst drug-polymer interactions are important, solubility of the solutes in both solvents is also significant. Changes to the polymer may

enhance drug-polymer interactions they may also affect polymer solubility. However, this could have the opposite effect on encapsulation efficiency than intended. For this reason carrier and drug solubility should also be considered when optimising a drug delivery system.

Chapter 5

Incorporation of DXMP into PGA Nanoparticles: Atomistic Model

The simulation of nanoprecipitation, including the dispersion of acetone, requires a large amount of molecules to interact simultaneously. Specifically the amount of solvent is vast, slowing down the speed of the simulation significantly. To overcome this, solvent molecules were coarse-grained and a multiscale model was used to enable AA solute molecules to interact with CG solvent molecules.

However, it has always been the case that a fully atomistic MD simulation is the most realistic MD model possible. An AA model is also more accurate than the multiscale model because it does not require the mixing of two force fields. AA force fields are well optimised and widely used in the field of computational modelling. CG models have several caveats, the most important being the loss of detailed electrostatic interactions and long-range

electrostatics. This was a major obstacle in optimising the multiscale model used in the previous chapter.

Previously AA simulations were used as reference simulations often at small scales due to their computationally demanding nature. Resolution transformation on small subsections of the multiscale nanoprecipitation simulation enabled comparison of the multiscale force field with an AA force field. However, these simulations are not ideal as only a small subsection of the entire simulation box was analysed. Preferably the entire system would be simulated for a realistic comparison between the two force fields.

Whilst we were confident in the results obtained with the multiscale force field in the previous chapter based on the resolution transformation, we were interested in the dynamics of an entirely atomistic simulation of nanoprecipitation. Without an atomistic reference simulation of the entire simulation it is difficult to be 100% sure of the accuracy of the multiscale model.

Our results so far have also shown that solvent plays a large role in encapsulation efficiency and drug loading for a polymer drug delivery system. Acetone dispersion rate and its interaction with both the polymer and drug affected how the polymer and drug interact. As we have simplified the acetone in our multiscale simulation using CG acetone, we were interested in simulating nanoprecipitation using atomistic solvent.

Our aim with this simulation was to analyse every aspect of it and compare it with our previous work. Through comparison we should be able to see faults in the multiscale model and address them in an updated force field.

5.1 Acetone Dispersion

We previously calculated that an 80ns fully atomistic simulation of PGA₂₀-co-C18PGA₈₀ in the presence of DXMP would contain over 20 million atoms. On our computational resources available this would take around 6 months to run including queuing time. As such we wanted to ensure that the simulation was as good as possible before it was run. This involved ensuring every aspect of the model was as close as possible to experimental conditions.

Based on the results from the multiscale model we knew that the dispersion of acetone would have a profound effect on the simulation. Therefore we decided to analyse the rate of atomistic acetone dispersion using an AA force field again to ensure accuracy in relation to experimental conditions.

We previously optimised the dispersion of CG acetone in CG water using AA acetone obtained from the Automated Topology Database (ATB) version 1.0. At the time this topology was considered sufficient for our needs. However, recently this acetone topology has been updated and this has altered the diffusion constant of AA acetone in AA water.

Experimentally the diffusion constant for acetone in water at various temperatures and molar fractions was determined by Tyn et al. in 1975. Our aim was to simulate the diffusion of acetone in a box of water and compare the diffusion constant with these experimental results.

Whilst AMBER and OPLS provide acetone topologies, the GROMOS force field does not and so the ATB was used to obtain one. Our original acetone model was obtained from version 1.0 of the ATB compatible with the

GROMOS 53A6 force field. This united atom topology contained neutral methyl atoms and had a +/-0.450 charge on the central carbonyl group.

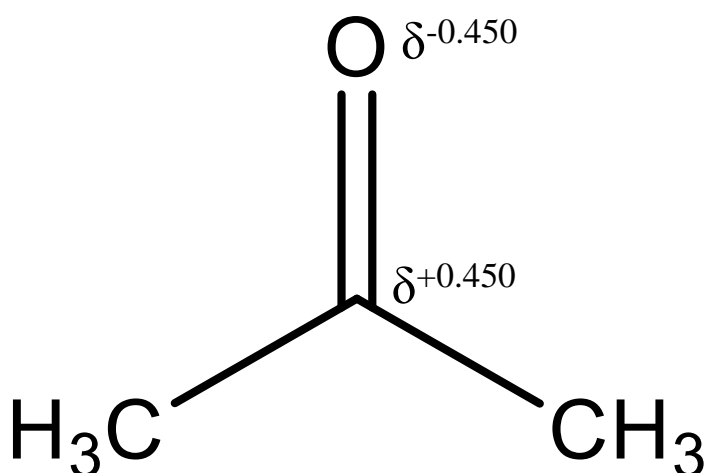


Figure 5.62 Chemical structure of acetone showing methyl groups and central carbonyl group.

Other acetone models available from the literature include WS (Weerasinghe and Smith), Perera, Vlugt and TraPPE (Transferable Potentials for Phase Equilibria) models. The WS model optimised using Kirkwood-Buff (KB) integrals has shown good performance over a range of acetone molar ratios. The KB theory relates the structure of a solution to its thermodynamic properties. KB integrals using the radial distribution function from a solvent mixture can create a topology for a molecule through optimisation against experimental data.

The WS parameters for acetone differ from the ATB v1.0 acetone topology used previously as the charge on the central carbonyl is increased to +/- 0.565. There are also differences in the sigma and epsilon values that define the Lennard Jones potential for the carbon, oxygen and methyl united atoms. Additionally the bonded parameters of the model slightly differ.

5.1.1 Molecular Dynamics Optimisation

To determine the optimal acetone topology we compared the ATB models and the WS model to determine which matched the experimental values from Tyn et al. closest.

Mixtures of acetone and water at two molar ratios: 0.024 and 0.28 were created. These ratios were chosen due to the experimental data available. The molecules were first allowed to mix fully, then a production MD simulation of 1ns was used to analyse the acetone diffusion constant in SPC/E water. As the diffusion constant varies with molar ratio we wanted to ensure that our acetone topology would have a diffusion constant similar to the experimental values at these two molar ratios.

| | Exp. | ATB v1.0 | ATB v1.2 | ATB v2.0 | WS | WS_RM |
|--|-------|-------------|-------------|-------------|--------|---------------|
| Diffusion Constant ($1 \times 10^{-5} \text{ cm}^2/\text{s}$) | 0.650 | 2.263 | 0.477 | 1.461 | 0.934 | 0.655 |
| Oxygen Charge | n/a | -0.450 | -0.652 | -0.568 | -0.565 | -0.626 |
| Carbon Charge | n/a | +0.450 | +0.652 | +0.734 | +0.565 | +0.626 |

Table 5.1 Summary of the atomistic acetone models tested and compared with experimental data for the diffusion constant of acetone in water at a molar ratio of 0.28.

At a 0.28 molar ratio the diffusion constant of acetone experimentally is $0.650 \times 10^{-5} \text{ cm}^2/\text{s}$. The original WS model produced a diffusion constant of $0.934 \times 10^{-5} \text{ cm}^2/\text{s}$, this was adjusted to $0.655 \times 10^{-5} \text{ cm}^2/\text{s}$ by increasing the charge on the carbonyl of acetone to ± 0.626 . The other bonded parameters of the WS model were left unchanged but this slight increase in the polarity of the molecule changed its diffusion constant to match the experimental data.

This new model, named WS_RM henceforth, was tested with a 0.024 molar ratio acetone-water mixture. This molar ratio is closer to the ratio used in the nanoprecipitation simulation (0.002). At this molar ratio the diffusion constant using the WS_RM model was $1.088 \times 10^{-5} \text{ cm}^2/\text{s}$ which is in good agreement with the experimental value of $1.140 \times 10^{-5} \text{ cm}^2/\text{s}$.

Our results show that the latest ATB parameters were unable to generate the dynamics required to match the experimental diffusion constant of acetone in water. The original version 1.0 ATB and version 2.0 acetone parameters resulted in diffusion constants that were vastly different to the experimental value.

Version 1.2 has a carbonyl charge that is similar to our optimised WS_RM model. But other parameters in the topology result in a decrease in the diffusion constant with respect to the experimental data.

The ATB acetone model may be more suited to other simulations that do not involve its dispersion in water. However, for nanoprecipitation we require the most accurate dispersion of acetone in water and so we have chosen to use the WS_RM model.

5.2 Fully Atomistic Simulation of PGA₂₀-co-C18PGA₈₀ nanoprecipitation in the presence of DXMP

The WS_RM model for acetone differs from the original ATB v1.0 acetone model to which the multiscale force field was parameterised. Compared to the multiscale model, the dispersion of acetone using WS_RM is faster. The time taken for full dispersion of acetone during nanoprecipitation is

almost halved with a full nanoparticle forming around 20-30ns into the simulation.

This difference between the models means that this fully atomistic simulation will not be identical to the multiscale simulations due to the change in acetone dispersion. A decrease in the drug loading and encapsulation efficiency is expected based on previous results on faster dispersing acetone. However, the increased dispersion speed of acetone is advantageous as the total simulation time required for nanoprecipitation is greatly reduced. The total required time required to run the simulation was reduced to ~3 months.

The fully atomistic simulation was created using identical concentrations to the previous multiscale simulations. We chose to simulate PGA₂₀-co-C18PGA₈₀ as this polymer showed the highest encapsulation efficiency and drug loading using the multiscale force field and also experimentally. Unfortunately due to time constraints we were unable to simulate nanoprecipitation with the other two polymers using a fully atomistic force field.

With the new WS_RM acetone topology the acetone drop dispersed into to the surrounding water at around double the speed. This caused faster aggregation of the polymer chains during the simulation. At 10ns almost all of the C18 chains had collapsed onto the surface of the nanoparticle and full aggregation into a nanoparticle occurred at around 20ns into the simulation (Figure 5.63).

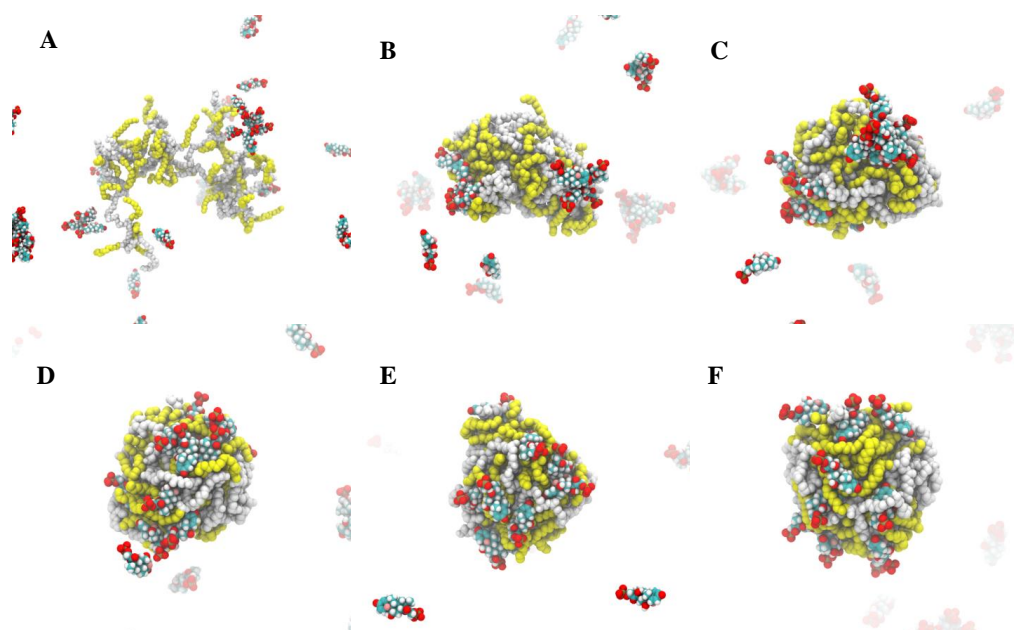


Figure 5.63 Snapshots taken during the 50ns atomistic simulation of PGA₂₀-co-C18PGA₈₀ with DXMP. A: 2ns, B: 10ns, C: 20ns, D: 30ns, E: 40ns , F: 50ns. DXMP (red/blue/white), PGA (white), C18 chains (yellow), acetone (blue). Water and acetone not shown for clarity.

Faster polymer aggregation reduced the interactions the polymer can make with surrounding drug molecules; something which was observed in the multiscale simulations. Still, C18 chains were still exposed on the surface of the polymer cluster. Similarly to the multiscale simulation these chains became buried into the polymer upon full exposure to water towards the end of the simulation.

Drug molecules that start close to the polymer chains at the beginning of the simulation formed strong interactions as the polymer quickly aggregates. Later in the simulation drug molecules bound to the surface of the nanoparticle by chance interaction whilst diffusing through the solvent. The expected orientation of the drug molecules was consistent with the multiscale simulations. Drug molecules lay flat on the surface of the nanoparticle with the charged phosphate group exposed to surrounding water and counter ions. As

the simulation progressed the polymer chains rearranged to form tighter contacts with drugs at the nanoparticle surface. This buried some drug molecules slightly deeper into the nanoparticle.

This process of the nanoparticle adapting to DXMP was also seen in multiscale simulations of polymer/drug nanoparticles in pure water after the 80ns multiscale simulation. The steroid part of DXMP is hydrophobic enough to promote stronger interactions with the polymer once it has interacted with the polymer nanoparticle surface initially (Figure 5.64).

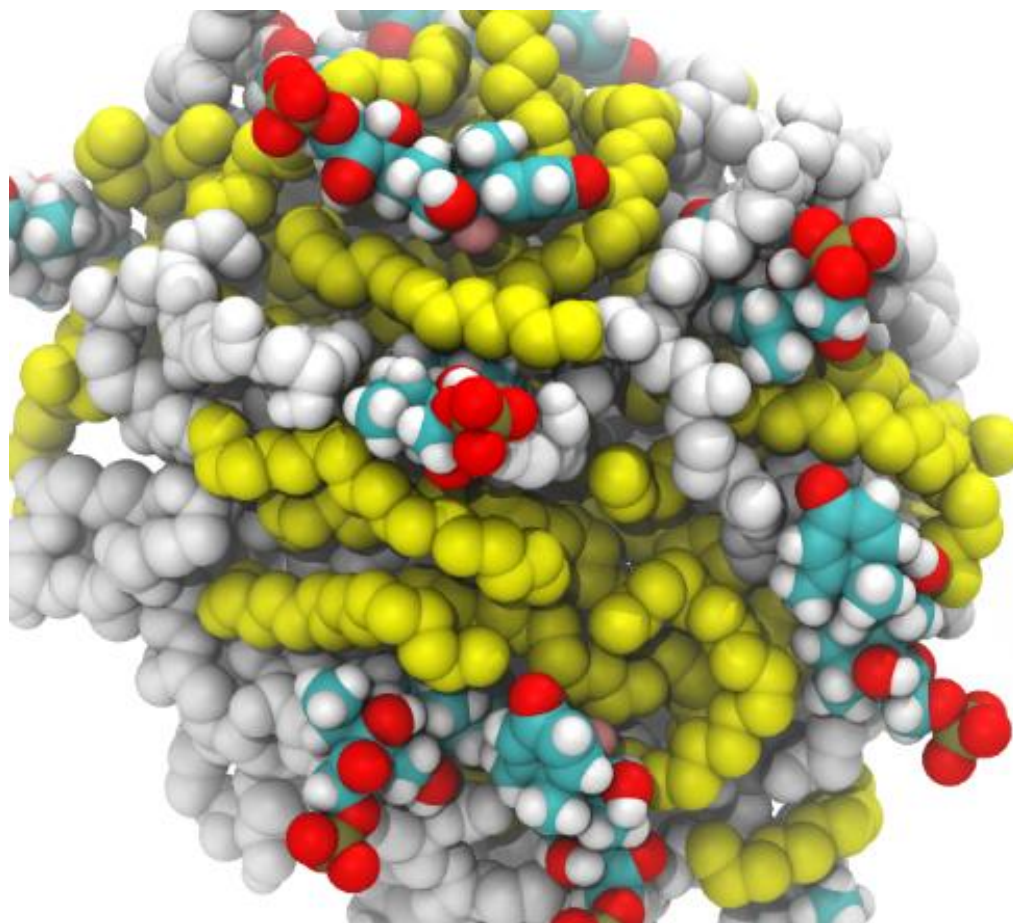


Figure 5.64 Snapshot taken at the end of the 50ns atomistic nanoprecipitation simulation. Some drug molecules are buried into the nanoparticle whilst others rest on the surface.

This highlights a potential flaw in the multiscale model. Interactions between the polymer nanoparticle and drug molecules may be reduced due to

the force field. An increase in the relative dielectric constant used for the multiscale simulation could be reducing the electrostatic interactions between these molecules. Whilst the orientation of the drug molecules is correct DXMP was unable to bury itself into the nanoparticle in the multiscale simulations.

Another reason could be due to the difference in the dispersion of acetone. Acetone maintains a droplet shape during the multiscale simulation but in the atomistic simulation acetone this does not happen. For the atomistic simulation this reduces the amount of acetone present at the surface of the nanoparticle, resulting in a more aqueous environment at the exterior of the nanoparticles compared with the multiscale model. This causes the hydrophobic steroid backbone of DXMP to become buried into the hydrophobic nanoparticle (Figure 5.65B).

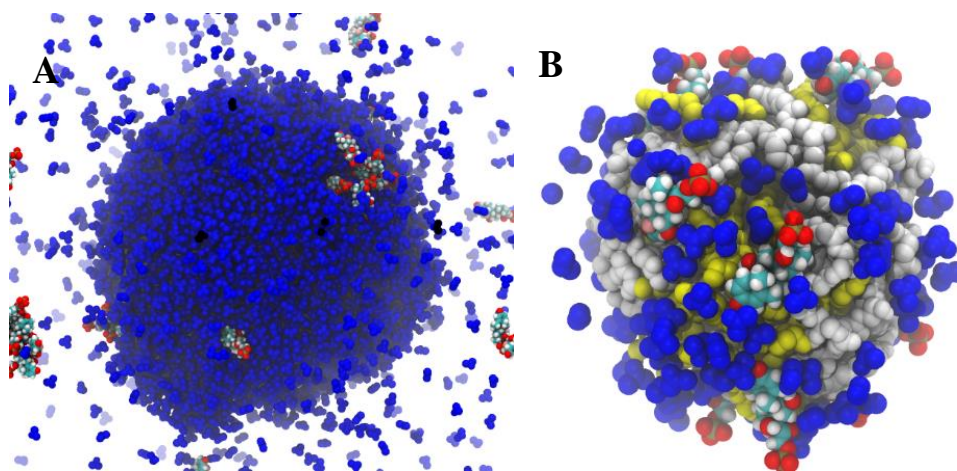


Figure 5.65 The location of acetone at the start (A) and end (B) of the 50ns fully atomistic nanoprecipitation simulation.

Furthermore acetone could be preventing further DXMP molecules from interacting with the surface of the polymer nanoparticle if they happen to drift close by. As acetone shields the hydrophobic surface of the nanoparticle further drug encapsulation could be reduced.

Experimentally nanoparticles are left to ‘harden’ overnight after they form, allowing acetone in the water to evaporate. This could allow drug molecules to make stronger contacts with the nanoparticle. However, we are unable to test this in our simulation due to time constraints.

5.3 Encapsulation Efficiency and Drug Loading

As expected the increased speed of acetone dispersion had an impact on encapsulation efficiency. As with our previous experiments on faster dispersing acetone using the multiscale force field (section 4.7), a decrease in both drug loading and encapsulation efficiency was seen. This was due to the decreased interaction between DXMP and acetone and faster aggregation of the polymer chains.

When acetone dispersed at a slower rate, as in the multiscale force field, the surface of the drop was present for longer allowing more drug molecules to interact with it. The acetone drop appeared to dissolve into the surrounding water instead of all the acetone molecules dispersing equally. This was due to strong interactions between the CG acetone beads holding them together. The result is that acetone remained as a drop for a longer time which allowed DXMP molecules to interact with its surface.

At a faster acetone dispersion rate using the WS_RM model, the acetone drop surface was less prevalent (Figure 5.66). DXMP was unable to interact with an acetone drop and therefore drugs were not brought onto the surface of the polymer as acetone dispersed.

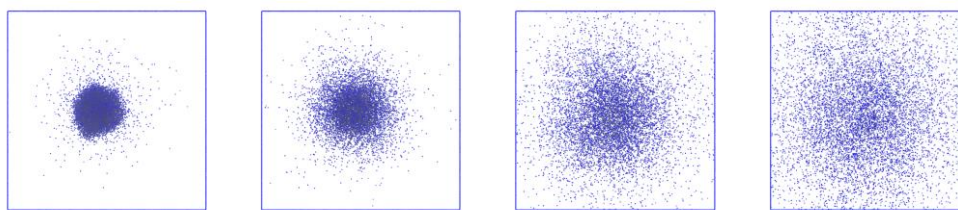


Figure 5.66 The dispersion of atomistic acetone over 50ns during the fully atomistic nanoprecipitation simulation.

In our fully atomistic simulation we found that 12 DXMP molecules were encapsulated by PGA₂₀-co-C18PGA₈₀ after 50ns. This translates to an EE of 2.4% and a DL of 24.7%. When compared with the multiscale simulation of PGA₂₀-co-C18PGA₈₀ with DXMP the EE has dropped by roughly a third and DL has halved. It should be noted this data is from a single simulation as repeats were not feasible due to time constraints.

This result reaffirms our previous understanding that acetone dispersion rate has a major role in the EE and DL for DXMP with PGA₂₀-co-C18PGA₈₀. Our results indicate that a slower dispersing solvent may increase drug loading for this polymer drug delivery system. This could be tested experimentally by using a solvent with a lower diffusion rate in water than acetone. If amphiphilic DXMP is still able to interact with this solvent then the slower dispersing solvent will allow for a greater amount of drug molecules to interact with the solvent drop before it fully disperses.

5.4 Sodium Ion Interactions

In the multiscale force field there are no electrostatic interactions between the CG solvent and the atomistic molecules in the system. As a consequence the interaction between sodium counter ions and DXMP's

phosphate group was strong. This caused almost all of the drugs to interact strongly with at least one sodium counter ion in solution during the 80ns multiscale simulation. Although electrostatics were decreased by increasing the relative dielectric constant, drugs that were unable to pair with a counter ion buried their charged phosphate groups into the polymer nanoparticle as the only other source of counter charge.

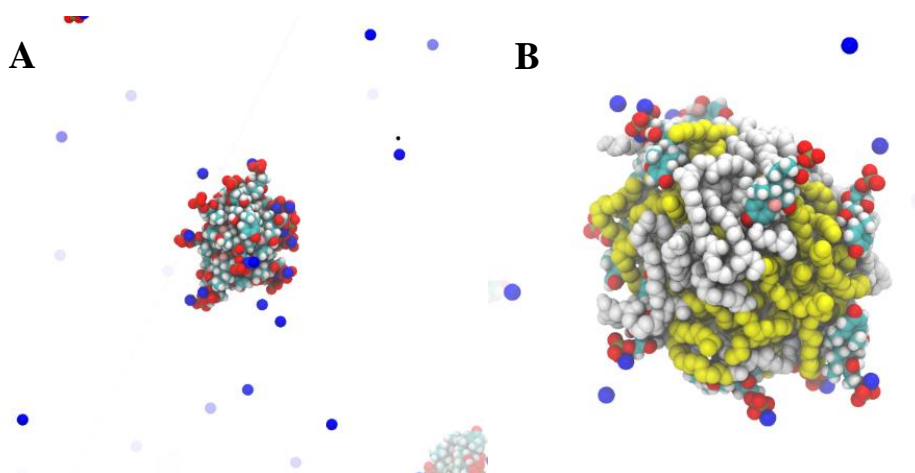


Figure 5.67 (A) A large cluster of DXMP molecules forms with sodium counter ions for the phosphate charge. (B) Phosphate groups on DXMP molecules encapsulated by PGA₂₀-co-C18PGA₈₀ interact with surrounding ions.

In the fully atomistic system solvent molecules have electrostatic interactions with the solute molecules. Whilst the interaction of sodium counter ions with the phosphate groups on DXMP was still observed, it was less pronounced. In addition we were able to observe that clusters of DXMP formed with counter ions. These clusters were also observed during the multiscale simulation. The use of particle mesh Ewald allowed for long range electrostatics between DXMP and the sodium ions resulting in presumably more realistic behaviour between these molecules.

This is difficult to replicate in the multiscale model as long range electrostatics were not used, instead a short range 1.2 nm shifted potential was used. Whilst PME could be used it is likely not the solution as the primary problem was a lack of electrostatic interactions between the solute and solvent. In bulk water the sodium counter ions were the only major counter charge for DXMP and so they bound tightly when CG solvent is used.

The phosphate group of DXMP is water soluble due to its phosphate group making hydrogen bonds with water. Dexamethasone is far less water soluble than DXMP as it has a hydroxyl group in place of the charged phosphate found on DXMP. When sodium forms strong electrostatic interactions with DXMP a salt forms that decreases interactions with the polar water molecules. This could promote its aggregation with other drug molecules that have also formed sodium salts (Figure 5.67A).

5.5 Drug Cluster Binding to the Polymer Nanoparticle

As with the multiscale simulations, DXMP clusters formed relatively quickly during the nanoprecipitation simulation in bulk water. Around 25ns into the atomistic simulation we observed a single drug cluster merging with the surface of the nascent polymer nanoparticle (Figure 5.68).

As the drug cluster contains several drugs, the binding of this cluster contributed about half of the overall encapsulated drug found in the nanoparticle at the end of the simulation.

Once the nanoparticle had formed, drug encapsulation occurred due to chance interactions with DXMP molecules diffusing through the bulk water.

When these drug molecules formed a cluster, the surface area to interact with the polymer nanoparticle increased. This might have increased the chances of drug being encapsulated.

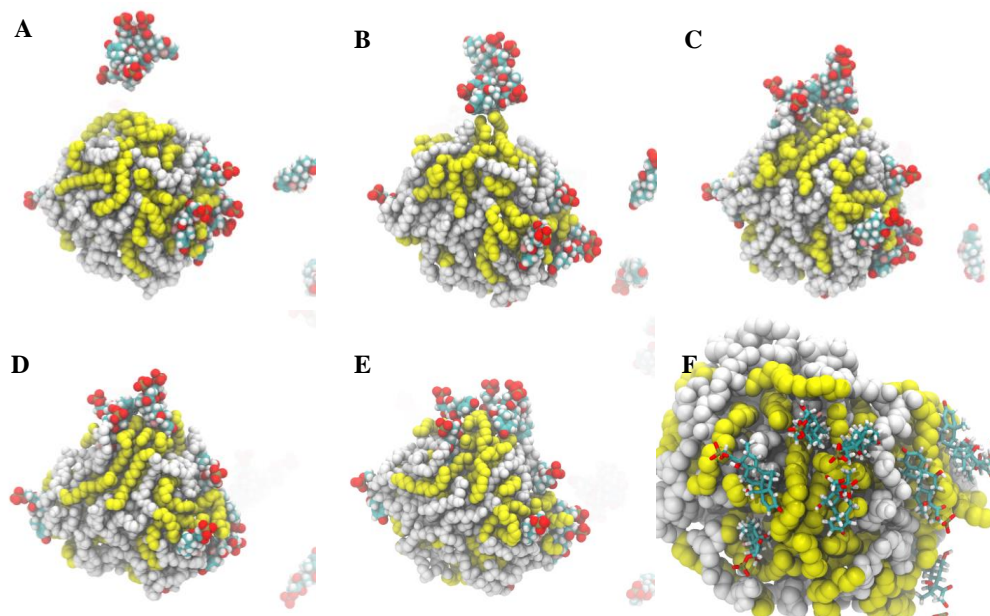


Figure 5.68 The process of a DXMP cluster merging with the surface of the polymer nanoparticle is shown over 2ns A-E. F: Close-up of where the drug bound to the surface of the polymer (drug shown with liquorice representation for clarity).

In Figure 5.68F it can be seen that DXMP preferentially bound to the yellow C18 chains of the polymer. These hydrophobic chains make strong interactions with the hydrophobic steroid rings on DXMP. The C18 chains can be seen to reach out and interact with the drug cluster (Figure 5.68B). The cluster was then brought onto the surface of the nanoparticle and broken up. The drug molecules then moved across the nanoparticle surface where they found optimal interactions predominately with the C18 chains on the polymer.

Unfortunately we were only able to run a single fully atomistic simulation of nanoprecipitation so we were unable to confirm the probability of these clusters binding to the polymer nanoparticle.

5.6 Conclusion

This simulation and the multiscale simulations in the previous chapter have shown that not only is drug-polymer compatibility important, but also interactions with solvent. An ideal solvent will ensure high solubility for the polymer and form good interactions with the drug to promote encapsulation. Slow diffusion of the polymer solvent into the counter solvent may increase the amount of drug that is brought onto the polymer nanoparticle surface and subsequently encapsulated. When optimising nanoparticle formation for a drug delivery system not only does the polymer need to be optimised through trial and error but the solvents used for nanoprecipitation should also be adjusted.

The atomistic simulation described in this chapter has shown that when acetone diffuses in accordance with experimental data, fewer drug molecules were drawn onto the polymer surface. This results in the majority of drug-polymer interactions occurring once the nanoparticle had already formed. This suggests that drug-polymer interactions may be more prevalent than first thought.

During the simulation drug clusters were able to interact with the nascent nanoparticle. These drug clusters break up on contact with the nanoparticle and individual drug molecules embed into the nanoparticle surface. This atomistic simulation showed that C18 chains facilitated this interaction.

The multiscale simulations also showed drug cluster interaction with an extant $\text{PGA}_{20}\text{-co-C18PGA}_{80}$ nanoparticle. However, DXMP did not interact with C18 chains but DXMP molecules already bound to the surface of the

nanoparticles. The atomistic simulation using a more accurate acetone dispersion rate revealed that drug loading in the multiscale simulations was artificially increased. This suggests that drug-polymer interactions rather than drug-drug interactions are most likely to facilitate the interaction with surrounding drug clusters.

This may explain why we have not observed drug cluster binding to PGA_{100} or C18PGA_{100} . PGA_{100} lacks C18 chains and may be unable to interact strongly enough with nearby drug clusters present in solution. C18PGA_{100} may lack the correct packing of the polymer in order for it to be mobile enough to extend its C18 chains out into the surrounding solution. This was shown in the multiscale simulations in the previous chapter where C18PGA_{100} forms a very tight nanoparticle compared to the other two polymers simulated. Additionally this hypothesis could explain the reduction in encapsulation efficiency and drug loading with these polymers. As they are less likely to bind DXMP clusters their overall drug loading of DXMP is reduced compared with PGA_{20} -co- C18PGA_{80} .

Chapter 6

Incorporation of DXMP into PGA Nanoparticles: Updated Multiscale Model

The fully atomistic simulation described in the previous chapter unveiled some new interactions between DXMP and $\text{PGA}_{20\text{-co-C18PGA}_{80}}$. Most notably the change in diffusion rate of acetone affected the encapsulation efficiency of the polymer. This faster dispersing acetone is believed to be a more accurate representation of experimental conditions as it is based on experimentally determined diffusion constants of acetone in water.

Whilst the accuracy of the AA simulation is superlative, the time taken for the simulation was extremely long. In order to use a nanoprecipitation model to aid in the experimental creation of polymer-based drug delivery systems the simulations must be relatively quick. Our initial 80ns multiscale nanoprecipitation simulations took around five days using the fastest available computational resources at the time. The shorter fully atomistic simulation (50ns) took around three months to complete. Whilst this simulation offers the

most relative accuracy it is too slow for our needs. Fully atomistic simulations may serve a purpose in analysing some experimental results but they cannot achieve rapid results.

A computational model needs to be able to quickly ascertain the compatibility of a drug-polymer pairing. This includes running multiple simulations to check for errors in the simulation. Our multiscale model is ideal for this, as although it has a slight decrease in accuracy it is significantly faster than fully atomistic simulations.

We have established that acetone should be dispersing at a faster rate than previously thought; at 50ns the simulations are completed in roughly three days. Triplicate repeats of a simulation are completed quicker and results obtained faster.

The original multiscale simulation described in Chapter 4 was optimised vis-a-vis atomistic “gold standard” simulations of small subsystems. However, with the completion of the fully atomistic simulation we have access to a full scale reference simulation.

Our aim at this stage was to attempt to replicate the dynamics observed in the fully atomistic simulation using the multiscale force field. If we can optimise the multiscale force field for the nanoprecipitation $\text{PGA}_{20}\text{-CO-C18PGA}_{80}$ with DXMP, these optimisations should hopefully work for the other two polymers. Overall this allows for another detailed analysis of the experimental data and may reveal new explanations for the experimental trend.

It should be noted that when attempting to perfectly match two things that are inherently different it is highly non-trivial. CG acetone is a simple sphere compared to the united AA acetone model that contains partial charges

and four separate atoms. As such we are merely attempting to reach the best possible match for the multiscale simulation as an exact replica is likely to be impossible.

For clarity, in this chapter we will refer to the original multiscale force field used in Chapter 4 as MS1 and the updated force field used for this chapter as MS2.

6.1 Optimisation

6.1.1 Acetone Dispersion

In the original multiscale force field (MS1), the CG acetone diffusion constant was matched with the diffusion constant of AA acetone using a topology obtained from the ATB. The new acetone topology, WS_RM, was created to match the experimental diffusion constant of acetone in water at two different molar ratios. As such this topology was considered superior to the previous AA topology and resulted in faster dispersion of the acetone drop during the nanoprecipitation simulation.

As with the original optimisation we wanted to match the diffusion constant and mean squared diffusion over time using CG acetone in CG water. Adjusting the non-bonded interactions between these two CG molecules enables adjustment of the diffusion constant of acetone in water.

Using the same 5ns simulation of a small sphere of acetone dispersing in water, we calculated the mean squared displacement (MSD) of acetone. The AA WS_RM acetone topology changes the MSD of AA acetone to $1.3456 \times 10^{-5} \text{ cm}^2/\text{s}$. This value was matched using CG acetone to reach an MSD of $1.3758 \times 10^{-5} \text{ cm}^2/\text{s}$.

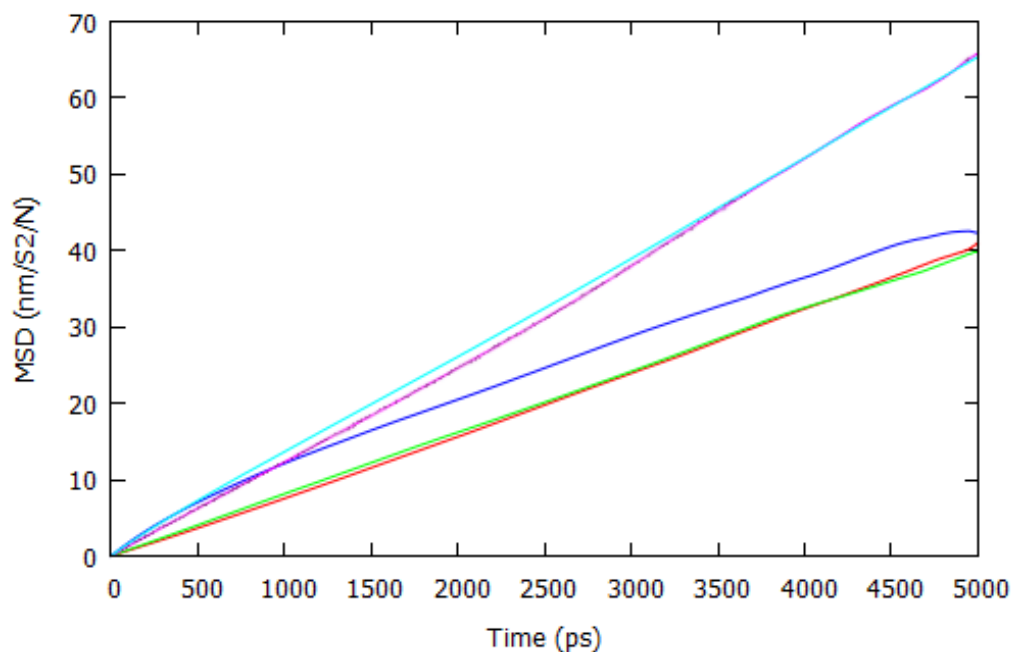


Figure 6.69 Plots for the mean squared displacement of acetone in water using various force fields. Original ATB AA (cyan), original multiscale (MS1) (purple), MARTINI CG (blue), WS_RM AA (green), new multiscale (MS2) (red).

Using MS1 the MSD over time for acetone in water was larger than with the updated multiscale force field (MS2). The overall diffusion constant for the 5ns simulation was also larger. However, we know that for our larger scale nanoprecipitation simulation this acetone dispersed into water at a faster rate. With MS1 the diffusion constant was larger ($2.213 \times 10^{-5} \text{ cm}^2/\text{s}$) but acetone dispersed into water over a longer time frame (60-80ns).

The diffusion constant indicates that on average acetone using MS1 diffuses faster than with MS2. However, the time taken for the acetone drop to disperse in water was shorter with MS2. This is due to the behaviour of the acetone drop in the two different force fields. Using MS1 acetone dissolves into water whereas with MS2 the acetone drop disperses equally and does not remain as a spherical droplet (Figure 6.70).

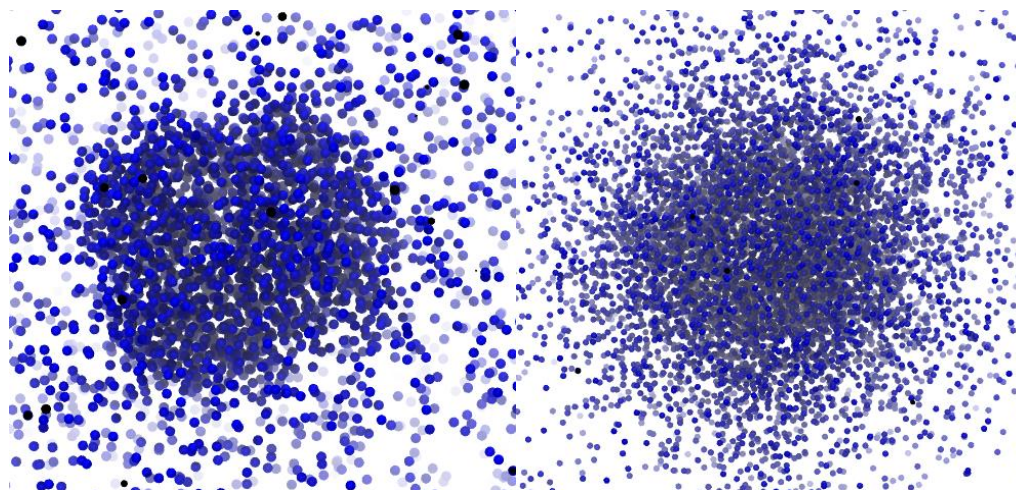


Figure 6.70 The dispersion of acetone differs between the original MS1 force field (left) and the atomistic force field WS_RM (right). Acetone is shown as a single sphere in both images for comparison.

CG acetone beads have a smoother surface than the atomistic acetone and this promotes faster dynamics. To match the atomistic acetone model using CG acetone it was necessary to increase the interaction between these beads to retard the diffusion/dispersion of the beads. Whilst this decreased the diffusion constant to ensure that acetone dispersed evenly and did not remain as a droplet, the interaction with solvent was also increased.

For a 5ns simulation this worked as is seen in Figure 6.69, however by increasing intermolecular interactions for acetone the chance of the solvent freezing is drastically increased. The MARTINI force field has been documented as having a propensity for freezing, specifically when the water is at 290K +/- 5K. This is due to relatively strong interaction between water molecules sometimes generating a nucleation point for water to freeze. When using a shift potential there are no long-range electrostatics in the simulation to prevent freezing.

To slow the overall MSD of acetone in water the short range interactions between the CG molecules were increased but this results in

“freezing” of acetone in a larger simulation. Therefore these parameters for CG acetone were not suitable for our nanoprecipitation simulation.

To prevent freezing, the MARTINI force field uses antifreeze particles. These particles have extremely high attractive interactions with the solvent to prevent clustering into a nucleus from which the solvent can freeze. Attempts were made to introduce an antifreeze particle for acetone without success. Additionally the complication of having an unrealistic particle in the system was undesirable.

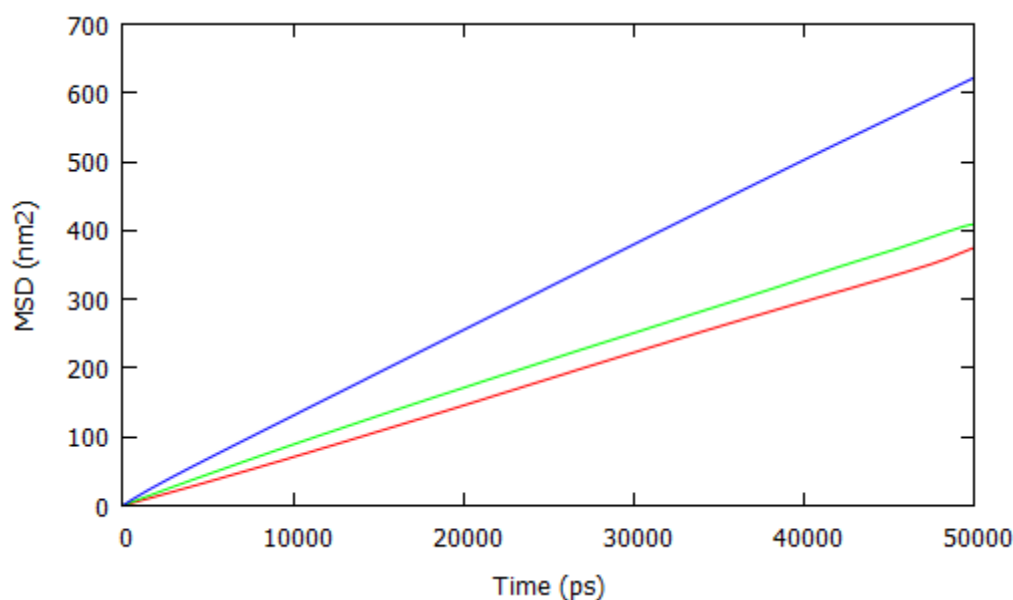


Figure 6.71 The MSD of acetone in water during 50ns of nanoprecipitation simulation time. Original multiscale (blue), fully atomistic (red), optimised multiscale (green).

Consequently the diffusion of acetone for the new multiscale force field was optimised based on a direct comparison of the MSD of acetone during the fully atomistic simulation (Figure 6.71). The initial Lennard-Jones epsilon and sigma parameters were based on the results from the smaller 5ns simulation and then tested on a 50ns nanoprecipitation simulation. These parameters were

further optimised until they were able to reasonably match acetone dispersion in the fully atomistic simulation.

6.1.2 PGA₂₀-co-C18PGA₈₀ Radius of Gyration

Additionally the radius of gyration for the two polymer chains in the simulation was optimised. The interaction between PGA₂₀-co-C18PGA₈₀ and CG acetone was adjusted such that the aggregation of the polymer chains matched the fully atomistic simulation (Figure 6.72).

The attraction of the polymer to CG acetone was increased to retard the aggregation of the polymer chains. This allowed the R_g over time to match the fully atomistic simulation from polymer chains starting in similar configurations. Whilst the initial drop in R_g is steeper with the MS2 force field the R_g when the polymer nanoparticle forms is slightly larger.

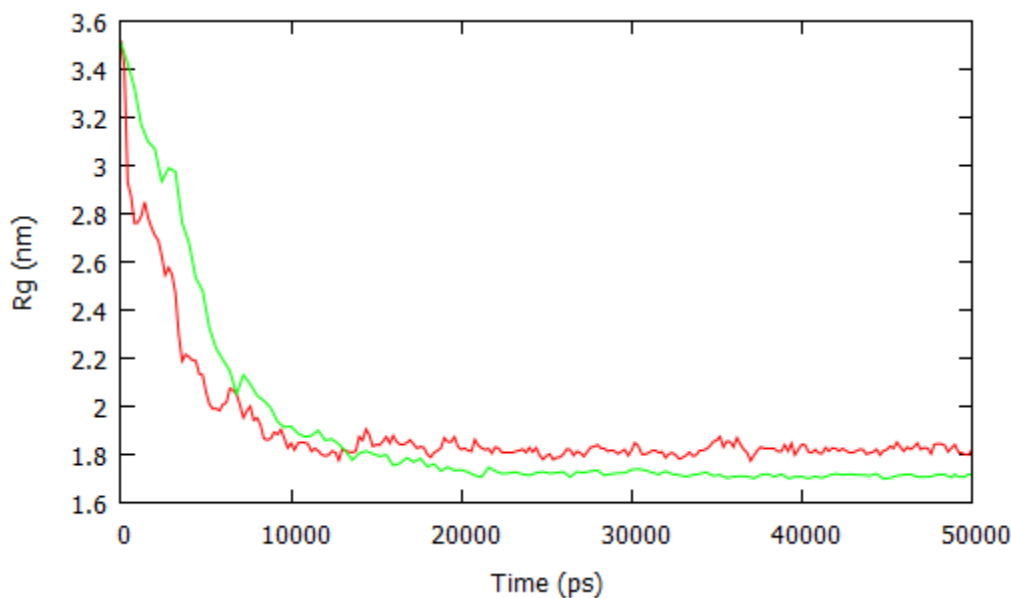


Figure 6.72 The total radius of gyration for a two polymer cluster is analysed over a 50ns nanoprecipitation simulations. Fully AA (green), MS2 (red).

Upon analysing the simulation we found that acetone was being retained around the polymer nanoparticle which lubricated the chains reducing nanoparticle density.

Although the MSD over time was matched against the fully atomistic simulation, the dispersion of acetone using the MS2 force field is still slightly different. This may be a flaw in using CG solvent molecules. The CG interactions between the virtual sites on the atomistic polymer and the CG acetone prevented correct aggregation of the polymer chains during the simulation. The interaction with acetone had to be increased to correct the radius of gyration but this resulted in incorrect acetone dispersion (Figure 6.73).

Acetone remained as a droplet due to stronger interactions with the polymer chains than the surrounding water. It is possible to correct this and prevent clustering of acetone around the polymer chains however the overall dispersion of acetone becomes too quick. Full dispersion of the acetone drop occurred over a short time frame and this is unreasonable if we want to match the atomistic simulation. As explained at the start of this chapter it may be impossible to perfectly match the AA dynamics of nanoprecipitation.

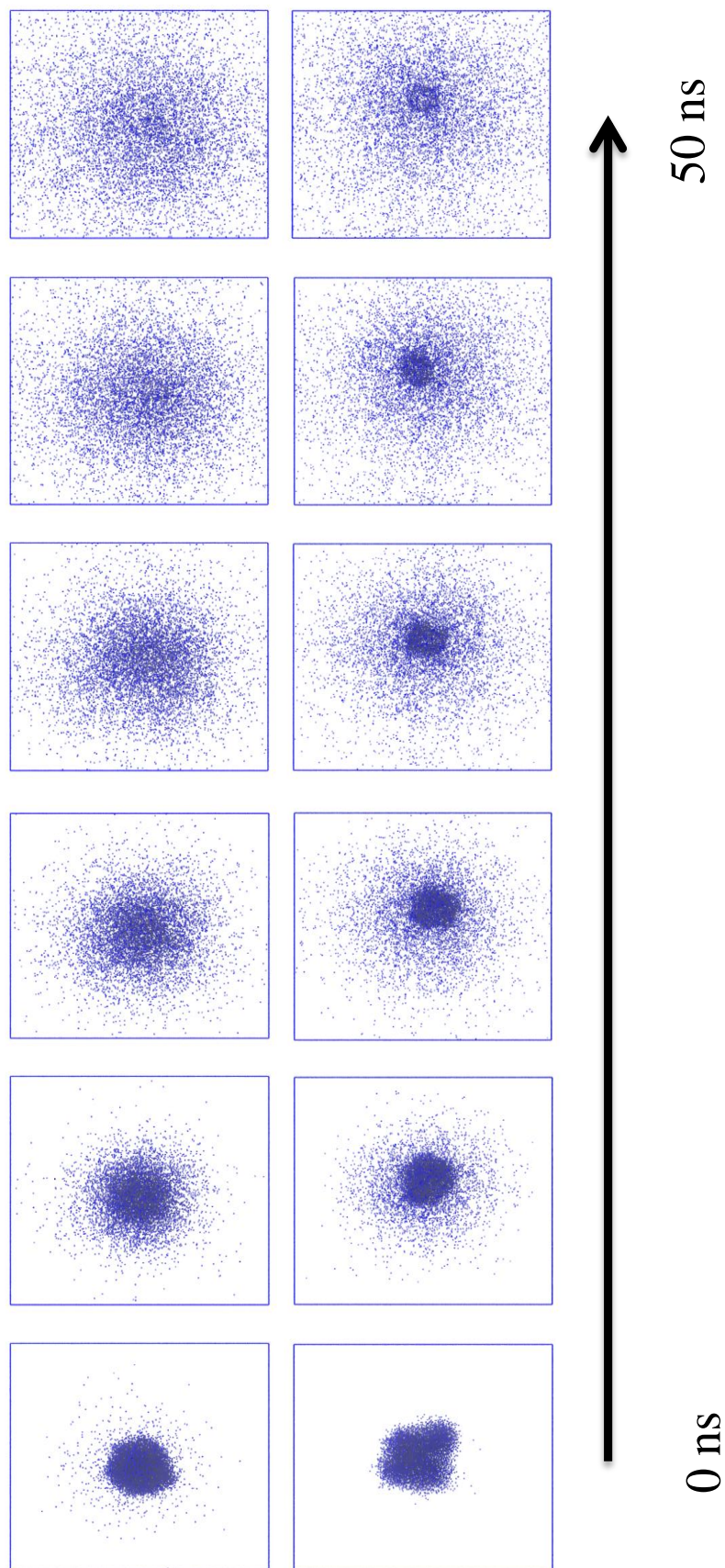


Figure 6.73 The dispersion of acetone is shown over the 50ns nanoprecipitation simulation using the fully atomistic force field (top) and MS2 force field (bottom). Snapshots were taken at 0, 10, 20, 30, 40 and 50ns from bottom to right.

6.2 Simulation of PGA₂₀-co-C18PGA₈₀ nanoprecipitation in the presence of DXMP

Visual analysis revealed that despite the flaws in the MS2 force field; the nanoprecipitation of PGA₂₀-co-C18PGA₈₀ was very similar to the fully atomistic simulation (Figure 6.74). The polymer nanoparticle aggregates over a similar time frame to the atomistic simulation. Compared with MS1, polymer chains aggregated earlier in the simulation using MS2 due to faster dispersing acetone.

Drug loading was fairly similar also with the MS2 simulation binding 15 drug molecules, an increase of 3 over the atomistic simulation. This equates to a 0.6% increase in EE and 4.3% increase in drug loading. Repeats would need to be performed to confirm these values.

Whilst the number of drugs encapsulated in the simulation was similar, the interaction between the polymer and drug molecules was different. Firstly the drugs appeared to bind less tightly to the nanoparticle than in the atomistic simulation. The orientation of the drug was similar, but drugs were not buried into the nanoparticle. This could be explained by the layer of acetone that remained around the nanoparticle (Figure 6.75). Acetone surrounded the nanoparticle solvating drug molecules at the surface. This prevented them from binding tightly to the nanoparticle and burying their hydrophobic steroid rings.

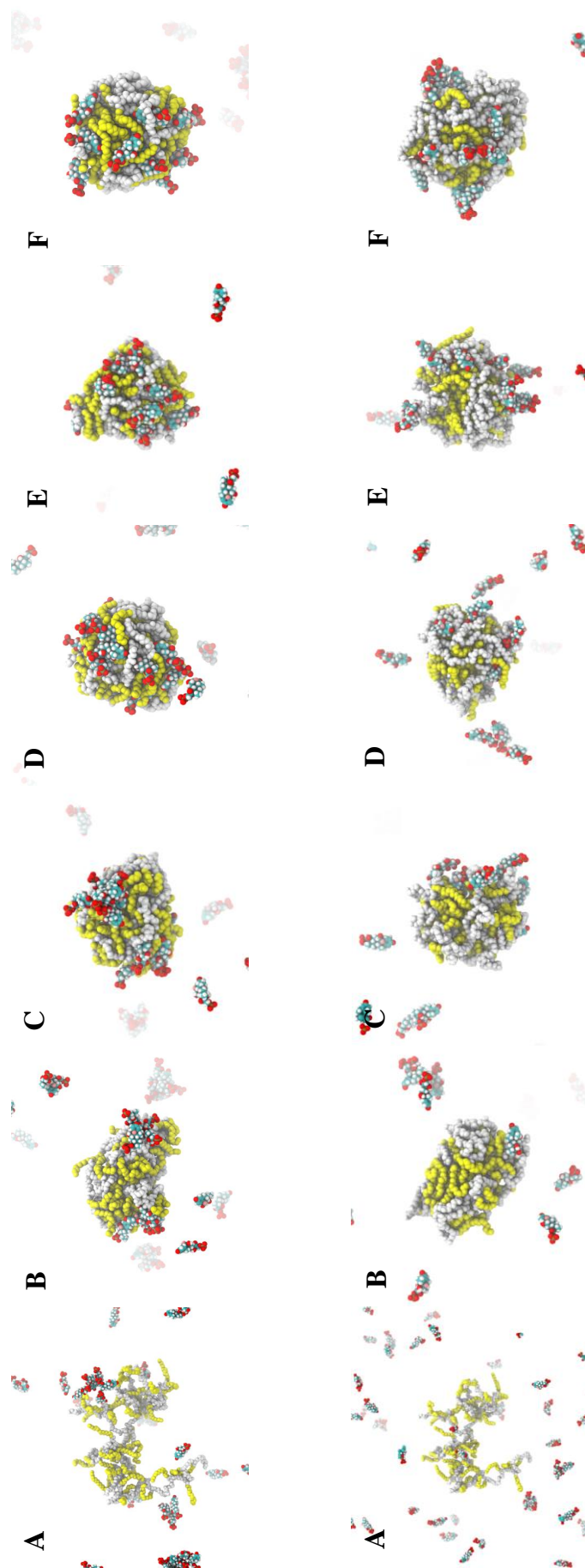


Figure 6.74 Snapshots taken during the 50ns MS2 simulation of PGA₂₀-co-C18PGA₈₀ with DXMP (bottom). Snapshots from the fully atomistic are shown for comparison (top). A: 2ns, B: 10ns, C: 20ns, D: 30ns, E: 40ns, F: 50ns. DXMP (red/blue/white), PGA (white). Water and acetone not shown for clarity.

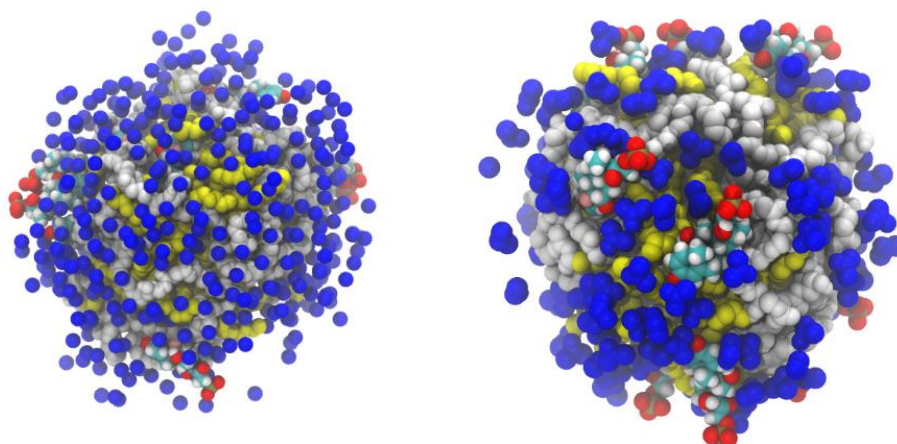


Figure 6.75 Snapshots taken at the end of the nanoprecipitation simulation of $\text{PGA}_{20}\text{-co-C18PGA}_{80}$ with DXMP using the MS2 force field (left) and atomistic force field (right). Acetone surrounding the polymer is shown for comparison.

Additionally drugs appear to initially bind the nanoparticle in the incorrect orientation (Figure 6.76). The negative charge on the phosphate group of DXMP buried into the nanoparticle if the drug was unable to partner with a sodium counter ion. Efforts were made to prevent this in the MS1 force field such as increasing the relative dielectric constant and those are unchanged with MS2. However, the presence of the acetone drop in the MS1 simulations prevented drug from reaching the polymer nanoparticle before the drug partnered with a counter ion.

Acetone dispersed faster with MS2, so there was still somewhat of an acetone drop around the polymer chains but it was not enough to prevent drug molecules from interacting with the polymer at early stages in the simulation before the drug found a counter ion. If a counter ion was able to interact with the phosphate group of DXMP the orientation of the drug was reversed (Figure 6.76).

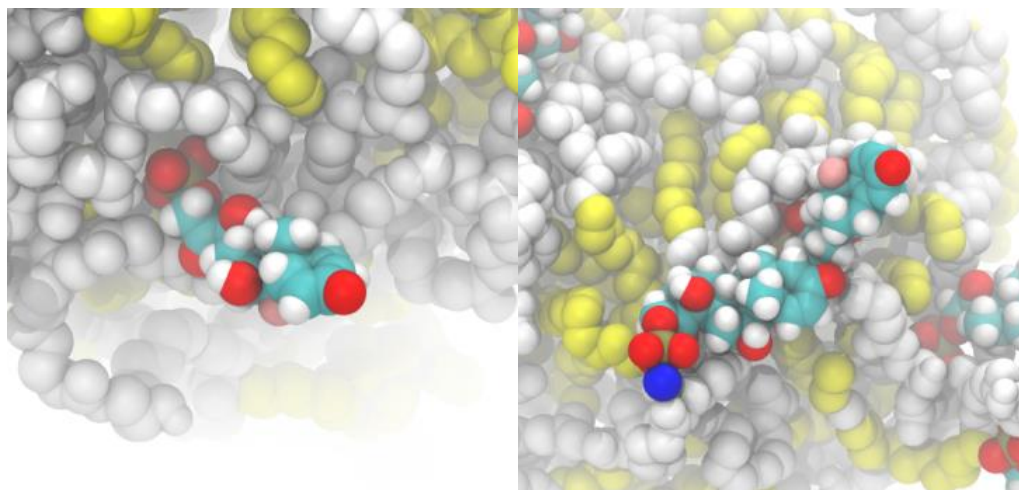


Figure 6.76 The binding of DXMP to PGA₂₀-co-C18PGA₈₀ during the MS2 simulation (left). If DXMP binds an ion the orientation of the drug molecule is reversed (right).

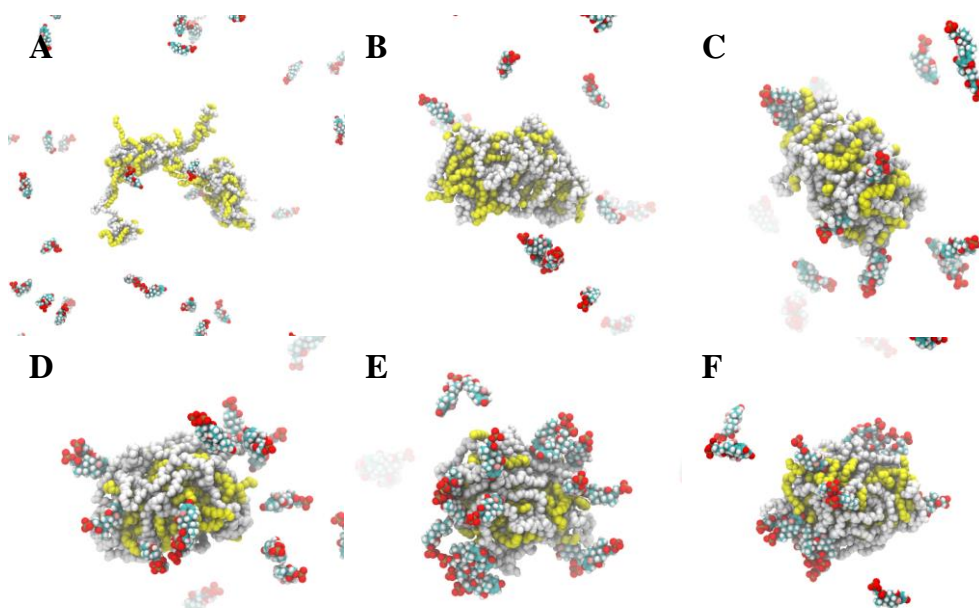


Figure 6.77 Snapshots taken during the 50ns MS2 simulation of PGA₂₀-co-C18PGA₈₀ with DXMP salt. A: 2ns, B: 10ns, C: 20ns, D: 30ns, E: 40ns, F: 50ns. DXMP (red/blue/white), PGA (white). Water and acetone not shown for clarity.

Whilst counter ions were able to reverse the orientation of DXMP and the encapsulation efficiency is comparable to the atomistic simulation, the way the drug interacts with the nanoparticle was different. As we wanted to match

the atomistic dynamics as closely as possible we decided that starting the simulation with DXMP as a disodium salt would correct this erroneous binding. This involved adding DXMP to the simulation box with two counter ions in close proximity to the phosphate group of the drug. This contrast with the normal method where counter ions are introduced randomly throughout the simulation box by replacing water beads.

Starting DXMP as a salt prevented the drug from burying its negative charge into the nanoparticle during the simulation (Figure 6.77). The diffusion constant of DXMP was unchanged when it was present as a salt. This new model is named MS2_salt hereafter.

DXMP bound in the correct orientation to the polymer but the large amount of acetone surrounding the nanoparticle prevented the drugs from being buried into the particle as they were in the fully atomistic simulation.

To check this hypothesis, a 10ns “wash” simulation in pure CG water was run where acetone surrounding the polymer was removed. In this simulation the drug molecules were able to bind tighter to the nanoparticle (Figure 6.78).

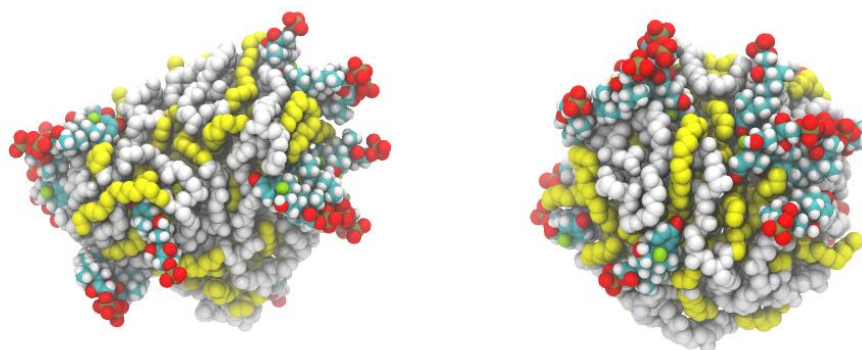


Figure 6.78 Snapshots taken from the 10ns wash simulation in pure CG water at the start (left) and end (right) of the simulation using the MS2 force field.

Additionally the radius of gyration of the polymer cluster changed due to the removal of acetone. During the first 100 ps of the simulation the R_g decreases and by the end of the 10ns “wash” simulation the R_g matched closely with the R_g obtained at the end of the fully atomistic simulation (Figure 6.79).

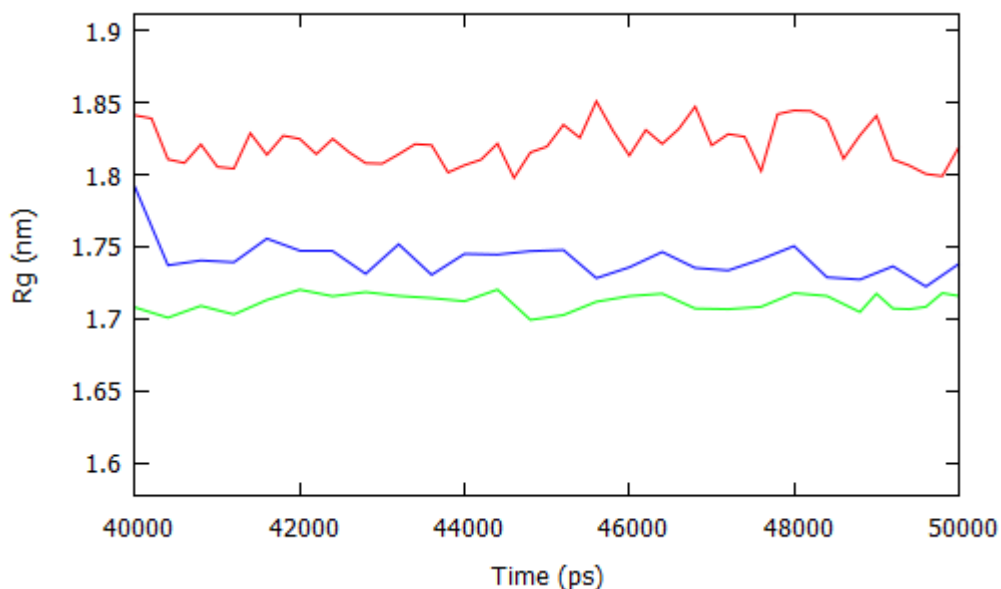


Figure 6.79 The radius of gyration (R_g) for the $\text{PGA}_{20}\text{-co-C18PGA}_{80}$ nanoparticle during a 10ns wash simulation (blue) is overlaid with the R_g from the last 10ns of the MS2 simulation (red) and fully atomistic simulation (green).

The presence of acetone at the surface of the polymer nanoparticle was affecting its compaction and interaction with DXMP molecules at the surface. The removal of acetone alleviated these problems and allowed the model to behave similarly to the fully atomistic simulation.

6.3 Simulation of C18PGA_{100} nanoprecipitation in the presence of DXMP (MS2_salt)

The simulation for C18PGA_{100} is similar to that of $\text{PGA}_{20}\text{-co-C18PGA}_{80}$. DXMP was present as a disodium salt again to correct its

orientation. Again drug molecules were unable to form tight interactions with the polymer due to a layer of acetone that surrounded the nanoparticle at the end of the simulation. Upon removal of acetone these drugs will form tighter interactions and so we considered these drugs encapsulated within the nanoparticle.

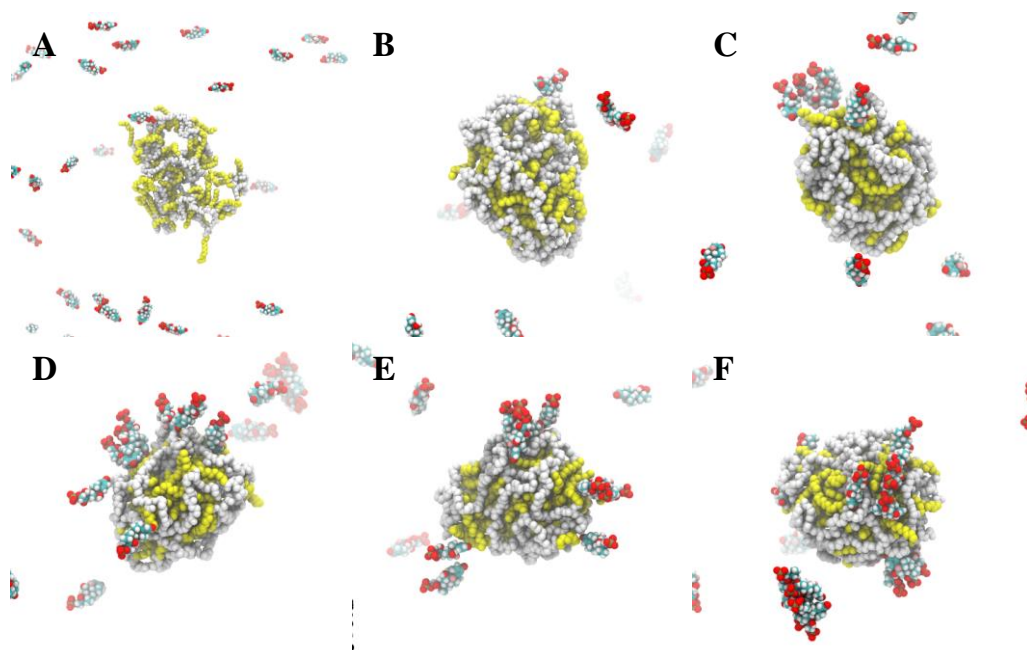


Figure 6.80 Snapshots taken during the 50ns MS2 simulation of C18PGA₁₀₀ with DXMP salt. A: 2ns, B: 10ns, C: 20ns, D: 30ns, E: 40ns, F: 50ns. DXMP (red/blue/white), PGA (white). Water and acetone not shown for clarity.

In Figure 6.80D we observed a few DXMP molecules interacting with the layer of acetone that coated the polymer. This acetone could artificially increase the encapsulation of DXMP in this model compared with the atomistic simulation. In the atomistic simulation acetone dispersed evenly (Figure 6.73) therefore DXMP was able to directly interact with the nanoparticle surface. As DXMP preferentially interacts at the acetone water interface, a layer of acetone around the polymer chains attracts more drug molecules to the nascent nanoparticle.

20ns into the simulation the nanoparticle appeared more compacted than $\text{PGA}_{20\text{-co-C18PGA}_{80}}$ at this time point. The increased hydrophobicity of this polymer and decreased solubility in acetone may cause tighter compaction and increased density of the C18PGA_{100} nanoparticle. This could reduce the ability for DXMP molecules to interact with the surface of C18PGA_{100} .

6.4 Simulation of PGA_{100} nanoprecipitation in the presence of DXMP (MS2_salt)

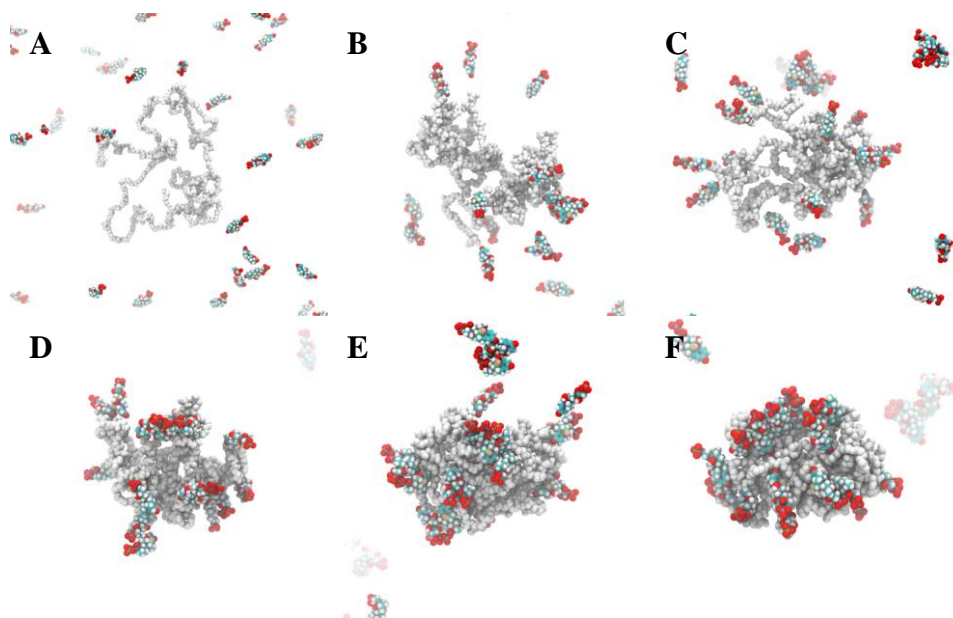


Figure 6.81 Snapshots taken during the 50ns MS2 simulation of PGA_{100} with DXMP salt. A: 2ns, B: 10ns, C: 20ns, D: 30ns, E: 40ns, F: 50ns. DXMP (red/blue/white), PGA (white). Water and acetone not shown for clarity.

For PGA_{100} the radius of gyration of the polymer during the simulation was different than with the other two polymers tested. This can be seen visually in Figure 6.81. With the $\text{PGA}_{20\text{-co-C18PGA}_{80}}$ and C18PGA_{100} the polymer chains fully aggregated within 10ns. However for PGA_{100} full aggregation of the polymer chains into a nanoparticle did not occur until 40ns into the simulation. This was due to the reduction in hydrophobicity for this polymer

when compared with the acylated versions of PGA. The hydroxyl groups on PGA kept the polymer chains in an extended conformation for a longer duration during nanoprecipitation.

DXMP was able to bind the polymer in the correct orientation due to the presence of the counter ion bound to its charged phosphate group. The increased solubility of this polymer reduced the nanoparticle density and forms nooks throughout the nanoparticle surface. This could aid in binding DXMP at the surface of the nascent nanoparticle.

6.5 Drug Loading and Encapsulation Efficiency

| Polymer | Model | No. DXMP bound | Encapsulation Efficiency (%) | Drug Loading (%) |
|--|-----------|----------------|------------------------------|------------------|
| PGA₂₀-co-C18PGA₈₀ | AA | 12 | 2.4 | 24.70 |
| | MS2 | 15 | 3 | 29.08 |
| | MS2_salt | 18 | 3.6 | 32.98 |
| C18PGA ₁₀₀ | MS2 | 25 | 5 | 40.60 |
| | MS2_salt | 19 | 3.8 | 34.19 |
| PGA ₁₀₀ | MS2 | 25 | 5 | 40.60 |
| | MS2_salt | 14 | 2.8 | 27.68 |

Table 6.1 The encapsulation efficiency and drug loading for three polymers with DXMP was analysed using different models.

For the new MS2 force field we were unable to run triplicate repeats due to time constraints. However, we were able to compare the effect of starting DXMP as a disodium salt as opposed to free drug with counter ions. For C18PGA₁₀₀ and PGA₁₀₀ there was a marked decrease in drug loading when DXMP started as a salt. This is because the phosphate group of DXMP is less attracted to the polymer as it did not need to bury its negative charge as it is countered by two sodium ions. The electrostatic attraction of DXMP to the

polymer chains was increased in the absence of a counter ion for its phosphate group. However, for PGA_{20-co-C18PGA}₈₀ we saw little change when DXMP started as a salt. Therefore this hypothesis would need to be tested with repeat simulations.

All of the MS2 simulations had higher DL and EE than the fully atomistic simulation. This is likely due to the layer of acetone that surround the nanoparticle as it forms. DXMP was drawn to the acetone and this artificially increased the number of drug molecules that interact with the nanoparticle compared with the atomistic simulation where acetone did not form layer around the polymer chains.

Compared with the results of the original MS1 simulations we were unable to perfectly match the experimental trend for the polymers. Obviously this would need to be tested with triplicate repeats. Nonetheless, the acylated polymers PGA_{20-co-C18PGA}₈₀ and C18PGA₁₀₀ were able to encapsulate more drug than PGA₁₀₀ when starting DXMP as a salt. Despite PGA₁₀₀ sustaining a considerably larger radius of gyration throughout the simulation the lack of C18 chains on the polymer appear to reduce its encapsulation efficiency with DXMP.

The lack of disparity between PGA_{20-co-C18PGA}₈₀ and C18PGA₁₀₀ may be due to the presence of acetone around the polymer during the simulation. This acetone layer was similar for both polymers and so similar amounts of drug interact with these two polymers. Correction of acetone dispersion to perfectly match the atomistic simulation may yield more accurate drug loading results.

Additionally differences between the acylated polymers are less pronounced due to the faster aggregation of the polymer chains. As acetone dispersed faster when compared with the original MS1 model it is unlikely that we will observe differences in the polymers radius of gyration that could affect encapsulation of DXMP. By having polymer at a concentration much higher than experimental conditions the aggregation of the polymer chains was very fast. Therefore we would expect to see little difference in the encapsulation of DXMP between these two polymers.

6.6 Conclusion

In the updated multiscale force field MS2 we were able to closely match the diffusion constant for acetone in water based on the diffusion constant obtained from the fully atomistic simulation of $\text{PGA}_{20}\text{-co-C18PGA}_{80}$ with DXMP. We also match the radius of gyration of $\text{PGA}_{20}\text{-co-C18PGA}_{80}$ during nanoprecipitation. However, we still observed a layer of acetone coating the polymer chains as they aggregated. This may be a problem with the use of a CG solvent model as it was very difficult to match the AA acetone dynamics perfectly.

Additionally DXMP was prone to binding the nanoparticle in an incorrect orientation so an updated model where DXMP started as a salt bound to two counter ions was used. This corrected the orientation of DXMP during the simulation yet the levels of DL and EE using the MS2 force field were higher than for the atomistic simulation. This was due to the layer of acetone that surrounded the polymer cluster during nanoprecipitation. DXMP interacts with this acetone increasing the amount of drug molecules drawn onto the

surface of the aggregating nanoparticle. Subsequent simulations in pure CG water with the acetone removed revealed that DXMP will bind the polymer similarly to the atomistic simulation.

Whilst we have improved certain aspects of the simulation the MS2 force field is still not perfect. We were able to show that levels of DL and EE do decrease compared with the MS1 force field due to the faster dispersion of acetone. Unfortunately we are unable to match the dispersion of AA acetone in AA water using a CG model. This has proven the most difficult optimisation and will need further work in the future.

Chapter 7

Conclusions and Future Work

In this thesis a computational model to simulate the nanoprecipitation of PGA with DXMP was presented. The conception of the model and use of a multiscale force field was discussed. DPD and other coarse-grained simulation techniques were considered less accurate than a multiscale model that allowed for atomistic drug-polymer interactions.

The multiscale force field was optimised via comparison with atomistic simulations. Metrics were designed to ensure the dynamics in the multiscale simulation matched the atomistic simulation. The dispersion of acetone into water was of particular importance due to its solubilising effect on both drug and polymer molecules in the model.

After simulating three polymers the drug loading and encapsulation efficiency data matched an experimentally determined trend. The hydrophobicity of the polymer and its solubility in acetone affected its radius of gyration. This was found to influence its attraction to drug molecules surrounding the acetone drop.

It would be useful to explore the effect of PGA acylation in more depth. Whilst the experimental trend is matched for three polymers we would have

more confidence in the multiscale model created if more polymers were tested. For example experimental data exists for a 40% acylated polymer. Additionally simulating a 70% or 90% acylated polymer would help determine the optimal C18 acylated polymer for DXMP.

Our initial hypothesis is that hydroxyl groups on the polymer influence its solubility in acetone and water. Other functional groups that would help increase the solubility of the polymer without effecting its hydrophobic interactions with DXMP could also be beneficial. PGA has been functionalised experimentally with amino acids in the past. A copolymer with amino acid groups and C18 chains could increase encapsulation efficiency with DXMP. However, the packing of the polymer nanoparticle may change due to steric effects of large amino acid groups.

The length of the acyl chain was not tested by simulation. Experimentally varying the length of the acyl chain had profound effects on the encapsulation of DXMP within nanoparticles. A computational model offers an easy method to explore these modifications to PGA and will also provide a molecular level understanding of how a change in acyl chain length affects polymer dynamics, solubility and interactions with DXMP.

An increase in chain length increases the polymer's hydrophobicity. These longer chains may be able to interact with more drug molecules at the surface of the acetone drop. However, more hydrophilic groups may be required to balance the polymers solubility in acetone and water. Hydroxyl groups may be insufficient to maintain optimal compaction of the polymer. Again an amino acid may be a useful hydrophilic group to add to the polymer to balance its hydrophobicity with longer hydrophobic acyl chains.

When acetone disperses into water at a faster rate the loading of DXMP within a $\text{PGA}_{20}\text{-co-C18PGA}_{80}$ nanoparticle decreased. This suggests that a slower dispersing solvent may be able to increase the encapsulation efficiency of this particular polymer drug mixture. The model could be used to test new solvents that are slower at dispersing in water than acetone. Any potential candidates should be subsequently tested experimentally.

The atomistic simulation of $\text{PGA}_{20}\text{-co-C18PGA}_{80}$ with DXMP revealed that the dispersion of acetone in our original multiscale model (MS1) was not accurate with regards to experimentally determined diffusion constants of acetone in water. However, atomistic simulations were very slow and due to limited computational resources we were only able to run a single simulation for this thesis. It would be useful to have atomistic simulations of the other two polymers tested: PGA_{100} and C18PGA_{100} so that the multiscale force field for these polymers can also be optimised.

For the update multiscale force field, MS2, we corrected the dispersion of acetone and the aggregation of $\text{PGA}_{20}\text{-co-C18PGA}_{80}$ using the atomistic simulation as a reference. Additionally to correct the orientation of DXMP during nanoprecipitation, using the atomistic simulation as a reference, the drug was started as a disodium salt. Whilst this ensured DXMP bound in the correct orientation it is not accurate to experimental conditions. Additionally we were unable to perfectly match the atomistic dispersion of acetone in water using a CG model. The overall dispersion of acetone had to be slowed but also disperse more evenly without remaining as a droplet. To achieve this strong interactions between the CG acetone beads themselves and CG water were required. However, this caused CG acetone to freeze at 300 kelvin. It may be

possible to use “antifreeze” particles that have been used in the MARTINI force field to prevent the freezing of acetone. Correcting this flaw in the MS2 force field will bring it in line with the dynamics of the atomistic simulation.

The DL and EE values obtained using the MS2 force field did not match the experimental trend as well as the MS1 model. This is likely due to a lack of repeats and further optimisation for the MS2 force field using PGA₁₀₀ and C18PGA₁₀₀ is required. Having the atomistic simulation of PGA₂₀-co-C18PGA₈₀ with DXMP helped in optimising MS2 for this polymer, but resolution transformation could be used in the future with the PGA₁₀₀ and C18PGA₁₀₀ MS2 simulations to improve the force field for these polymers.

When optimising the multiscale force field a consistent problem was the large charge on DXMP. This charge meant that the system required counterions and a careful adjustment of the relative dielectric constant for the simulation. This problem has also been observed by Wassenaar et al. when using a multiscale force field with charged protein side chains. They were unable to match the potential of mean force (PMF) between charged amino acids when compared with an atomistic force field.

The likely cause of this disparity is the lack of polarity of CG water. Converting four mobile polar water molecules into a neutral bead has profound implications on charged moieties using a multiscale force field. However, Wassenaar et al. found that even polarisable CG water models such as BMW and MARTINI PW were unable to match the PMF between charged amino acids produced using AA SPC/E. The PMF for a sodium and chloride ion was different to SPC/E for all CG water models tested.

We have also observed inaccurate electrostatic interactions in our own multiscale simulations. The interaction of the sodium counter ions with the phosphate group of DXMP was exaggerated. In the atomistic simulation using PME with AA water, DXMP had weaker interactions with the counter ions in the system.

Therefore the simulation of neutral drug molecules is expected to be more accurate with the multiscale force field. Not only are counter ions not required for neutral drug molecules but the relative dielectric constant of the simulation can be substantially decreased from the large value used for DXMP. The ideal relative dielectric constant (ϵ_r) for atomistic interactions is 1 as this ensures accurate electrostatics between the atomistic molecules in the system. We had to use an ϵ_r of 6 for our multiscale simulations to reduce the strength of electrostatic interactions with the charged phosphate group of DXMP. However, if the system contains all neutral molecules the ϵ_r could be set to a much lower value. The optimisation of neutral molecules is likely much faster and easier than for charged ones.

In theory a fully CG model of nanoprecipitation is also possible if the CG interactions are adjusted such that the dynamics match a fully atomistic reference simulation such as the one completed for PGA₂₀-co-C18PGA₈₀ with DXMP. A CG model has many advantages over a multiscale force field, the most important being the possibility to simulate much larger systems. CG simulations can be run with a time step around 20 times longer than multiscale and AA simulations. A larger time step drastically reduces the amount of equations that must be computed for a simulation.

Large scale simulations of nanoprecipitation could provide insight into that formation of nanoparticles closer in size to those formed experimentally. The particles formed in our multiscale and AA simulations were around 30 times smaller than those formed experimentally. Larger particles could reveal new ways in which DXMP binds to PGA and its derivatives.

Our initial simulations found the MARTINI force field unable to accurately simulate nanoprecipitation of PGA with DXMP. As such a fully CG simulation would require re-parameterisation of the MARTINI force field in a similar manner to how the multiscale CG interactions were optimised. The fully atomistic simulation could be used as the ideal reference to which a new CG force field could be optimised.

However, it is likely that the CG force field created may be specific to the polymer it is optimised for. Whilst the optimisation may be quick due to the decreased time to run CG simulations, the lack of atomistic detail makes analysis difficult. It is probable that drug-polymer interactions would be inferior in a CG simulation. Furthermore CG drug molecules are difficult to create with no established method. Usually the CG beads on the molecule must be tightly constrained which often reduces flexibility such that the drug becomes a rigid block of connected CG beads.

Ideally the removal of water would be the best way to speed up the simulation of nanoprecipitation. The majority of the model is comprised of water and so the bulk of simulation time is spent on interactions between water molecules. An implicit solvent model may be possible however this would likely result in inaccurate acetone dispersion. A key conclusion from this work has been that the dispersion of acetone has a major impact on the encapsulation

of DXMP into PGA polymers. We were unable to match the dispersion of AA acetone using CG acetone in CG water so it is likely that it will be more difficult using implicit water.

In the literature there is little focus on how nanoparticles form but rather how drug molecules are encapsulated into preformed particles. Our results have demonstrated that the formation of nanoparticles influences their encapsulation efficiency. However, the majority of DXMP bound to the nanoparticle was on the surface. This indicates that it is possible for preformed nanoparticles to achieve similar encapsulation efficiency to nanoparticles that are formed in the presence of drug molecules.

This difference in encapsulation efficiency between forming and preformed particles was analysed by Woodhead et al. in the introduction²⁶. The advantage of simulating with preformed particles is that there is no need to simulate the dispersion of acetone in water that is a big limitation to the nanoprecipitation simulations in this thesis. However, in order to achieve the correct polymer entanglement, nanoprecipitation using an acetone drop must be performed. One method would involve running a multiscale simulation of nanoprecipitation in the absence of drug at a large scale. This would form a polymer nanoparticle which could, when stripped of its virtual sites, be used for fully atomistic simulations. AA nanoparticles in pure water could be simulated with AA drug molecules at a relevant concentration to observe their interactions.

We have also considered that the nanoprecipitation simulation we have designed may not be completely accurate compared to how it occurs experimentally. In our simulations acetone starts as a drop surrounded by water. However, we know that the acetone can diffuse quickly in water so it is unrealistic to assume that a droplet could stay intact as it enters the water such that it can become surrounded by it.

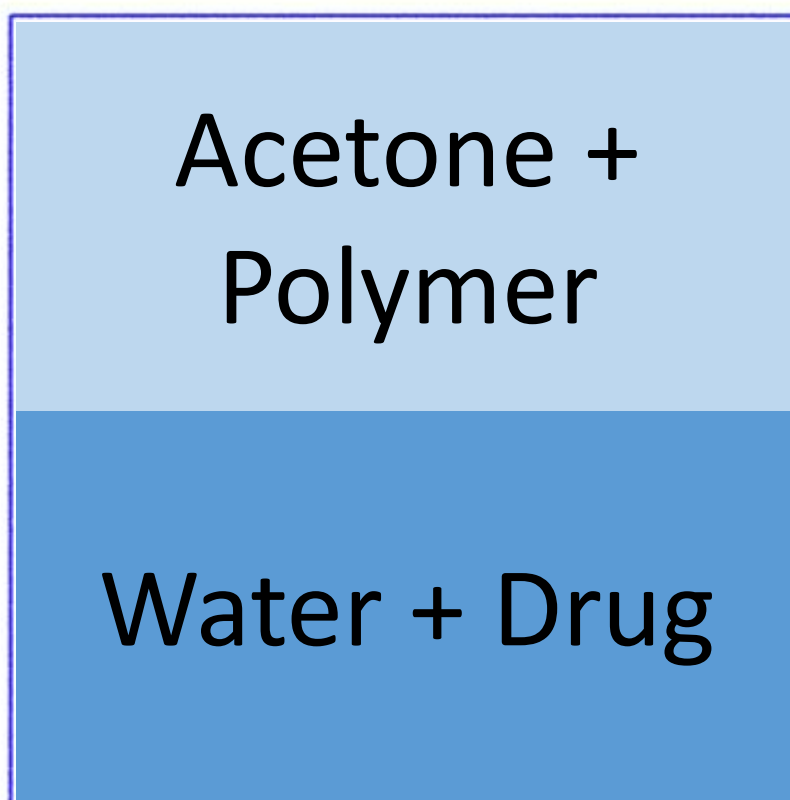


Figure 7.82 An alternative model for nanoprecipitation where the aqueous and organic phases are separated into planes and allowed to mix during the simulation.

A more realistic simulation could involve simulating two planes of solvent mixing with each other. As the acetone drop makes contact with the water it is likely that it disperses into the water in this way as opposed to a droplet dispersing in all directions. In addition to being potentially more

accurate, this model may also require less water than our nanoprecipitation model.

One limitation of this model is in dealing with boundary conditions. Normal xyz boundary conditions would allow for water to diffuse into acetone through the y boundary. This results in acetone diffusing not only with water below but also through the boundary above. To prevent mixing of solvent across the y boundary it is possible to use the walls feature in GROMACS. This allows the construction of a wall of Lennard-Jones particles that prevent the movement of particles across the y boundary.

This thesis has focused heavily on nanoprecipitation and the formation of nanoparticles. Whilst this provides understanding of this complicated process there are other techniques that can be used to aid in developing polymer-based drug delivery systems. These techniques also help address the inability for MD to help understand drug released from nanoparticles. As drug release occurs over a long time frame we are currently unable to observe this using conventional MD.

The first is the free energy of binding of the drug to polymer nanoparticle. This technique is traditionally used for drug molecules bound within an active site of a protein. However, it is possible to apply techniques such as MM-PBSA (Molecular Mechanics Poisson Boltzmann Surface Area) to calculate the free energy of binding DXMP to a nanoparticle.

GMXPBSA⁵² allows for the calculation of free energies using GROMACS and could be used on the nanoparticles formed in this thesis. Our initial studies are not presented in this thesis as the results were inconclusive

but there is potential to use free energy of binding to indicate the relative strength of drug-polymer interactions in a drug delivery system.

Similarly umbrella sampling could be used to obtain the free energy profile for drug release from a nanoparticle. Using steered MD in a similar manner to Maiti et al.³² it is possible to remove single DXMP molecules from PGA nanoparticles formed using the multiscale force field. Umbrella sampling can be used to calculate the potential of mean force for that particular delivery system.

Not only is this an interesting method to compare the drug-polymer interactions between different polymers, but it can also give an indication of the drug release profile for a particular delivery system. DXMP molecules that have a lower free energy barrier from the umbrella sampling form weaker interactions with the nanoparticle and should be more readily released in solution.

The advantage of this technique is that it gives an insight into drug-polymer interactions without need to simulate nanoprecipitation. However, to form the drug delivery systems nanoprecipitation will have to be run initially.

Our studies in this area were inconclusive due to the variation in the drug-polymer interactions at the surface of the polymer. Umbrella sampling requires multiple simulations to be run with a large amount of optimisation. Some drugs were bound more tightly than others and so to gain an accurate representation of the drug-polymer interactions multiple DXMP molecules would need to be analysed.

It would be beneficial to automate the process of umbrella sampling for all the drugs bound to a particular nanoparticle. The larger the sample size the

more accurate the comparison between polymers as it is likely the free energy barrier could be quite similar if drugs are bound in similar positions on the nanoparticle. This is especially true for drugs that are bound to the surface of the polymer. A “wash” simulation in pure water could ensure drug molecules form optimal interactions with the nanoparticle before umbrella sampling is performed.

References

1. Galindo-Rodriguez, S., Allémann, E., Fessi, H. & Doelker, E. Physicochemical parameters associated with nanoparticle formation in the salting-out, emulsification-diffusion, and nanoprecipitation methods. *Pharm. Res.* **21**, 1428–39 (2004).
2. Singer, J. W. Paclitaxel poliglumex (XYOTAX, CT-2103): a macromolecular taxane. *J. Control. Release* **109**, 120–6 (2005).
3. Wang, A. Z., Langer, R. & Farokhzad, O. C. Nanoparticle delivery of cancer drugs. *Annu. Rev. Med.* **63**, 185–98 (2012).
4. Van der Meel, R., Vehmeijer, L. J. C., Kok, R. J., Storm, G. & van Gaal, E. V. B. Ligand-targeted particulate nanomedicines undergoing clinical evaluation: current status. *Adv. Drug Deliv. Rev.* **65**, 1284–98 (2013).
5. Tong, R. *et al.* Nanopolymeric Therapeutics. *MRS Bull.* **34**, 422–431 (2009).
6. Mattheolabakis, G., Rigas, B. & Constantinides, P. P. Nanodelivery strategies in cancer chemotherapy: biological rationale and pharmaceutical perspectives. *Nanomedicine (Lond)*. **7**, 1577–90 (2012).
7. Cai, K. *et al.* Dimeric drug polymeric nanoparticles with exceptionally high drug loading and quantitative loading efficiency. *J. Am. Chem. Soc.* **137**, 3458–61 (2015).
8. Gu, X. *A Novel Approach to Formulation of Anticancer Drugs in Nanoparticles.* (ProQuest, 2008). at <https://books.google.com/books?id=zAVbUFo0IjYC&pgis=1>
9. *Pharmaceutical Manufacturing Handbook: Production and Processes.* (John Wiley & Sons, 2008). at <https://books.google.com/books?id=4c0Hp3AOi8UC&pgis=1>

10. Vendruscolo, M. & Dobson, C. M. Protein dynamics: Moore's law in molecular biology. *Curr. Biol.* **21**, R68–70 (2011).
11. Puri, S., Kallinteri, P., Higgins, S., Hutcheon, G. A. & Garnett, M. C. Drug incorporation and release of water soluble drugs from novel functionalized poly(glycerol adipate) nanoparticles. *J. Control. Release* **125**, 59–67 (2008).
12. Kallinteri, P., Higgins, S., Hutcheon, G. A., St Pourçain, C. B. & Garnett, M. C. Novel functionalized biodegradable polymers for nanoparticle drug delivery systems. *Biomacromolecules* **6**, 1885–94 (2005).
13. Hewitt, M. *et al.* Ensuring confidence in predictions: A scheme to assess the scientific validity of in silico models. *Adv. Drug Deliv. Rev.* (2015). doi:10.1016/j.addr.2015.03.005
14. Vauthier, C. & Bouchemal, K. Methods for the preparation and manufacture of polymeric nanoparticles. *Pharm. Res.* **26**, 1025–58 (2009).
15. Prieto, F., Gómez-Déniz, E. & Sarabia, J. M. Modelling road accident blackspots data with the discrete generalized Pareto distribution. *Accid. Anal. Prev.* **71**, 38–49 (2014).
16. Noonan, M. J., Abidur Rahman, M., Newman, C., Buesching, C. D. & Macdonald, D. W. Avoiding verisimilitude when modelling ecological responses to climate change: The influence of weather conditions on trapping efficiency in European badgers (*Meles meles*). *Glob. Chang. Biol.* (2015). doi:10.1111/gcb.12942
17. Hodak, H. The Nobel Prize in chemistry 2013 for the development of multiscale models of complex chemical systems: a tribute to Martin Karplus, Michael Levitt and Arieh Warshel. *J. Mol. Biol.* **426**, 1–3 (2014).
18. Warshel, A. & Levitt, M. Theoretical studies of enzymic reactions: dielectric, electrostatic and steric stabilization of the carbonium ion in the reaction of lysozyme. *J. Mol. Biol.* **103**, 227–49 (1976).
19. Spaeth, J. R., Kevrekidis, I. G. & Panagiotopoulos, A. Z. Dissipative particle dynamics simulations of polymer-protected nanoparticle self-assembly. *J. Chem. Phys.* **135**, 184903 (2011).
20. Capretto, L. *et al.* Mechanism of co-nanoprecipitation of organic actives and block copolymers in a microfluidic environment. *Nanotechnology* **23**, 375602 (2012).

21. Subashini, M., Devarajan, P. V, Sonavane, G. S. & Doble, M. Molecular dynamics simulation of drug uptake by polymer. *J. Mol. Model.* **17**, 1141–7 (2011).
22. Lemkul, J. A., Allen, W. J. & Bevan, D. R. Practical considerations for building GROMOS-compatible small-molecule topologies. *J. Chem. Inf. Model.* **50**, 2221–35 (2010).
23. Luo, Z. & Jiang, J. pH-sensitive drug loading/releasing in amphiphilic copolymer PAE-PEG: integrating molecular dynamics and dissipative particle dynamics simulations. *J. Control. Release* **162**, 185–93 (2012).
24. Nie, S. Y. *et al.* Dissipative particle dynamics studies of doxorubicin-loaded micelles assembled from four-arm star triblock polymers 4AS-PCL-b-PDEAEMA-b-PPEGMA and their pH-release mechanism. *J. Phys. Chem. B* **117**, 13688–97 (2013).
25. Ahmad, S. *et al.* In silico modelling of drug-polymer interactions for pharmaceutical formulations. *J. R. Soc. Interface* **7 Suppl 4**, S423–33 (2010).
26. Woodhead, J. L. & Hall, C. K. Encapsulation Efficiency and Micellar Structure of Solute-Carrying Block Copolymer Nanoparticles. *Macromolecules* **44**, 5443–5451 (2011).
27. Kumar, V. & Prud'homme, R. K. Thermodynamic limits on drug loading in nanoparticle cores. *J. Pharm. Sci.* **97**, 4904–14 (2008).
28. Loverde, S. M., Klein, M. L. & Discher, D. E. Nanoparticle shape improves delivery: rational coarse grain molecular dynamics (rCG-MD) of taxol in worm-like PEG-PCL micelles. *Adv. Mater.* **24**, 3823–30 (2012).
29. Tanis, I. & Karatasos, K. Association of a weakly acidic anti-inflammatory drug (ibuprofen) with a poly(amidoamine) dendrimer as studied by molecular dynamics simulations. *J. Phys. Chem. B* **113**, 10984–93 (2009).
30. Patel, S. K., Lavasanifar, A. & Choi, P. Molecular dynamics study of the encapsulation capability of a PCL-PEO based block copolymer for hydrophobic drugs with different spatial distributions of hydrogen bond donors and acceptors. *Biomaterials* **31**, 1780–6 (2010).
31. Costache, A. D., Sheihet, L., Zaveri, K., Knight, D. D. & Kohn, J. Polymer-drug interactions in tyrosine-derived triblock copolymer nanospheres: a computational modeling approach. *Mol. Pharm.* **6**, 1620–7 (2009).

32. Maingi, V., Kumar, M. V. S. & Maiti, P. K. PAMAM dendrimer-drug interactions: effect of pH on the binding and release pattern. *J. Phys. Chem. B* **116**, 4370–6 (2012).
33. Samanta, S. & Roccatano, D. Interaction of Curcumin with PEO-PPO-PEO block copolymers: a molecular dynamics study. *J. Phys. Chem. B* **117**, 3250–7 (2013).
34. Rossi, G., Monticelli, L., Puisto, S. R., Vattulainen, I. & Ala-Nissila, T. Coarse-graining polymers with the MARTINI force-field: polystyrene as a benchmark case. *Soft Matter* **7**, 698 (2011).
35. Ortiz, V., Nielsen, S. O., Klein, M. L. & Discher, D. E. Computer simulation of aqueous block copolymer assemblies: Length scales and methods. *J. Polym. Sci. Part B Polym. Phys.* **44**, 1907–1918 (2006).
36. Praprotnik, M., Delle Site, L. & Kremer, K. Adaptive resolution scheme for efficient hybrid atomistic-mesoscale molecular dynamics simulations of dense liquids. *Phys. Rev. E. Stat. Nonlin. Soft Matter Phys.* **73**, 066701 (2006).
37. Levitt, M. & Warshel, A. Computer simulation of protein folding. *Nature* **253**, 694–8 (1975).
38. Rzepiela, A. J., Louhivuori, M., Peter, C. & Marrink, S. J. Hybrid simulations: combining atomistic and coarse-grained force fields using virtual sites. *Phys. Chem. Chem. Phys.* **13**, 10437–48 (2011).
39. Wassenaar, T. A., Ingólfsson, H. I., Priess, M., Marrink, S. J. & Schäfer, L. V. Mixing MARTINI: electrostatic coupling in hybrid atomistic-coarse-grained biomolecular simulations. *J. Phys. Chem. B* **117**, 3516–30 (2013).
40. Orafai, H. *et al.* Novel Poly (glycerol-adipate) Polymers Used for Nanoparticle Making: A Study of Surface Free Energy. *Iran. J. Pharm. Res.* **7**, 11–19 (2008).
41. Tawfeek, H. *et al.* Poly(glycerol adipate-co- ω -pentadecalactone) spray-dried microparticles as sustained release carriers for pulmonary delivery. *Pharm. Res.* **28**, 2086–97 (2011).
42. Marrink, S. J., Risselada, H. J., Yefimov, S., Tieleman, D. P. & de Vries, A. H. The MARTINI force field: coarse grained model for biomolecular simulations. *J. Phys. Chem. B* **111**, 7812–24 (2007).
43. Hess, B., Kutzner, C., Van Der Spoel, D. & Lindahl, E. GROMACS 4: Algorithms for Highly Efficient, Load-Balanced, and Scalable Molecular Simulation. *J. Chem. Theory Comput.* **4**, 435–447 (2008).

44. Hanwell, M. D. *et al.* Avogadro: an advanced semantic chemical editor, visualization, and analysis platform. *J. Cheminform.* **4**, 17 (2012).
45. D.A. Case, V. Babin, J.T. Berryman, R.M. Betz, Q. Cai, D.S. Cerutti, T.E. Cheatham, III, T.A. Darden, R.E. Duke, H. Gohlke, A.W. Goetz, S. Gusarov, N. Homeyer, P. Janowski, J. Kaus, I. Kolossváry, A. Kovalenko, T.S. Lee, S. LeGrand, T. Luchko, R. Luo, B., X. W. and P. A. K. AMBER 14. (2014).
46. Malde, A. K. *et al.* An Automated force field Topology Builder (ATB) and repository: version 1.0. *J. Chem. Theory Comput.* **7**, 111027125018002 (2011).
47. Weerasinghe, S. & Smith, P. E. Kirkwood–Buff derived force field for mixtures of acetone and water. *J. Chem. Phys.* **118**, 10663 (2003).
48. Rühle, V., Junghans, C., Lukyanov, A., Kremer, K. & Andrienko, D. Versatile Object-Oriented Toolkit for Coarse-Graining Applications. *J. Chem. Theory Comput.* **5**, 3211–3223 (2009).
49. Wassenaar, T. A., Pluhackova, K., Böckmann, R. A., Marrink, S. J. & Tieleman, D. P. Going Backward: A Flexible Geometric Approach to Reverse Transformation from Coarse Grained to Atomistic Models. *J. Chem. Theory Comput.* **10**, 676–690 (2014).
50. Shaw, D. E. *et al.* Anton, a Special-purpose Machine for Molecular Dynamics Simulation. in *Proc. 34th Annu. Int. Symp. Comput. Archit.* 1–12 (ACM, 2007). doi:10.1145/1250662.1250664
51. Harmandaris, V. A., Reith, D., van der Vegt, N. F. A. & Kremer, K. Comparison Between Coarse-Graining Models for Polymer Systems: Two Mapping Schemes for Polystyrene. *Macromol. Chem. Phys.* **208**, 2109–2120 (2007).
52. Paissoni, C., Spiliotopoulos, D., Musco, G. & Spitaleri, A. GMXPBSA 2.0: A GROMACS tool to perform MM/PBSA and computational alanine scanning. *Comput. Phys. Commun.* **185**, 2920–2929 (2014).

Appendix

WS_RM Acetone Topology

[moleculetype]

; Name nrexcl

AON 3

[atoms]

| ; nr | type | resnr | resid | atom | cgnr | charge | mass | total_charge |
|------|------|-------|-------|------|------|--------|---------|--------------|
| 1 | CHA | 1 | AON | C1 | 1 | 0.000 | 15.0350 | ; 0.000 |
| 2 | CAC | 1 | AON | C2 | 2 | 0.626 | 12.0110 | |

```

3 OAC 1 AON O1 2 -0.626 15.9994 ; 0.000
4 CHA 1 AON C3 3 0.000 15.0350 ; 0.000
; total charge of the molecule: 0.000
[ bonds ]
; ai aj funct c0 c1
1 2 2 0.1507 7.1500e+06
2 3 2 0.1222 1.6600e+07
2 4 2 0.1507 7.1500e+06
[ pairs ]
; ai aj funct ; all 1-4 pairs but the ones excluded in GROMOS itp
[ angles ]
; ai aj ak funct angle fc
1 2 3 2 121.44 730.00
1 2 4 2 117.12 670.00
3 2 4 2 121.44 730.00
[ dihedrals ]
; GROMOS improper dihedrals
; ai aj ak al funct angle fc
2 3 4 1 2 0.00 167.36

```

Multiscale DXMP.gro

Gromacs Runs On Most of All Computer Systems

68

```

1DXM C7 1 1.266 0.954 1.154
1DXM H4 2 1.349 0.946 1.223
1DXM H5 3 1.190 0.882 1.183
1DXM H6 4 1.224 1.053 1.162
1DXM C5 5 1.425 1.026 0.970
1DXM C6 6 1.318 0.922 1.010
1DXM C11 7 1.206 0.930 0.896
1DXM F1 8 1.277 0.917 0.777
1DXM C4 9 1.554 1.005 0.992
1DXM H2 10 1.627 1.081 0.966
1DXM C1 11 1.609 0.875 1.043
1DXM O1 12 1.725 0.861 1.080
1DXM C2 13 1.509 0.762 1.040
1DXM H1 14 1.548 0.662 1.054
1DXM C3 15 1.381 0.783 1.020
1DXM H3 16 1.311 0.701 1.018
1DXM C8 17 1.380 1.155 0.900
1DXM H7 18 1.395 1.142 0.793
1DXM H8 19 1.443 1.238 0.932
1DXM C9 20 1.232 1.189 0.926
1DXM H9 21 1.205 1.277 0.867
1DXM H10 22 1.219 1.217 1.030
1DXM C10 23 1.136 1.073 0.890
1DXM H12 24 1.108 1.084 0.785
1DXM C13 25 1.006 1.083 0.974

```

| | | | | | |
|---------|---------|---------|-------|-------|-------|
| 1DXM | H16 | 26 | 1.032 | 1.078 | 1.080 |
| 1DXM | C14 | 27 | 0.907 | 0.969 | 0.947 |
| 1DXM | H22 | 28 | 0.879 | 0.970 | 0.841 |
| 1DXM | C15 | 29 | 0.971 | 0.833 | 0.979 |
| 1DXM | H14 | 30 | 0.999 | 0.828 | 1.084 |
| 1DXM | H15 | 31 | 0.902 | 0.752 | 0.958 |
| 1DXM | C12 | 32 | 1.095 | 0.817 | 0.886 |
| 1DXM | H13 | 33 | 1.057 | 0.829 | 0.783 |
| 1DXM | O2 | 34 | 1.154 | 0.687 | 0.897 |
| 1DXM | H11 | 35 | 1.080 | 0.625 | 0.874 |
| 1DXM | C16 | 36 | 0.919 | 1.208 | 0.952 |
| 1DXM | H17 | 37 | 0.913 | 1.231 | 0.846 |
| 1DXM | H18 | 38 | 0.959 | 1.296 | 1.002 |
| 1DXM | C17 | 39 | 0.779 | 1.170 | 1.007 |
| 1DXM | H23 | 40 | 0.766 | 1.214 | 1.106 |
| 1DXM | C18 | 41 | 0.665 | 1.223 | 0.917 |
| 1DXM | H19 | 42 | 0.673 | 1.331 | 0.910 |
| 1DXM | H20 | 43 | 0.567 | 1.199 | 0.957 |
| 1DXM | H21 | 44 | 0.673 | 1.182 | 0.817 |
| 1DXM | C19 | 45 | 0.781 | 1.012 | 1.027 |
| 1DXM | C20 | 46 | 0.653 | 0.939 | 0.974 |
| 1DXM | O4 | 47 | 0.634 | 0.920 | 0.855 |
| 1DXM | O3 | 48 | 0.805 | 0.978 | 1.165 |
| 1DXM | H24 | 49 | 0.741 | 1.033 | 1.216 |
| 1DXM | C21 | 50 | 0.552 | 0.887 | 1.081 |
| 1DXM | H25 | 51 | 0.517 | 0.971 | 1.142 |
| 1DXM | H26 | 52 | 0.606 | 0.819 | 1.148 |
| 1DXM | O5 | 53 | 0.445 | 0.812 | 1.021 |
| 1DXM | P1 | 54 | 0.308 | 0.906 | 0.979 |
| 1DXM | O8 | 55 | 0.192 | 0.822 | 0.897 |
| 1DXM | O6 | 56 | 0.376 | 1.045 | 0.907 |
| 1DXM | O7 | 57 | 0.268 | 0.979 | 1.128 |
| 1DXC | AD | 58 | 1.609 | 0.874 | 1.042 |
| 1DXC | BD | 59 | 1.322 | 0.886 | 1.061 |
| 1DXC | CD | 60 | 1.346 | 1.123 | 0.932 |
| 1DXC | DD | 61 | 1.218 | 0.964 | 0.842 |
| 1DXC | ED | 62 | 0.842 | 1.171 | 0.962 |
| 1DXC | FD | 63 | 1.081 | 0.770 | 0.918 |
| 1DXC | GD | 64 | 0.828 | 0.985 | 1.058 |
| 1DXC | HD | 65 | 0.615 | 0.916 | 0.959 |
| 1DXC | ID | 66 | 0.316 | 0.912 | 0.985 |
| 1.96400 | 1.96400 | 1.96400 | | | |

Multiscale DXMP.itp

```
[ moleculetype ]
; Name nrexcl
DXM 3
```

```

[ atoms ]
; nr type resnr resid atom cgnr charge mass total_charge
 1  C  1  DXM  C7  1 -0.192 12.0110
 2  HC  1  DXM  H4  1  0.064 1.0080
 3  HC  1  DXM  H5  1  0.064 1.0080
 4  HC  1  DXM  H6  1  0.064 1.0080 ; 0.000
 5  C  1  DXM  C5  2  0.028 12.0110
 6  CH0 1  DXM  C6  2  0.017 12.0110
 7  CH0 1  DXM  C11 2  0.150 12.0110
 8  F  1  DXM  F1  2 -0.179 18.9984 ; 0.016
 9  C  1  DXM  C4  3 -0.114 12.0110
10  HC  1  DXM  H2  3  0.064 1.0080 ; -0.050
11  C  1  DXM  C1  4  0.189 12.0110
12  O  1  DXM  O1  4 -0.249 15.9994 ; -0.060
13  C  1  DXM  C2  5 -0.107 12.0110
14  HC  1  DXM  H1  5  0.068 1.0080 ; -0.039
15  C  1  DXM  C3  6 -0.054 12.0110
16  HC  1  DXM  H3  6  0.100 1.0080 ; 0.046
17  C  1  DXM  C8  7 -0.122 12.0110
18  HC  1  DXM  H7  7  0.061 1.0080
19  HC  1  DXM  H8  7  0.061 1.0080 ; 0.000
20  C  1  DXM  C9  8 -0.112 12.0110
21  HC  1  DXM  H9  8  0.056 1.0080
22  HC  1  DXM  H10 8  0.056 1.0080 ; 0.000
23  C  1  DXM  C10 9 -0.055 12.0110
24  HC  1  DXM  H12 9  0.055 1.0080 ; 0.000
25  C  1  DXM  C13 10 -0.047 12.0110
26  HC  1  DXM  H16 10  0.047 1.0080 ; 0.000
27  C  1  DXM  C14 11 -0.049 12.0110
28  HC  1  DXM  H22 11  0.049 1.0080 ; 0.000
29  C  1  DXM  C15 12 -0.124 12.0110
30  HC  1  DXM  H14 12  0.062 1.0080
31  HC  1  DXM  H15 12  0.062 1.0080 ; 0.000
32  C  1  DXM  C12 13  0.060 12.0110
33  HC  1  DXM  H13 13  0.054 1.0080 ; 0.114
34  OA  1  DXM  O2  14 -0.306 15.9994
35  H  1  DXM  H11 14  0.192 1.0080 ; -0.114
36  C  1  DXM  C16 15 -0.112 12.0110
37  HC  1  DXM  H17 15  0.056 1.0080
38  HC  1  DXM  H18 15  0.056 1.0080 ; 0.000
39  C  1  DXM  C17 16 -0.047 12.0110
40  HC  1  DXM  H23 16  0.047 1.0080 ; 0.000
41  C  1  DXM  C18 17 -0.192 12.0110
42  HC  1  DXM  H19 17  0.064 1.0080
43  HC  1  DXM  H20 17  0.064 1.0080
44  HC  1  DXM  H21 17  0.064 1.0080 ; 0.000
45  CH0 1  DXM  C19 18  0.108 12.0110
46  C  1  DXM  C20 18  0.188 12.0110
47  O  1  DXM  O4  18 -0.249 15.9994 ; 0.047
48  OA  1  DXM  O3  19 -0.309 15.9994

```

| | | | | | | | | |
|----|----|---|-----|-----|----|--------|---------|----------|
| 49 | H | 1 | DXM | H24 | 19 | 0.187 | 1.0080 | ; -0.122 |
| 50 | C | 1 | DXM | C21 | 20 | 0.230 | 12.0110 | |
| 51 | HC | 1 | DXM | H25 | 20 | 0.066 | 1.0080 | |
| 52 | HC | 1 | DXM | H26 | 20 | 0.066 | 1.0080 | ; 0.140 |
| 53 | OA | 1 | DXM | O5 | 21 | -0.559 | 15.9994 | |
| 54 | P | 1 | DXM | P1 | 21 | 0.921 | 30.9738 | |
| 55 | OM | 1 | DXM | O8 | 21 | -0.854 | 15.9994 | ; 0.329 |
| 56 | OM | 1 | DXM | O6 | 21 | -0.854 | 15.9994 | |
| 57 | OM | 1 | DXM | O7 | 21 | -0.854 | 15.9994 | |
| 58 | AD | 1 | DXC | AD | 22 | | 0 | |
| 59 | BD | 1 | DXC | BD | 23 | | 0 | |
| 60 | CD | 1 | DXC | CD | 24 | | 0 | |
| 61 | DD | 1 | DXC | DD | 25 | | 0 | |
| 62 | ED | 1 | DXC | ED | 26 | | 0 | |
| 63 | FD | 1 | DXC | FD | 27 | | 0 | |
| 64 | GD | 1 | DXC | GD | 28 | | 0 | |
| 65 | HD | 1 | DXC | HD | 29 | | 0 | |
| 66 | ID | 1 | DXC | ID | 30 | | 0 | |

[bonds]

| | ai | aj | funct | c0 | c1 |
|--|----|----|-------|--------|------------|
| | 1 | 2 | 2 | 0.1090 | 1.2300e+07 |
| | 1 | 3 | 2 | 0.1090 | 1.2300e+07 |
| | 1 | 4 | 2 | 0.1090 | 1.2300e+07 |
| | 1 | 6 | 2 | 0.1530 | 7.1500e+06 |
| | 5 | 6 | 2 | 0.1530 | 7.1500e+06 |
| | 5 | 9 | 2 | 0.1330 | 1.1800e+07 |
| | 5 | 17 | 2 | 0.1530 | 7.1500e+06 |
| | 6 | 7 | 2 | 0.1570 | 2.7500e+06 |
| | 6 | 15 | 2 | 0.1530 | 7.1500e+06 |
| | 7 | 8 | 2 | 0.1360 | 4.7700e+06 |
| | 7 | 23 | 2 | 0.1570 | 2.7500e+06 |
| | 7 | 32 | 2 | 0.1570 | 2.7500e+06 |
| | 9 | 10 | 2 | 0.1090 | 1.2300e+07 |
| | 9 | 11 | 2 | 0.1520 | 5.4300e+06 |
| | 11 | 12 | 2 | 0.1230 | 1.6600e+07 |
| | 11 | 13 | 2 | 0.1520 | 5.4300e+06 |
| | 13 | 14 | 2 | 0.1090 | 1.2300e+07 |
| | 13 | 15 | 2 | 0.1330 | 1.1800e+07 |
| | 15 | 16 | 2 | 0.1090 | 1.2300e+07 |
| | 17 | 18 | 2 | 0.1090 | 1.2300e+07 |
| | 17 | 19 | 2 | 0.1090 | 1.2300e+07 |
| | 17 | 20 | 2 | 0.1530 | 7.1500e+06 |
| | 20 | 21 | 2 | 0.1090 | 1.2300e+07 |
| | 20 | 22 | 2 | 0.1090 | 1.2300e+07 |
| | 20 | 23 | 2 | 0.1530 | 7.1500e+06 |
| | 23 | 24 | 2 | 0.1090 | 1.2300e+07 |
| | 23 | 25 | 2 | 0.1530 | 7.1500e+06 |
| | 25 | 26 | 2 | 0.1090 | 1.2300e+07 |
| | 25 | 27 | 2 | 0.1530 | 7.1500e+06 |

| | | | | |
|----|----|---|--------|------------|
| 25 | 36 | 2 | 0.1530 | 7.1500e+06 |
| 27 | 28 | 2 | 0.1090 | 1.2300e+07 |
| 27 | 29 | 2 | 0.1530 | 7.1500e+06 |
| 27 | 45 | 2 | 0.1530 | 7.1500e+06 |
| 29 | 30 | 2 | 0.1090 | 1.2300e+07 |
| 29 | 31 | 2 | 0.1090 | 1.2300e+07 |
| 29 | 32 | 2 | 0.1530 | 7.1500e+06 |
| 32 | 33 | 2 | 0.1100 | 1.2100e+07 |
| 32 | 34 | 2 | 0.1435 | 6.1000e+06 |
| 34 | 35 | 2 | 0.1000 | 1.5700e+07 |
| 36 | 37 | 2 | 0.1090 | 1.2300e+07 |
| 36 | 38 | 2 | 0.1090 | 1.2300e+07 |
| 36 | 39 | 2 | 0.1530 | 7.1500e+06 |
| 39 | 40 | 2 | 0.1090 | 1.2300e+07 |
| 39 | 41 | 2 | 0.1530 | 7.1500e+06 |
| 39 | 45 | 2 | 0.1570 | 2.7500e+06 |
| 41 | 42 | 2 | 0.1090 | 1.2300e+07 |
| 41 | 43 | 2 | 0.1090 | 1.2300e+07 |
| 41 | 44 | 2 | 0.1090 | 1.2300e+07 |
| 45 | 46 | 2 | 0.1570 | 2.7500e+06 |
| 45 | 48 | 2 | 0.1435 | 6.1000e+06 |
| 46 | 47 | 2 | 0.1230 | 1.6600e+07 |
| 46 | 50 | 2 | 0.1530 | 7.1500e+06 |
| 48 | 49 | 2 | 0.1000 | 1.5700e+07 |
| 50 | 51 | 2 | 0.1090 | 1.2300e+07 |
| 50 | 52 | 2 | 0.1090 | 1.2300e+07 |
| 50 | 53 | 2 | 0.1360 | 1.0200e+07 |
| 53 | 54 | 2 | 0.1760 | 1.2900e+06 |
| 54 | 55 | 2 | 0.1530 | 3.5700e+06 |
| 54 | 56 | 2 | 0.1530 | 3.5700e+06 |
| 54 | 57 | 2 | 0.1530 | 3.5700e+06 |

[pairs]

; ai aj funct ; all 1-4 pairs but the ones excluded in GROMOS itp

| | | |
|---|----|---|
| 1 | 8 | 1 |
| 1 | 9 | 1 |
| 1 | 13 | 1 |
| 1 | 16 | 1 |
| 1 | 17 | 1 |
| 1 | 23 | 1 |
| 1 | 32 | 1 |
| 2 | 5 | 1 |
| 2 | 7 | 1 |
| 2 | 15 | 1 |
| 3 | 5 | 1 |
| 3 | 7 | 1 |
| 3 | 15 | 1 |
| 4 | 5 | 1 |
| 4 | 7 | 1 |
| 4 | 15 | 1 |
| 5 | 8 | 1 |

5 12 1
5 13 1
5 16 1
5 21 1
5 22 1
5 23 1
5 32 1
6 10 1
6 11 1
6 14 1
6 18 1
6 19 1
6 20 1
6 24 1
6 25 1
6 29 1
6 33 1
6 34 1
7 9 1
7 13 1
7 16 1
7 17 1
7 21 1
7 22 1
7 26 1
7 27 1
7 30 1
7 31 1
7 35 1
7 36 1
8 15 1
8 20 1
8 24 1
8 25 1
8 29 1
8 33 1
8 34 1
9 14 1
9 15 1
9 18 1
9 19 1
9 20 1
10 12 1
10 13 1
10 17 1
11 16 1
11 17 1
12 14 1
12 15 1
14 16 1

15 17 1
15 23 1
15 32 1
17 24 1
17 25 1
18 21 1
18 22 1
18 23 1
19 21 1
19 22 1
19 23 1
20 26 1
20 27 1
20 32 1
20 36 1
21 24 1
21 25 1
22 24 1
22 25 1
23 28 1
23 29 1
23 33 1
23 34 1
23 37 1
23 38 1
23 39 1
23 45 1
24 26 1
24 27 1
24 32 1
24 36 1
25 30 1
25 31 1
25 32 1
25 40 1
25 41 1
25 46 1
25 48 1
26 28 1
26 29 1
26 37 1
26 38 1
26 39 1
26 45 1
27 33 1
27 34 1
27 37 1
27 38 1
27 40 1
27 41 1

27 47 1
27 49 1
27 50 1
28 30 1
28 31 1
28 32 1
28 36 1
28 39 1
28 46 1
28 48 1
29 35 1
29 36 1
29 39 1
29 46 1
29 48 1
30 33 1
30 34 1
30 45 1
31 33 1
31 34 1
31 45 1
32 45 1
33 35 1
36 42 1
36 43 1
36 44 1
36 46 1
36 48 1
37 40 1
37 41 1
37 45 1
38 40 1
38 41 1
38 45 1
39 47 1
39 49 1
39 50 1
40 42 1
40 43 1
40 44 1
40 46 1
40 48 1
41 46 1
41 48 1
42 45 1
43 45 1
44 45 1
45 51 1
45 52 1
45 53 1

```

46 49 1
46 54 1
47 48 1
47 51 1
47 52 1
47 53 1
48 50 1
50 55 1
50 56 1
50 57 1
51 54 1
52 54 1

```

[angles]

```

; ai aj ak funct angle fc
 2  1  3  2 107.00 987.00
 2  1  4  2 107.00 987.00
 2  1  6  2 109.00 842.00
 3  1  4  2 107.00 987.00
 3  1  6  2 109.00 842.00
 4  1  6  2 114.00 928.00
 6  5  9  2 120.00 560.00
 6  5 17  2 120.00 560.00
 9  5 17  2 120.00 560.00
 1  6  5  2 109.50 285.00
 1  6  7  2 111.00 530.00
 1  6 15  2 109.50 285.00
 5  6  7  2 109.50 285.00
 5  6 15  2 109.50 285.00
 7  6 15  2 111.00 530.00
 6  7  8  2 104.00 490.00
 6  7 23  2 111.00 530.00
 6  7 32  2 120.00 560.00
 8  7 23  2 106.75 503.00
 8  7 32  2 104.00 490.00
23  7 32  2 109.50 285.00
 5  9 10  2 120.00 505.00
 5  9 11  2 125.00 750.00
10  9 11  2 120.00 505.00
 9 11 12  2 125.00 750.00
 9 11 13  2 111.00 530.00
12 11 13  2 125.00 750.00
11 13 14  2 120.00 505.00
11 13 15  2 120.00 560.00
14 13 15  2 120.00 505.00
 6 15 13  2 125.00 750.00
 6 15 16  2 114.00 928.00
13 15 16  2 120.00 505.00
 5 17 18  2 109.00 842.00
 5 17 19  2 109.00 842.00

```

| | | | | | |
|----|----|----|---|--------|--------|
| 5 | 17 | 20 | 2 | 111.00 | 530.00 |
| 18 | 17 | 19 | 2 | 107.00 | 987.00 |
| 18 | 17 | 20 | 2 | 109.00 | 842.00 |
| 19 | 17 | 20 | 2 | 109.00 | 842.00 |
| 17 | 20 | 21 | 2 | 109.00 | 842.00 |
| 17 | 20 | 22 | 2 | 109.00 | 842.00 |
| 17 | 20 | 23 | 2 | 111.00 | 530.00 |
| 21 | 20 | 22 | 2 | 107.00 | 987.00 |
| 21 | 20 | 23 | 2 | 109.00 | 842.00 |
| 22 | 20 | 23 | 2 | 109.00 | 842.00 |
| 7 | 23 | 20 | 2 | 111.00 | 530.00 |
| 7 | 23 | 24 | 2 | 109.00 | 842.00 |
| 7 | 23 | 25 | 2 | 111.00 | 530.00 |
| 20 | 23 | 24 | 2 | 109.00 | 842.00 |
| 20 | 23 | 25 | 2 | 109.50 | 285.00 |
| 24 | 23 | 25 | 2 | 109.00 | 842.00 |
| 23 | 25 | 26 | 2 | 109.00 | 842.00 |
| 23 | 25 | 27 | 2 | 111.00 | 530.00 |
| 23 | 25 | 36 | 2 | 120.00 | 560.00 |
| 26 | 25 | 27 | 2 | 109.00 | 842.00 |
| 26 | 25 | 36 | 2 | 109.00 | 842.00 |
| 27 | 25 | 36 | 2 | 101.00 | 821.00 |
| 25 | 27 | 28 | 2 | 109.00 | 842.00 |
| 25 | 27 | 29 | 2 | 111.00 | 530.00 |
| 25 | 27 | 45 | 2 | 101.00 | 821.00 |
| 28 | 27 | 29 | 2 | 109.00 | 842.00 |
| 28 | 27 | 45 | 2 | 109.00 | 842.00 |
| 29 | 27 | 45 | 2 | 120.00 | 560.00 |
| 27 | 29 | 30 | 2 | 109.00 | 842.00 |
| 27 | 29 | 31 | 2 | 109.00 | 842.00 |
| 27 | 29 | 32 | 2 | 109.50 | 285.00 |
| 30 | 29 | 31 | 2 | 107.00 | 987.00 |
| 30 | 29 | 32 | 2 | 114.00 | 928.00 |
| 31 | 29 | 32 | 2 | 109.00 | 842.00 |
| 7 | 32 | 29 | 2 | 120.00 | 560.00 |
| 7 | 32 | 33 | 2 | 103.00 | 420.00 |
| 7 | 32 | 34 | 2 | 111.00 | 530.00 |
| 29 | 32 | 33 | 2 | 109.00 | 842.00 |
| 29 | 32 | 34 | 2 | 111.00 | 530.00 |
| 33 | 32 | 34 | 2 | 110.00 | 739.00 |
| 32 | 34 | 35 | 2 | 108.53 | 443.00 |
| 25 | 36 | 37 | 2 | 109.00 | 842.00 |
| 25 | 36 | 38 | 2 | 114.00 | 928.00 |
| 25 | 36 | 39 | 2 | 109.50 | 285.00 |
| 37 | 36 | 38 | 2 | 107.00 | 987.00 |
| 37 | 36 | 39 | 2 | 109.00 | 842.00 |
| 38 | 36 | 39 | 2 | 109.00 | 842.00 |
| 36 | 39 | 40 | 2 | 109.00 | 842.00 |
| 36 | 39 | 41 | 2 | 111.00 | 530.00 |
| 36 | 39 | 45 | 2 | 109.50 | 285.00 |

| | | | | | |
|----|----|----|---|--------|--------|
| 40 | 39 | 41 | 2 | 109.00 | 842.00 |
| 40 | 39 | 45 | 2 | 109.00 | 842.00 |
| 41 | 39 | 45 | 2 | 111.00 | 530.00 |
| 39 | 41 | 42 | 2 | 109.00 | 842.00 |
| 39 | 41 | 43 | 2 | 114.00 | 928.00 |
| 39 | 41 | 44 | 2 | 109.00 | 842.00 |
| 42 | 41 | 43 | 2 | 107.00 | 987.00 |
| 42 | 41 | 44 | 2 | 107.00 | 987.00 |
| 43 | 41 | 44 | 2 | 107.00 | 987.00 |
| 27 | 45 | 39 | 2 | 101.00 | 821.00 |
| 27 | 45 | 46 | 2 | 111.00 | 530.00 |
| 27 | 45 | 48 | 2 | 109.50 | 320.00 |
| 39 | 45 | 46 | 2 | 111.00 | 530.00 |
| 39 | 45 | 48 | 2 | 111.00 | 530.00 |
| 46 | 45 | 48 | 2 | 110.30 | 524.00 |
| 45 | 46 | 47 | 2 | 121.00 | 685.00 |
| 45 | 46 | 50 | 2 | 120.00 | 560.00 |
| 47 | 46 | 50 | 2 | 121.00 | 685.00 |
| 45 | 48 | 49 | 2 | 108.53 | 443.00 |
| 46 | 50 | 51 | 2 | 109.00 | 842.00 |
| 46 | 50 | 52 | 2 | 109.00 | 842.00 |
| 46 | 50 | 53 | 2 | 111.00 | 530.00 |
| 51 | 50 | 52 | 2 | 107.00 | 987.00 |
| 51 | 50 | 53 | 2 | 110.00 | 739.00 |
| 52 | 50 | 53 | 2 | 110.00 | 739.00 |
| 50 | 53 | 54 | 2 | 120.00 | 530.00 |
| 53 | 54 | 55 | 2 | 103.00 | 420.00 |
| 53 | 54 | 56 | 2 | 103.00 | 420.00 |
| 53 | 54 | 57 | 2 | 103.00 | 420.00 |
| 55 | 54 | 56 | 2 | 109.60 | 450.00 |
| 55 | 54 | 57 | 2 | 120.00 | 780.00 |
| 56 | 54 | 57 | 2 | 109.60 | 450.00 |

[dihedrals]

; GROMOS improper dihedrals

| ; ai | aj | ak | al | funct | angle | fc |
|------|----|----|----|-------|-------|--------|
| 11 | 9 | 12 | 13 | 2 | 0.00 | 167.36 |
| 13 | 11 | 14 | 15 | 2 | 0.00 | 167.36 |
| 15 | 6 | 13 | 16 | 2 | 0.00 | 167.36 |
| 9 | 5 | 10 | 11 | 2 | 0.00 | 167.36 |
| 5 | 6 | 9 | 17 | 2 | 0.00 | 167.36 |
| 46 | 45 | 47 | 50 | 2 | 0.00 | 167.36 |

[dihedrals]

| ; ai | aj | ak | al | funct | ph0 | cp | mult |
|------|----|----|----|-------|--------|------|------|
| 2 | 1 | 6 | 15 | 1 | 0.00 | 3.77 | 3 |
| 9 | 5 | 6 | 15 | 1 | 0.00 | 1.00 | 6 |
| 6 | 5 | 9 | 11 | 1 | 180.00 | 1.53 | 2 |
| 9 | 5 | 17 | 20 | 1 | 0.00 | 1.00 | 6 |
| 15 | 6 | 7 | 23 | 1 | 0.00 | 3.77 | 3 |
| 5 | 6 | 15 | 13 | 1 | 0.00 | 1.00 | 6 |

```

6 7 23 20 1 0.00 3.77 3
6 7 32 34 1 0.00 3.77 3
5 9 11 13 1 180.00 1.53 2
12 11 13 15 1 180.00 5.86 2
11 13 15 6 1 180.00 1.53 2
5 17 20 23 1 0.00 3.77 3
17 20 23 7 1 180.00 1.00 3
20 23 25 27 1 0.00 3.77 3
23 25 27 29 1 0.00 3.77 3
23 25 36 39 1 0.00 3.77 3
25 27 29 32 1 0.00 3.77 3
25 27 45 39 1 0.00 3.77 3
27 29 32 7 1 0.00 3.77 3
7 32 34 35 1 0.00 1.26 3
25 36 39 41 1 180.00 1.00 3
36 39 41 42 1 0.00 3.77 3
36 39 45 27 1 180.00 1.00 3
27 45 46 47 1 0.00 1.00 6
27 45 48 49 1 0.00 1.26 3
45 46 50 53 1 180.00 1.00 6
46 50 53 54 1 180.00 1.00 3
50 53 54 56 1 0.00 1.05 3

```

[virtual_sitesn]

```

58 2 12 9 13 14 10 11
59 2 15 6 1 2 3 4 16
60 2 5 17 20 18 19 21 22
61 2 23 7 8 24
62 2 25 36 39 41 26 37 38 42 43 44 40
63 2 32 29 34 33 30 31 35
64 2 27 45 48 28 49
65 2 51 52 47 46 50
66 2 53 54 55 56 57

```

grompp.mdp for Multiscale Simulations

```

integrator      = md
dt              = 0.002
nsteps         = 25000000

nstxout        = 0
nstvout        = 0
nstfout        = 0
nstlog         = 0
nstenergy      = 0
nstxtcout      = 100000

nstlist        = 5
rlist          = 1.4

```

```

coulombtype      = shift
rcoulomb_switch  = 0.0
rcoulomb         = 1.2
epsilon_r        = 6
vdw_type         = shift
rvdw_switch      = 0.9
rvdw            = 1.2

tcoupl           = v-rescale
tc-grps          = PGA STR STe PGs PCG AON DXM DXC W NA
tau_t            = 1.0 1.0 1.0 1.0 1.0 1.0 1.0 1.0 1.0 1.0
ref_t            = 310 310 310 310 310 310 310 310 310 310
;Pcoupl          = berendsen
Pcoupltype       = isotropic
tau_p            = 5.0
compressibility  = 1e-5
ref_p            = 1.0

constraints      = hbonds

```

MS2 force field

[defaults]

1 1

[atomtypes]

| ;name | at.num | mass | charge | ptype | c6 | c12 |
|-------|--------|---------|--------|-------|---------------|---------------|
| O | 8 | 15.9994 | 0.000 | A | 0.0022619536 | 1e-06 |
| OA | 8 | 15.9994 | 0.000 | A | 0.0022619536 | 1.505529e-06 |
| OM | 8 | 15.9994 | 0.000 | A | 0.0022619536 | 7.4149321e-07 |
| OE | 8 | 15.9994 | 0.000 | A | 0.0022619536 | 1.21e-06 |
| C | 6 | 12.011 | 0.000 | A | 0.0023406244 | 4.937284e-06 |
| CH0 | 6 | 12.011 | 0.000 | A | 0.0023970816 | 0.0002053489 |
| CH1 | 6 | 13.019 | 0.000 | A | 0.00606841 | 9.70225e-05 |
| CH2 | 6 | 14.027 | 0.000 | A | 0.0074684164 | 3.3965584e-05 |
| CH3 | 6 | 0.000 | 0.000 | A | 0.0096138025 | 2.6646244e-05 |
| HC | 1 | 1.0080 | 0.000 | A | 8.464e-05 | 1.5129e-08 |
| F | 9 | 18.9984 | 0.000 | A | 0.0011778624 | 7.6073284e-07 |
| P | 15 | 30.9738 | 0.000 | A | 0.01473796 | 2.2193521e-05 |
| H | 1 | 1.0080 | 0.000 | A | 0.0 | 0.0 |
| NA+ | 11 | 22.9898 | 0.000 | A | 7.2063121e-05 | 2.1025e-08 |
| AX | 0 | 0.000 | 0.000 | V | 0.0 | 0.0 |
| BX | 0 | 0.000 | 0.000 | V | 0.0 | 0.0 |
| CX | 0 | 0.000 | 0.000 | V | 0.0 | 0.0 |
| DX | 0 | 0.000 | 0.000 | V | 0.0 | 0.0 |
| EX | 0 | 0.000 | 0.000 | V | 0.0 | 0.0 |
| FX | 0 | 0.000 | 0.000 | V | 0.0 | 0.0 |
| GX | 0 | 0.000 | 0.000 | V | 0.0 | 0.0 |

| | | | | | |
|----|------|-------|-------|-------|-----|
| HX | 0 | 0.000 | 0.000 | V 0.0 | 0.0 |
| IX | 0 | 0.000 | 0.000 | V 0.0 | 0.0 |
| JX | 0 | 0.000 | 0.000 | V 0.0 | 0.0 |
| KX | 0 | 0.000 | 0.000 | V 0.0 | 0.0 |
| LX | 0 | 0.000 | 0.000 | V 0.0 | 0.0 |
| AD | 0 | 0.000 | 0.000 | V 0.0 | 0.0 |
| BD | 0 | 0.000 | 0.000 | V 0.0 | 0.0 |
| CD | 0 | 0.000 | 0.000 | V 0.0 | 0.0 |
| DD | 0 | 0.000 | 0.000 | V 0.0 | 0.0 |
| ED | 0 | 0.000 | 0.000 | V 0.0 | 0.0 |
| FD | 0 | 0.000 | 0.000 | V 0.0 | 0.0 |
| GD | 0 | 0.000 | 0.000 | V 0.0 | 0.0 |
| HD | 0 | 0.000 | 0.000 | V 0.0 | 0.0 |
| ID | 0 | 0.000 | 0.000 | V 0.0 | 0.0 |
| P4 | 72.0 | 0.000 | A 0.0 | 0.0 | |
| Na | 72.0 | 0.000 | A 0.0 | 0.0 | |

[nonbond_params]

| | | | | |
|-----|-----|---|--------------|---------------|
| OM | O | 1 | 0.0022619536 | 8.611e-07 |
| OA | O | 1 | 0.0022619536 | 1.38651e-06 |
| OA | OM | 1 | 0.0022619536 | 2.258907e-06 |
| OE | O | 1 | 0.0022619536 | 1.1e-06 |
| OE | OM | 1 | 0.0022619536 | 9.4721e-07 |
| OE | OA | 1 | 0.0022619536 | 1.505529e-06 |
| C | O | 1 | 0.0023009528 | 2.222e-06 |
| C | OM | 1 | 0.0023009528 | 1.9133642e-06 |
| C | OA | 1 | 0.0023009528 | 2.4442e-06 |
| C | OE | 1 | 0.0023009528 | 2.4442e-06 |
| CH0 | O | 1 | 0.0023285376 | 1.433e-05 |
| CH0 | OM | 1 | 0.0023285376 | 1.2339563e-05 |
| CH0 | OA | 1 | 0.0023285376 | 1.5763e-05 |
| CH0 | OE | 1 | 0.0023285376 | 1.5763e-05 |
| CH0 | C | 1 | 0.0023686848 | 3.184126e-05 |
| CH1 | O | 1 | 0.003704924 | 9.85e-06 |
| CH1 | OM | 1 | 0.003704924 | 8.481835e-06 |
| CH1 | OA | 1 | 0.003704924 | 1.0835e-05 |
| CH1 | OE | 1 | 0.003704924 | 1.0835e-05 |
| CH1 | C | 1 | 0.003768802 | 2.18867e-05 |
| CH1 | CH0 | 1 | 0.003813984 | 0.0001411505 |
| CH2 | O | 1 | 0.0041101352 | 5.828e-06 |
| CH2 | OM | 1 | 0.0041101352 | 5.0184908e-06 |
| CH2 | OA | 1 | 0.0041101352 | 6.4108e-06 |
| CH2 | OE | 1 | 0.0041101352 | 6.4108e-06 |
| CH2 | C | 1 | 0.0041809996 | 1.2949816e-05 |
| CH2 | CH0 | 1 | 0.0042311232 | 8.351524e-05 |
| CH2 | CH1 | 1 | 0.006732118 | 5.74058e-05 |
| CH3 | O | 1 | 0.004663258 | 5.162e-06 |
| CH3 | OM | 1 | 0.004663258 | 4.4449982e-06 |
| CH3 | OA | 1 | 0.004663258 | 5.6782e-06 |
| CH3 | OE | 1 | 0.004663258 | 5.6782e-06 |

| | | | | |
|-----|-----|---|---------------|---------------|
| CH3 | C | 1 | 0.004743659 | 1.1469964e-05 |
| CH3 | CH0 | 1 | 0.004800528 | 7.397146e-05 |
| CH3 | CH1 | 1 | 0.007638095 | 5.08457e-05 |
| CH3 | CH2 | 1 | 0.008473481 | 3.0084136e-05 |
| HC | O | 1 | 0.000437552 | 1.23e-07 |
| HC | OM | 1 | 0.000437552 | 1.059153e-07 |
| HC | OA | 1 | 0.000437552 | 1.353e-07 |
| HC | OE | 1 | 0.000437552 | 1.353e-07 |
| HC | C | 1 | 0.000445096 | 2.73306e-07 |
| HC | CH0 | 1 | 0.000450432 | 1.76259e-06 |
| HC | CH1 | 1 | 0.00071668 | 1.21155e-06 |
| HC | CH2 | 1 | 0.000795064 | 7.16844e-07 |
| HC | CH3 | 1 | 0.00090206 | 6.34926e-07 |
| H | O | 1 | 0 | 0 |
| H | OM | 1 | 0 | 0 |
| H | OA | 1 | 0 | 0 |
| H | OE | 1 | 0 | 0 |
| H | C | 1 | 0 | 0 |
| H | CH0 | 1 | 0 | 0 |
| H | CH1 | 1 | 0 | 0 |
| H | CH2 | 1 | 0 | 0 |
| H | CH3 | 1 | 0 | 0 |
| H | HC | 1 | 0 | 0 |
| P | O | 1 | 0.005773784 | 5.32343e-06 |
| P | OM | 1 | 0.005773784 | 1.4453348e-05 |
| P | OA | 1 | 0.005773784 | 5.780397e-06 |
| P | OE | 1 | 0.005773784 | 5.780397e-06 |
| P | C | 1 | 0.005873332 | 1.0467842e-05 |
| P | CH0 | 1 | 0.005943744 | 6.750863e-05 |
| P | CH1 | 1 | 0.00945706 | 4.640335e-05 |
| P | CH2 | 1 | 0.010491388 | 2.7455708e-05 |
| P | CH3 | 1 | 0.01190327 | 2.4318182e-05 |
| P | HC | 1 | 0.00111688 | 5.79453e-07 |
| P | H | 1 | 0 | 0 |
| F | O | 1 | 0.0016322592 | 8.722e-07 |
| F | OM | 1 | 0.0016322592 | 7.5105142e-07 |
| F | OA | 1 | 0.0016322592 | 1.505529e-06 |
| F | OE | 1 | 0.0016322592 | 9.5942e-07 |
| F | C | 1 | 0.0016604016 | 1.9380284e-06 |
| F | CH0 | 1 | 0.0016803072 | 1.2498626e-05 |
| F | CH1 | 1 | 0.002673528 | 8.59117e-06 |
| F | CH2 | 1 | 0.0029659344 | 5.0831816e-06 |
| F | CH3 | 1 | 0.003365076 | 4.5022964e-06 |
| F | HC | 1 | 0.000315744 | 1.072806e-07 |
| F | H | 1 | 0 | 0 |
| F | P | 1 | 0.004166448 | 5.780397e-06 |
| NA+ | O | 1 | 0.00040373684 | 1.6385e-07 |
| NA+ | OM | 1 | 0.00040373684 | 4.4486e-07 |
| NA+ | OA | 1 | 0.00040373684 | 1.77915e-07 |
| NA+ | OE | 1 | 0.00040373684 | 1.77915e-07 |

| | | | | |
|-----|-----|---|---------------|-------------|
| NA+ | C | 1 | 0.00041069782 | 3.2219e-07 |
| NA+ | CH0 | 1 | 0.00041562144 | 2.07785e-06 |
| NA+ | CH1 | 1 | 0.0006612931 | 1.42825e-06 |
| NA+ | CH2 | 1 | 0.00073361938 | 8.4506e-07 |
| NA+ | CH3 | 1 | 0.00083234645 | 7.4849e-07 |
| NA+ | HC | 1 | 7.80988e-05 | 1.7835e-08 |
| NA+ | H | 1 | 0 | 0 |
| NA+ | P | 1 | 0.0010305646 | 6.83095e-07 |
| NA+ | F | 1 | 0.00029134248 | 1.77915e-07 |

;solvent

| | | | | |
|-----|----|---|-------------|-------------|
| P4 | Na | 1 | 0.20002E-00 | 0.21514E-02 |
| Na | Na | 1 | 0.24145E-00 | 0.26027E-02 |
| P4 | P4 | 1 | 0.21558E-00 | 0.23238E-02 |
| NA+ | Na | 1 | 0.17246E-00 | 0.18590E-02 |
| NA+ | P4 | 1 | 0.24145E-00 | 0.26027E-02 |

;polymer

| | | | | |
|----|----|---|-------------|-------------|
| P4 | AX | 1 | 0.13366E-00 | 0.14408E-02 |
| P4 | BX | 1 | 0.11642E-00 | 0.12549E-02 |
| P4 | CX | 1 | 0.86233E-01 | 0.92953E-03 |
| P4 | DX | 1 | 0.11642E-00 | 0.12549E-02 |
| P4 | EX | 1 | 0.13366E-00 | 0.14408E-02 |
| P4 | FX | 1 | 0.13366E-00 | 0.14408E-02 |
| P4 | GX | 1 | 0.11642E-00 | 0.12549E-02 |
| P4 | HX | 1 | 0.86233E-01 | 0.92953E-03 |
| P4 | IX | 1 | 0.86233E-01 | 0.92953E-03 |
| P4 | JX | 1 | 0.86233E-01 | 0.92953E-03 |
| P4 | KX | 1 | 0.86233E-01 | 0.92953E-03 |
| P4 | LX | 1 | 0.86233E-01 | 0.92953E-03 |

| | | | | |
|----|----|---|-------------|-------------|
| Na | AX | 1 | 0.17246E-00 | 0.18590E-02 |
| Na | BX | 1 | 0.17246E-00 | 0.18590E-02 |
| Na | CX | 1 | 0.15091E-00 | 0.16267E-02 |
| Na | DX | 1 | 0.17246E-00 | 0.18590E-02 |
| Na | EX | 1 | 0.15091E-00 | 0.16267E-02 |
| Na | FX | 1 | 0.15091E-00 | 0.16267E-02 |
| Na | GX | 1 | 0.15091E-00 | 0.16267E-02 |
| Na | HX | 1 | 0.15091E-00 | 0.16267E-02 |
| Na | IX | 1 | 0.15091E-00 | 0.16267E-02 |
| Na | JX | 1 | 0.15091E-00 | 0.16267E-02 |
| Na | KX | 1 | 0.15091E-00 | 0.16267E-02 |
| Na | LX | 1 | 0.15091E-00 | 0.16267E-02 |

;drug

| | | | | |
|----|----|---|-------------|-------------|
| P4 | AD | 1 | 0.86233E-01 | 0.92953E-03 |
| P4 | BD | 1 | 0.86233E-01 | 0.92953E-03 |
| P4 | CD | 1 | 0.86233E-01 | 0.92953E-03 |
| P4 | DD | 1 | 0.86233E-01 | 0.92953E-03 |
| P4 | ED | 1 | 0.86233E-01 | 0.92953E-03 |

| | | | | |
|----|----|---|-------------|-------------|
| P4 | FD | 1 | 0.86233E-01 | 0.92953E-03 |
| P4 | GD | 1 | 0.86233E-01 | 0.92953E-03 |
| P4 | HD | 1 | 0.11642E-00 | 0.12549E-02 |
| P4 | ID | 1 | 0.24145E-00 | 0.26027E-02 |
| | | | | |
| Na | AD | 1 | 0.13366E-00 | 0.14408E-02 |
| Na | BD | 1 | 0.13366E-00 | 0.14408E-02 |
| Na | CD | 1 | 0.13366E-00 | 0.14408E-02 |
| Na | DD | 1 | 0.13366E-00 | 0.14408E-02 |
| Na | ED | 1 | 0.13366E-00 | 0.14408E-02 |
| Na | FD | 1 | 0.15091E-00 | 0.16267E-02 |
| Na | GD | 1 | 0.15091E-00 | 0.16267E-02 |
| Na | HD | 1 | 0.15091E-00 | 0.16267E-02 |
| Na | ID | 1 | 0.13366E-00 | 0.14408E-02 |

[pairtypes]

| ;i | j | func | c6 | c12 |
|-----|-----|------|--------------|---------------|
| O | O | 1 | 0.0022619536 | 7.4149321e-07 |
| OM | O | 1 | 0.0022619536 | 7.4149321e-07 |
| OM | OM | 1 | 0.0022619536 | 7.4149321e-07 |
| OA | O | 1 | 0.0022619536 | 9.687375e-07 |
| OA | OM | 1 | 0.0022619536 | 9.687375e-07 |
| OA | OA | 1 | 0.0022619536 | 1.265625e-06 |
| OE | O | 1 | 0.0022619536 | 9.687375e-07 |
| OE | OM | 1 | 0.0022619536 | 9.687375e-07 |
| OE | OA | 1 | 0.0022619536 | 1.265625e-06 |
| OE | OE | 1 | 0.0022619536 | 1.265625e-06 |
| C | O | 1 | 0.0023009528 | 1.5818407e-06 |
| C | OM | 1 | 0.0023009528 | 1.5818407e-06 |
| C | OA | 1 | 0.0023009528 | 2.066625e-06 |
| C | OE | 1 | 0.0023009528 | 2.066625e-06 |
| C | C | 1 | 0.0023406244 | 3.374569e-06 |
| CH0 | O | 1 | 0.0023009528 | 1.5818407e-06 |
| CH0 | OM | 1 | 0.0023009528 | 1.5818407e-06 |
| CH0 | OA | 1 | 0.0023009528 | 2.066625e-06 |
| CH0 | OE | 1 | 0.0023009528 | 2.066625e-06 |
| CH0 | C | 1 | 0.0023406244 | 3.374569e-06 |
| CH0 | CH0 | 1 | 0.0023406244 | 3.374569e-06 |
| CH1 | O | 1 | 0.0025663376 | 1.6645063e-06 |
| CH1 | OM | 1 | 0.0025663376 | 1.6645063e-06 |
| CH1 | OA | 1 | 0.0025663376 | 2.174625e-06 |
| CH1 | OE | 1 | 0.0025663376 | 2.174625e-06 |
| CH1 | C | 1 | 0.0026105848 | 3.550921e-06 |
| CH1 | CH0 | 1 | 0.0026105848 | 3.550921e-06 |
| CH1 | CH1 | 1 | 0.0029116816 | 3.736489e-06 |
| CH2 | O | 1 | 0.0032687988 | 1.8751283e-06 |
| CH2 | OM | 1 | 0.0032687988 | 1.8751283e-06 |
| CH2 | OA | 1 | 0.0032687988 | 2.4497959e-06 |
| CH2 | OE | 1 | 0.0032687988 | 2.4497959e-06 |
| CH2 | C | 1 | 0.0033251574 | 4.0002446e-06 |

| | | | | |
|-----|-----|---|--------------|---------------|
| CH2 | CH0 | 1 | 0.0033251574 | 4.0002446e-06 |
| CH2 | CH1 | 1 | 0.0037086708 | 4.2092938e-06 |
| CH2 | CH2 | 1 | 0.0047238129 | 4.7419261e-06 |
| CH3 | O | 1 | 0.0039370168 | 2.1146739e-06 |
| CH3 | OM | 1 | 0.0039370168 | 2.1146739e-06 |
| CH3 | OA | 1 | 0.0039370168 | 2.7627548e-06 |
| CH3 | OE | 1 | 0.0039370168 | 2.7627548e-06 |
| CH3 | C | 1 | 0.0040048964 | 4.5112715e-06 |
| CH3 | CH0 | 1 | 0.0040048964 | 4.5112715e-06 |
| CH3 | CH1 | 1 | 0.0044668088 | 4.7470266e-06 |
| CH3 | CH2 | 1 | 0.0056894694 | 5.347702e-06 |
| CH3 | CH3 | 1 | 0.0068525284 | 6.0308652e-06 |
| HC | O | 1 | 0.000437552 | 1.059153e-07 |
| HC | OM | 1 | 0.000437552 | 1.059153e-07 |
| HC | OA | 1 | 0.000437552 | 1.38375e-07 |
| HC | OE | 1 | 0.000437552 | 1.38375e-07 |
| HC | C | 1 | 0.000445096 | 2.25951e-07 |
| HC | CH0 | 1 | 0.000445096 | 2.25951e-07 |
| HC | CH1 | 1 | 0.000496432 | 2.37759e-07 |
| HC | CH2 | 1 | 0.000632316 | 2.6784436e-07 |
| HC | CH3 | 1 | 0.000761576 | 3.0206119e-07 |
| HC | HC | 1 | 8.464e-05 | 1.5129e-08 |
| H | O | 1 | 0 | 0 |
| H | OM | 1 | 0 | 0 |
| H | OA | 1 | 0 | 0 |
| H | OE | 1 | 0 | 0 |
| H | C | 1 | 0 | 0 |
| H | CH0 | 1 | 0 | 0 |
| H | CH1 | 1 | 0 | 0 |
| H | CH2 | 1 | 0 | 0 |
| H | CH3 | 1 | 0 | 0 |
| H | HC | 1 | 0 | 0 |
| H | H | 1 | 0 | 0 |
| P | O | 1 | 0.005773784 | 4.0566421e-06 |
| P | OM | 1 | 0.005773784 | 4.0566421e-06 |
| P | OA | 1 | 0.005773784 | 5.299875e-06 |
| P | OE | 1 | 0.005773784 | 5.299875e-06 |
| P | C | 1 | 0.005873332 | 8.654107e-06 |
| P | CH0 | 1 | 0.005873332 | 8.654107e-06 |
| P | CH1 | 1 | 0.006550744 | 9.106363e-06 |
| P | CH2 | 1 | 0.008343822 | 1.0258657e-05 |
| P | CH3 | 1 | 0.010049492 | 1.1569189e-05 |
| P | HC | 1 | 0.00111688 | 5.79453e-07 |
| P | H | 1 | 0 | 0 |
| P | P | 1 | 0.01473796 | 2.2193521e-05 |
| F | O | 1 | 0.0016322592 | 7.5105142e-07 |
| F | OM | 1 | 0.0016322592 | 7.5105142e-07 |
| F | OA | 1 | 0.0016322592 | 9.81225e-07 |
| F | OE | 1 | 0.0016322592 | 9.81225e-07 |
| F | C | 1 | 0.0016604016 | 1.6022314e-06 |

```

F   CH0  1  0.0016604016  1.6022314e-06
F   CH1  1  0.0018519072  1.6859626e-06
F   CH2  1  0.0023588136  1.8992996e-06
F   CH3  1  0.0028410096  2.1419331e-06
F   HC   1  0.000315744   1.072806e-07
F   H    1    0    0
F   P    1  0.004166448   4.1089342e-06
F   F    1  0.0011778624   7.6073284e-07
NA+  O    1  0.00040373684   1.248595e-07
NA+  OM   1  0.00040373684   1.248595e-07
NA+  OA   1  0.00040373684   1.63125e-07
NA+  OE   1  0.00040373684   1.63125e-07
NA+  C    1  0.00041069782   2.66365e-07
NA+  CH0  1  0.00041069782   2.66365e-07
NA+  CH1  1  0.00045806644   2.80285e-07
NA+  CH2  1  0.00058344897   3.1575148e-07
NA+  CH3  1  0.00070271942   3.5608839e-07
NA+  HC   1  7.80988e-05   1.7835e-08
NA+  H    1    0    0
NA+  P    1  0.0010305646   6.83095e-07
NA+  F    1  0.00029134248   1.26469e-07

```

```

#include "dxmpsalt.itp"
#include "hyb80c18.itp"

```

```

;;;;; ACETONE

```

```

[ moleculetype ]

```

```

; molname      nrexcl
AON           1

```

```

[ atoms ]

```

```

;id   type  resnr  residu  atom  cgnr  charge
1     Na    1       AON     Na    1     0

```

```

;;;;; SODIUM

```

```

[ moleculetype ]

```

```

; Name nrexcl
NA     1

```

```

[ atoms ]

```

```

; nr type resnr resid atom cgnr charge  mass  total_charge
1  NA+  1     NA  NA  1    1

```

```

;;;;; WATER (representing 4 H2O molecules)

```

```

[ moleculetype ]

```

```

; molname      nrexcl
W             1

```

```
[ atoms ]
;id   type  resnr  residu  atom  cgnr  charge
1     P4    1      W      W     1     0
```